# CHAPTER IV

# SIMULATION STUDIES

The simulation case studies were conducted by using a reservoir simulator to acquire pressure responses under particular conditions. The simulation results were then interpreted using a well test interpretation software. As a result, reservoirs properties are obtained.

The simulator used to generate results for all the models in this study is SimBestII, a commercial black oil simulator, which was kindly provided by Paradigm Geotechnology B.V. After running each case, the simulated pressure response is imported into Interpret2005, which was used for well test interpretation, also provided by Paradigm Geotechnology B.V.

A single well radial reservoir is used for all simulations in this study. The zone of interest is assumed to be occupied by water so that PVT data is not necessitated to be taken into account, and possible difficulties and errors are avoided.

Initially, a simple case study was simulated as a single layer homogenous reservoir for the verification of the homogenous behavior and to prove that a simulator can be used to generate the desirable condition of reservoir.

In the next step, the simulator was used to generate numerous cases in order to conduct an investigation of the effect of test duration, probe position, and permeability etc.

Finally, multilayer reservoir with different permeabilities between the layers was generated to appraise whether the permeabilities obtained from wireline formation testing in multilayer reservoirs is satisfactory compared to permeabilities obtained from conventional well tests.

## 4.1 Simulation of Single Layer Homogenous Reservoir

### 4.1.1 Base Case

The reservoir geometry was set to be a radial model with a single layer containing 20 circular grid blocks in the theta direction, 20 grid blocks in the radial direction, and 31 grid blocks in the z-direction as schematically shown in Figure 4.2. The grid sizes in all directions increase logarithmically because the pressure response changes logarithmically as a function of distance. Figure 4.1 compares the diagnostic plots of the pressure response when the block size was kept constant and the pressure response when the block size was increased logarithmically. As seen in the figure, at middle times, the negative half slope cannot be seen in the derivative plot of the linear series gridding. At late times, the stabilization in the derivative plot identifying radial flow cannot be seen. So, the regression cannot be fitted with the derivative plot and no parameter can be estimated. When the grid cells were resized logarithmically the negative half slope, which is an indicator of spherical flow can be observed. At late times, the stabilization indicating radial flow is present. The spherical and horizontal permeability can be estimated from the spherical flow and radial flow regimes. Therefore, logarithmical series gridding will be used for all the cases.

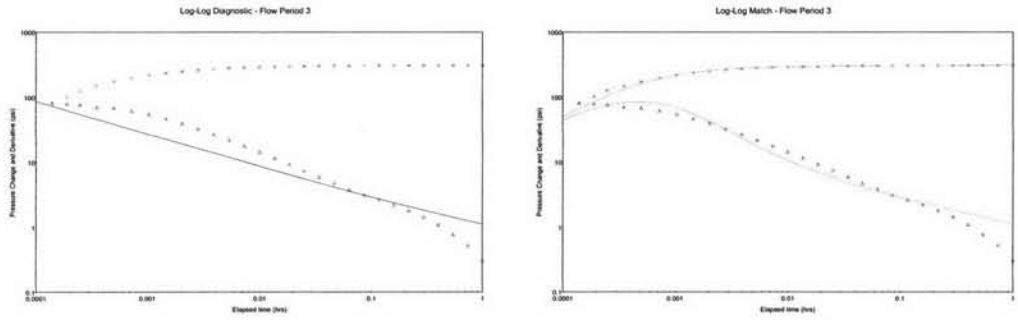


Diagnostic plot and regression of the linear series gridding.

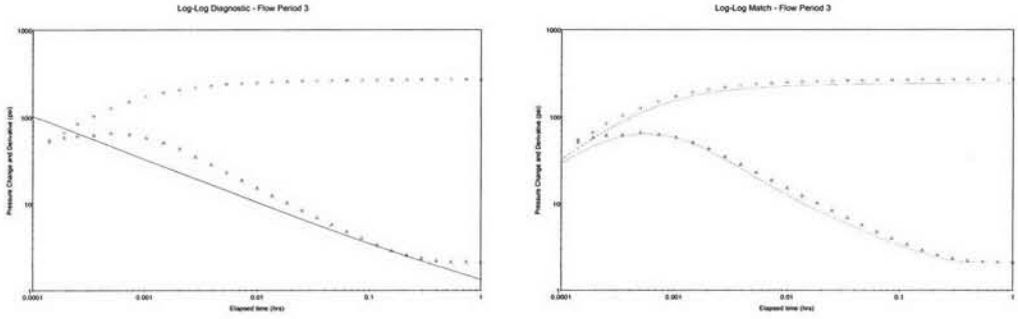


Diagnostic plot and regression of the logarithmical series gridding.

Figure 4.1: Comparison between different gridding methods.

The wellbore radius of a reservoir model was set to be 0.25 foot. In the radial direction, started from the wellbore radius, the first grid size was set to be 0.0369 foot. Subsequent grid sizes were increased logarithmically as tabulated in Table 4.1. The first grid cell in the theta direction was set to be 8.46 degrees. The angle was increased logarithmically in the clockwise and counter clockwise directions as summarized in Table 4.1 and shown in Figure 4.2. Note that grid 2 is adjacent to grid 1 in the counter clockwise direction while grid 20 is adjacent to grid 1 in the clockwise direction. In the z-direction, the initial grid size was set to be 0.0833 foot (1 inch), which is equal to the size of the actual probe, and all grid cells were logarithmically increased. For the grid sizes in the z-direction shown in Table 4.1, the probe is located at grid 16 which is in the middle of the formation. If the probe is to be located near the top or bottom boundary, the grid sizes have to be changed in a way

that the grid where the probe is located is the smallest grid with the size 0.0833 foot, and then the size is increased logarithmically.

Table 4.1: Grid sizes of the single layer radial model.

| Radial direction | |
|---|---|
| **Grid** | **Grid size (ft)** |
| 1 | 0.0369 |
| 2 | 0.0550 |
| 3 | 0.0821 |
| 4 | 0.1225 |
| 5 | 0.1828 |
| 6 | 0.2727 |
| 7 | 0.4068 |
| 8 | 0.6068 |
| 9 | 0.9053 |
| 10 | 1.3505 |
| 11 | 2.0147 |
| 12 | 3.0055 |
| 13 | 4.4837 |
| 14 | 6.6889 |
| 15 | 9.9787 |
| 16 | 14.8865 |
| 17 | 22.2081 |
| 18 | 33.1306 |
| 19 | 49.4250 |
| 20 | 73.7334 |
| Σ | 224 |

| Theta direction | |
|---|---|
| **Grid** | **Grid size (Degrees)** |
| 1 | 8.4600 |
| 2 | 9.8100 |
| 3 | 11.3753 |
| 4 | 13.1905 |
| 5 | 15.2953 |
| 6 | 17.7360 |
| 7 | 20.5661 |
| 8 | 23.8478 |
| 9 | 27.6532 |
| 10 | 32.0658 |
| 11 | 32.0658 |
| 12 | 27.6532 |
| 13 | 23.8478 |
| 14 | 20.5661 |
| 15 | 17.7360 |
| 16 | 15.2953 |
| 17 | 13.1905 |
| 18 | 11.3753 |
| 19 | 9.8100 |
| 20 | 8.4600 |
| Σ | 360 |

| z-direction | |
|---|---|
| **Grid** | **Grid size (ft)** |
| 1 | 1.9793 |
| 2 | 1.6024 |
| 3 | 1.2974 |
| 4 | 1.0504 |
| 5 | 0.8504 |
| 6 | 0.6885 |
| 7 | 0.5574 |
| 8 | 0.4513 |
| 9 | 0.3654 |
| 10 | 0.2958 |
| 11 | 0.2395 |
| 12 | 0.1939 |
| 13 | 0.157 |
| 14 | 0.1271 |
| 15 | 0.1029 |
| 16 | 0.0833 |
| 17 | 0.1029 |
| 18 | 0.1271 |
| 19 | 0.157 |
| 20 | 0.1939 |
| 21 | 0.2395 |
| 22 | 0.2958 |
| 23 | 0.3654 |
| 24 | 0.4513 |
| 25 | 0.5574 |
| 26 | 0.6885 |
| 27 | 0.8504 |
| 28 | 1.0504 |
| 29 | 1.2974 |
| 30 | 1.6024 |
| 31 | 1.9793 |
| Σ | 20 |

Figure 4.2 shows 3D perspective of the single layer radial model. It can be seen that grid cells were in logarithmical series in all directions. Figure 4.3 depicts grid cells from the top view. In the theta direction, the probe is at the smallest cell and the cell size increases logarithmically clockwise and counter clockwise so the biggest cell is at the opposite direction of the probe. In the radial direction, the cells near the wellbore are the smallest and logarithmically increase. Figures 4.4 and 4.5 show the cross section of the model in 3D and 2D, respectively. The probe was set at the smallest cell which is in the middle of the model.

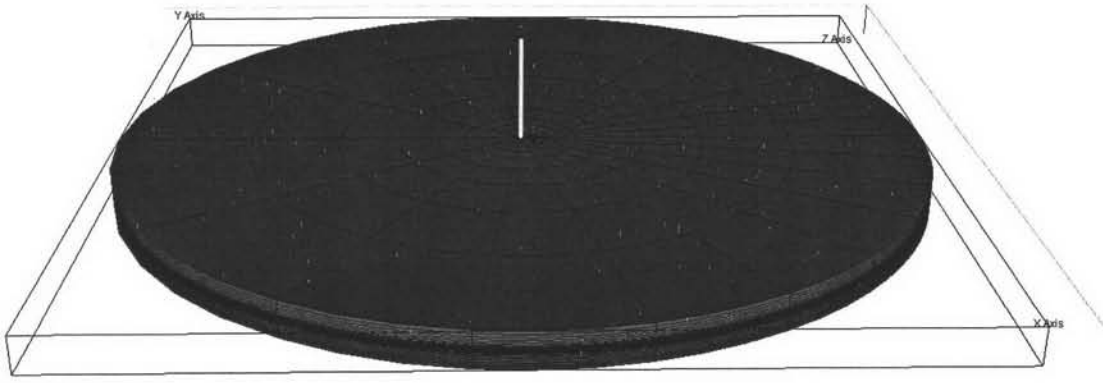


Figure 4.2: 3D view of a single layer radial model.

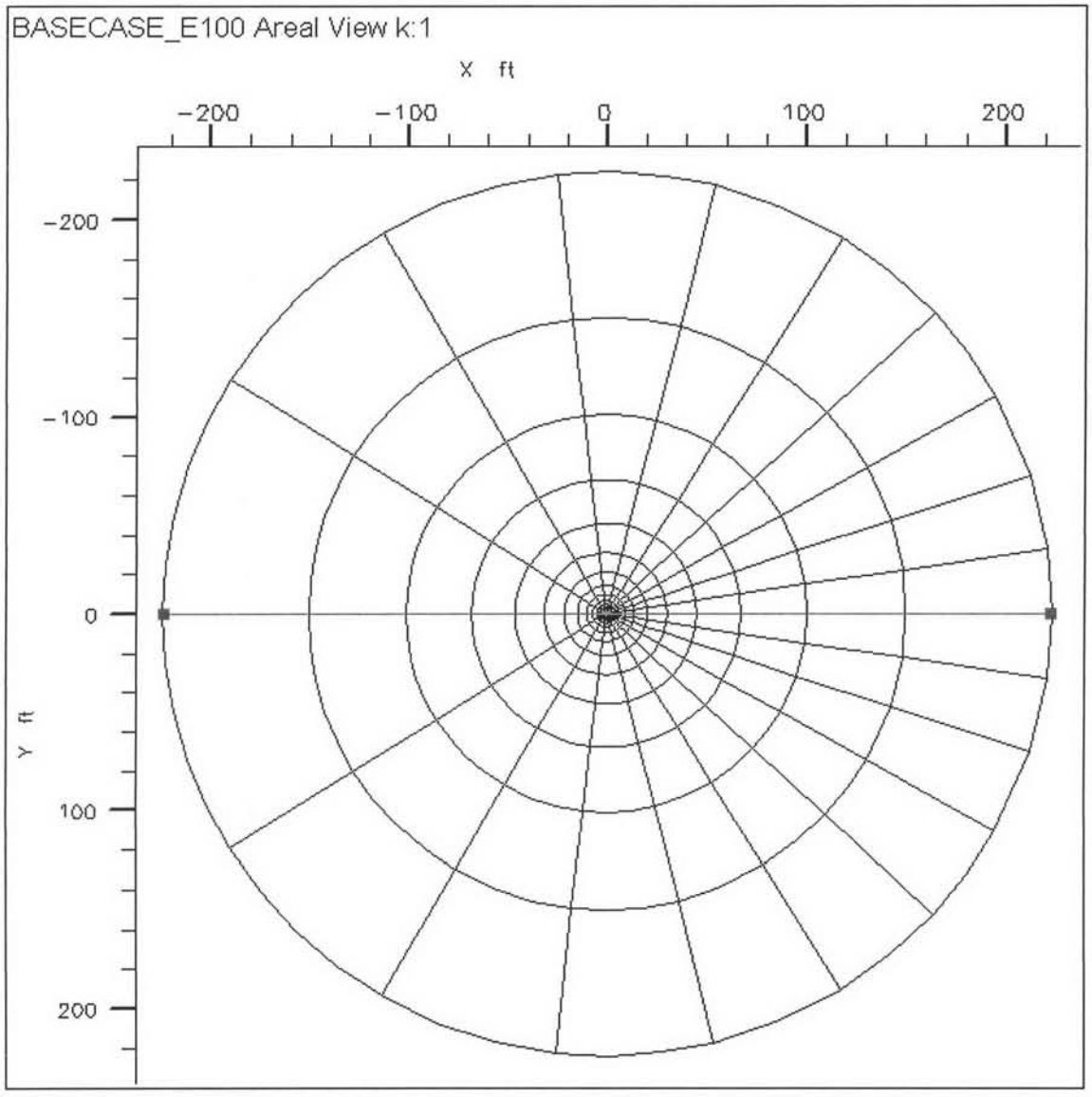


Figure 4.3: Top view of a single layer radial model.

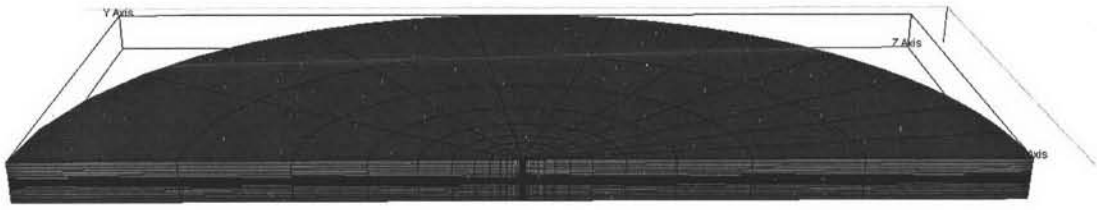

Figure 4.4: Cross section of a single layer radial model.

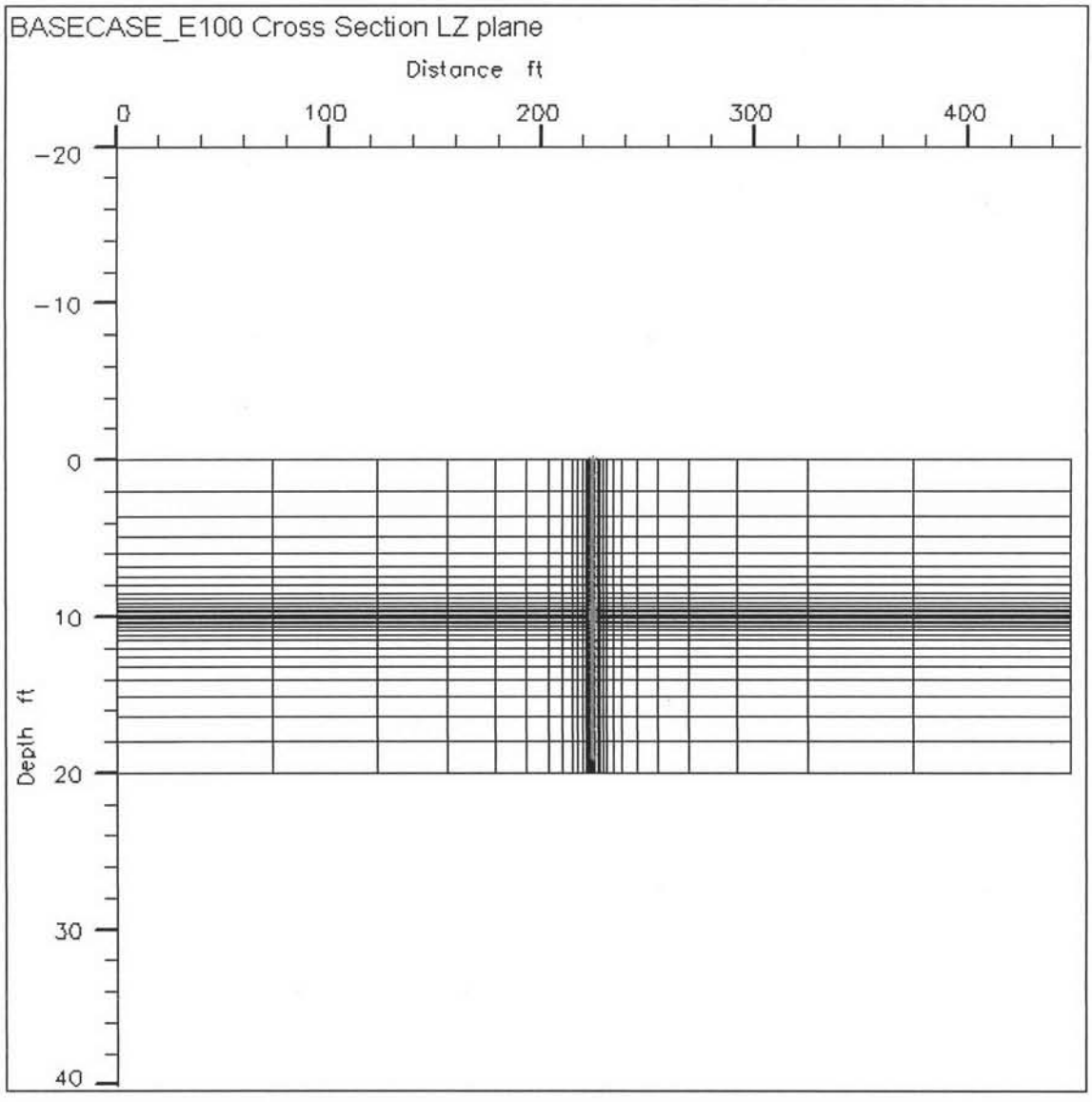


Figure 4.5: Side view of a single layer radial model.

The top depth of the reservoir was set at 8100 feet. The reservoir thickness is 20 feet. Water was used as the fluid in the reservoir to avoid any possibility of two-phase flow.

To simulate a homogenous reservoir, permeabilities in the theta and radial directions were set to be 10 mD. Therefore, the horizontal permeability ($k_{xy}$) is equal to 10 mD. In order to have the vertical and horizontal permeability ratio equal to 0.1 $\left(k_z/k_{hxy} = 0.1\right)$, the permeability in the z-direction was set to be 1.0 mD. As a result, by using Equation 3.6, the calculated spherical permeability is equal to 4.642 mD. The porosity was set to be 0.18. A schematic of a single layer homogenous reservoir is shown in Figure 4.6.

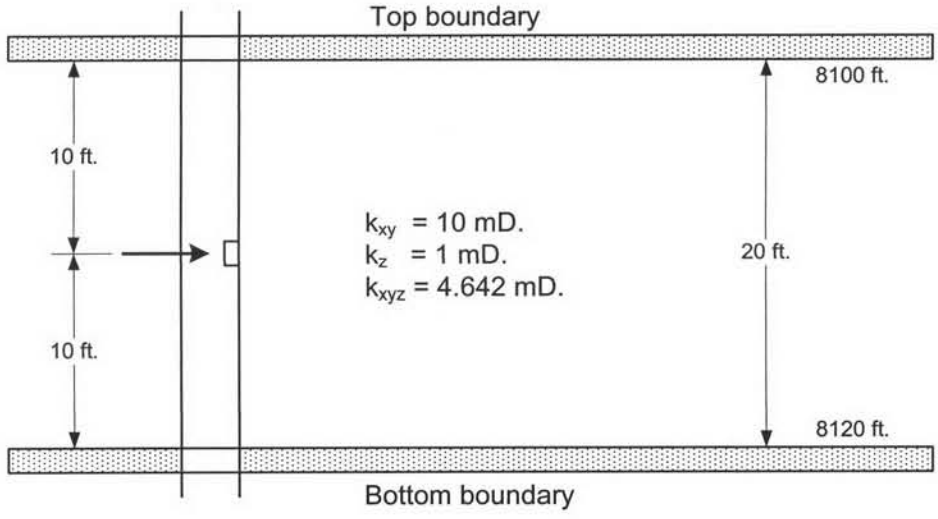


Figure 4.6: Schematic of a single layer homogenous reservoir.

Table 4.2 summarizes the conditions used in the simulation. The datum was set at 7348 feet and the initial datum pressure was set equal to 3216 psi. The reservoir temperature was set to be 160° F. The water has a viscosity of 1.0 cp, compressibility of $3\text{x}10^{-6}$ $\text{psi}^{-1}$, with a total compressibility equal to $9\text{x}10^{-6}$ $\text{psi}^{-1}$, and initial formation volume factor equal to 1.001. The probe position was set at the middle of the reservoir thickness, at depth 8110 feet. The flow rate was set at 2.54 bbl/day (4.67 cc/sec) over a total flow period of 120 minutes consisting of a 30-minute drawdown and a 90-minute buildup. This flow period is longer than that of an actual wireline formation test so that the radial flow regime can fully develop.

Table 4.2: Reservoir conditions of simulation model.

| Parameter | | Value | Unit |
|---|---|---|---|
| Top resevoir depth | | 8100 | ft |
| Bottom reservoir depth | | 8120 | ft |
| Datum | | 7348 | ft |
| Initial datum pressure | | 3216 | psi |
| Pressure at standard condition | $p_{sc}$ | 14.6 | psi |
| Temperature at standard condition | $T_{sc}$ | 60 | ° F |
| Water initial formatin volume factor | $B_{wi}$ | 1.001 | - |
| Water viscosity | $\mu_w$ | 1 | cp |
| Water compressibility | $c_w$ | $3 \times 10^{-6}$ | $psi^{-1}$ |
| Total compressibility | $c_t$ | $9 \times 10^{-6}$ | $psi^{-2}$ |

A test run of reservoir simulation was then conducted. The pressure response during the drawdown and buildup of the simulation is shown in Figure 4.7. The simulated pressure response was then interpreted using pressure transient analysis technique. As shown in Figure 4.8, at early times, the negative half slope can be seen in the derivative plot, indicating the spherical flow. At middle times, the horizontal straight line which is the indicator of the radial flow can be seen. After running a nonlinear regression using a probe model option in the well test software, the values of $k_{xy}$, $k_z$ and $k_{xyz}$ were determined. The results are shown in Table 4.3. Also shown in table is the values used or computed in the simulation. The estimates of parameters obtained from interpreting the pressure response from simulated WFT are consistent with the input used in simulating the WFT. The regression match of the pressure response is shown in Figure 4.9.

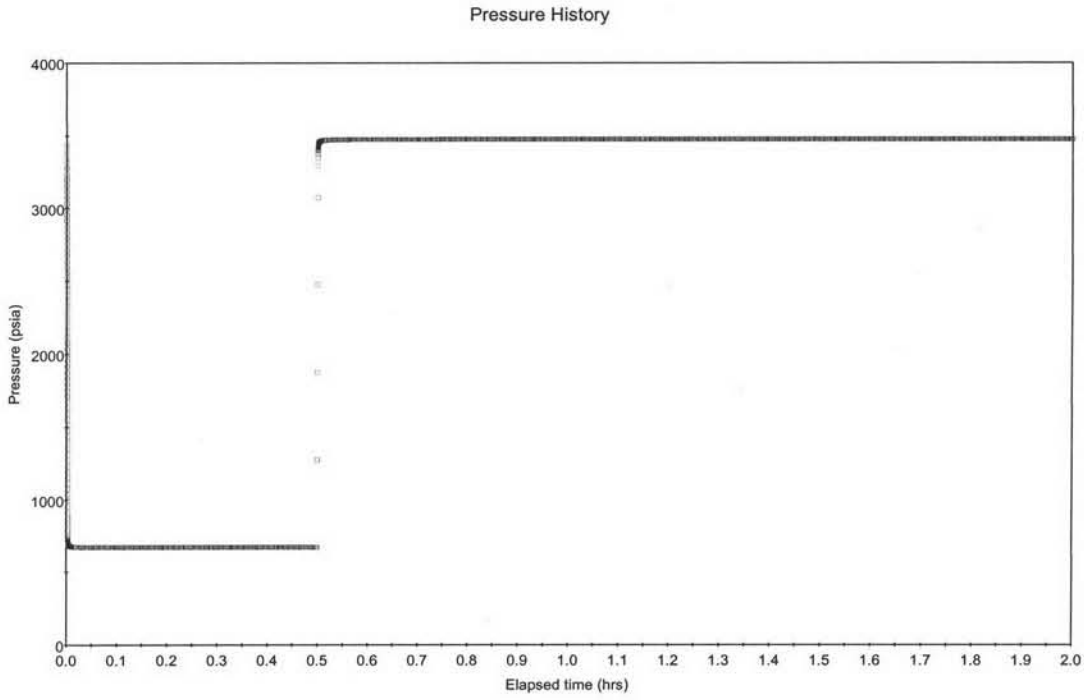


Figure 4.7: Pressure history of a single layer homogenous reservoir (base case).

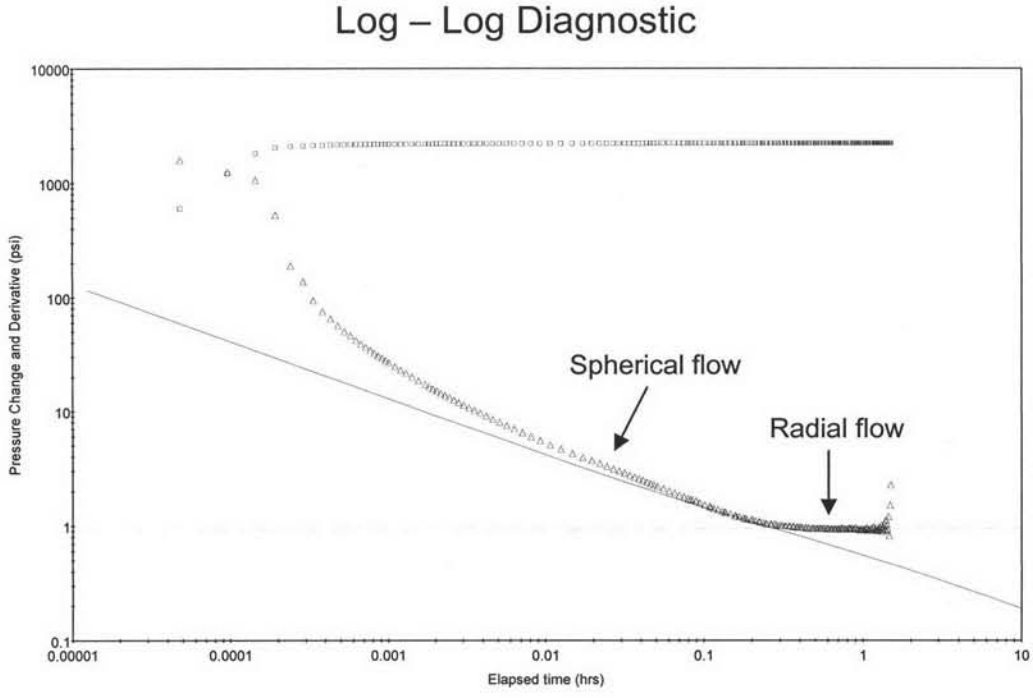


Figure 4.8: Diagnostic plot for a single layer homogenous reservoir (base case).

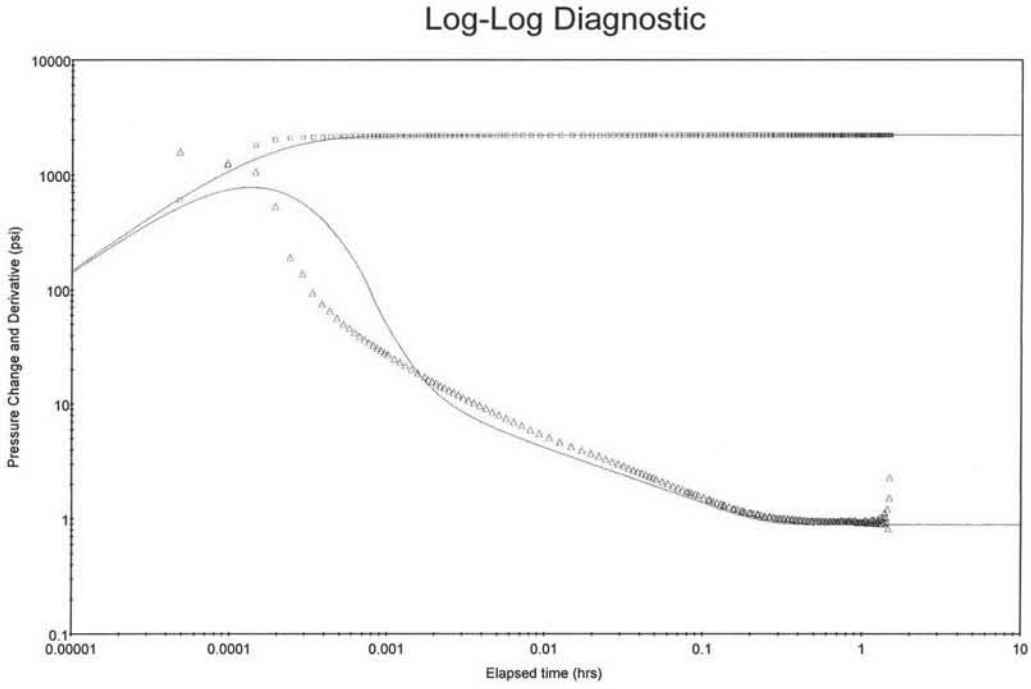


Figure 4.9: Regression for a single layer homogenous reservoir (base case).

Table 4.3: Comparison between input parameters and estimates from test interpretation.

| Parameter | Input | Interpreted result | Error (%) |
|---|---|---|---|
| $k_{xy}$ (mD) | 10 | 9.864 | -1.36 |
| $k_z$ (mD) | 1 | 0.946 | -5.40 |
| $k_{xyz}$ (mD) | 4.642 | 4.515 | -2.74 |
| $k_{xyz}/k_{xy}$ | 0.1 | 0.0959 | -4.10 |

### 4.1.2 Effects of Test Duration

To study the effect of test duration, tests with different durations of buildup and drawdown periods as shown in Table 4.4 were simulated. The simulation was conducted for the water reservoir having the same reservoir parameters and conditions. The probe position was set at the middle of the reservoir as shown in Figure 4.10. The horizontal permeability ($k_{xy}$) was set equal to 10 mD, and the vertical permeability ($k_z$) was set equal to 1 mD. Thus, from Equation 3.6, the calculated spherical permeability is 4.642 mD. The flow rate of the test was set at 2.54 bbl/day (4.67 cc/sec).

The pressure responses for these different cases are interpreted using Interpret2005. The diagnostic plots of the tests are depicted in Figure 4.11, and the interpretation results are tabulated in Table 4.4.

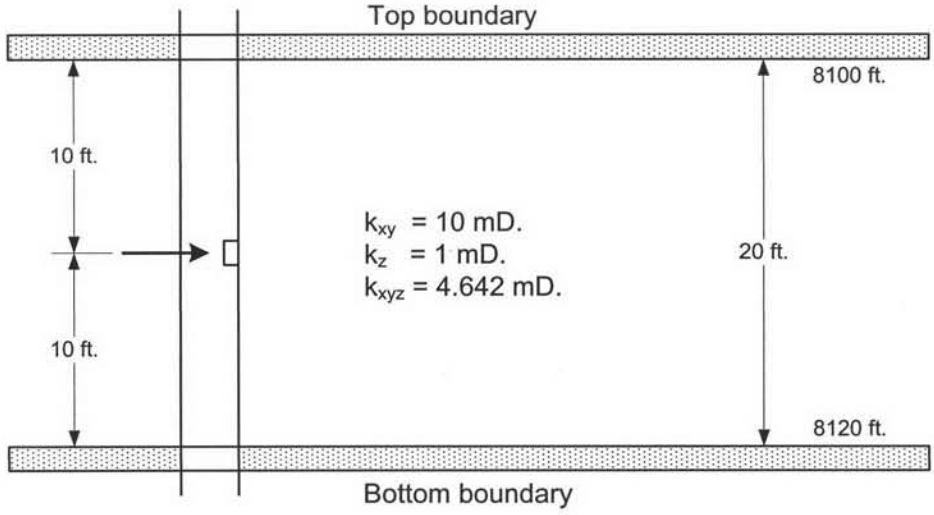


Figure 4.10: Schematic of a single layer reservoir with different test durations.

The derivative plot for case t11 in Figure 4.11 (a) depicts a spherical flow and a short period of radial flow. When the drawdown was increased to 30 minutes with a buildup period of 60 or 90 minutes, the radial flow is more noticeable as seen in Figure 4.11 (b) and (d). The longer the test was performed, the further the pressure response travels in the reservoir.

When comparing case t14 and case t15 which have the same total flow period of 120 minutes but with different drawdown and buildup time ratios, it can be seen that, the flow period consists of a 30-minute drawdown and a 90-minute buildup, gave a more satisfactory result. The pressure response went further in reservoir even though the total flow period is the same. Furthermore, when considering the radius of investigation ($r_{inv}$) as shown in Table 4.2, case t14 with a drawdown and buildup time ratio of 1:1, the pressure response traveled for a shorter distance compared to case t15 with the drawdown and buildup time ratio of 1:3.

The spherical and horizontal permeabilities obtained from the tests as shown in Table 4.4 illustrate that the estimated value are very close to those used in simulation (4.625 and 10 mD).

Table 4.4: Interpreted results for different test durations.

| Case | Drawdown time | Buildup time | Cumu. time | dd:bu ratio | Interpreted $k_{xyz}$ | Interpreted $k_{xy}$ | $r_{inv}$ |
|---|---|---|---|---|---|---|---|
| | mins | mins | mins | | mD | mD | ft |
| t11 | 10 | 30 | 40 | 1:3 | 4.590 | 9.905 | 72 |
| t12 | 30 | 60 | 90 | 1:2 | 4.531 | 9.733 | 71 |
| t14 | 60 | 60 | 120 | 1:1 | 4.417 | 9.491 | 99 |
| t15 | 30 | 90 | 120 | 1:3 | 4.515 | 9.864 | 124 |

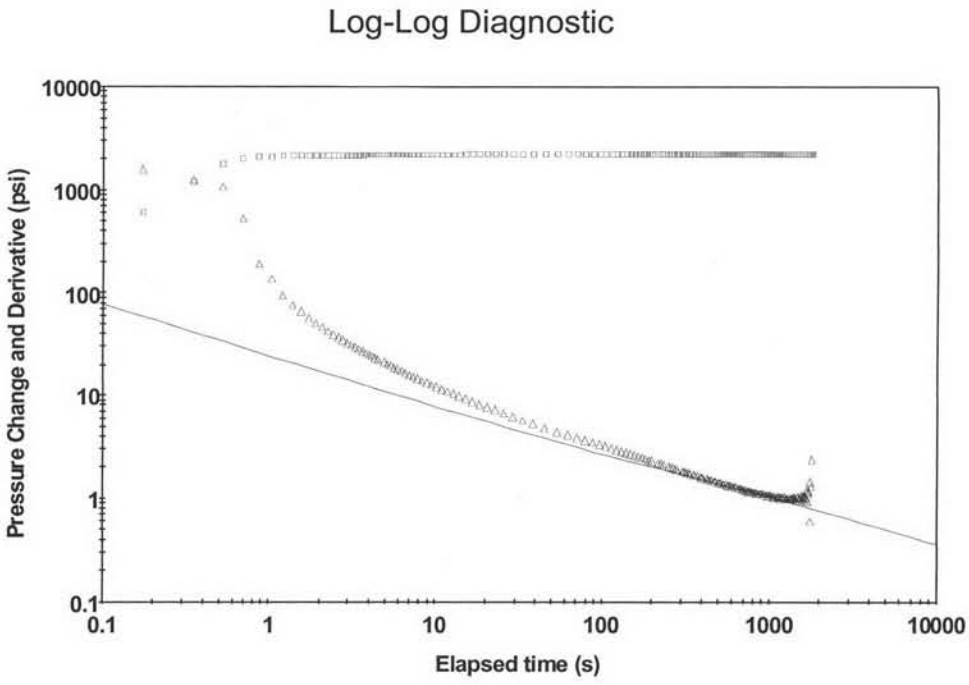


(a) Drawdown for 10 minutes and buildup for 30 minutes (case t11).

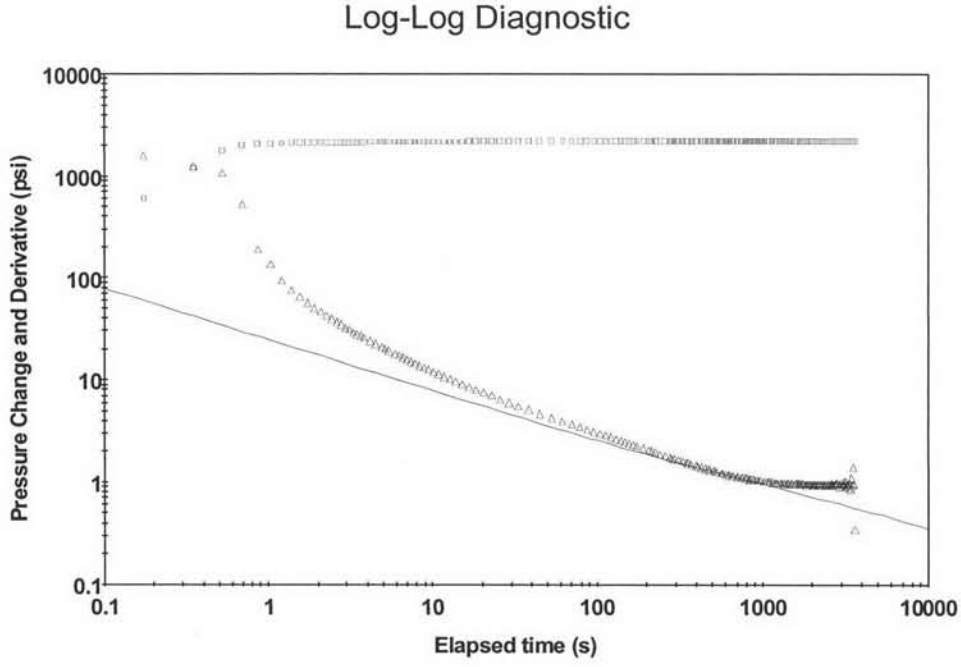


(b) Drawdown for 30 minutes and buildup for 60 minutes (case t12).

Figure 4.11: Diagnostic plots for different test durations.

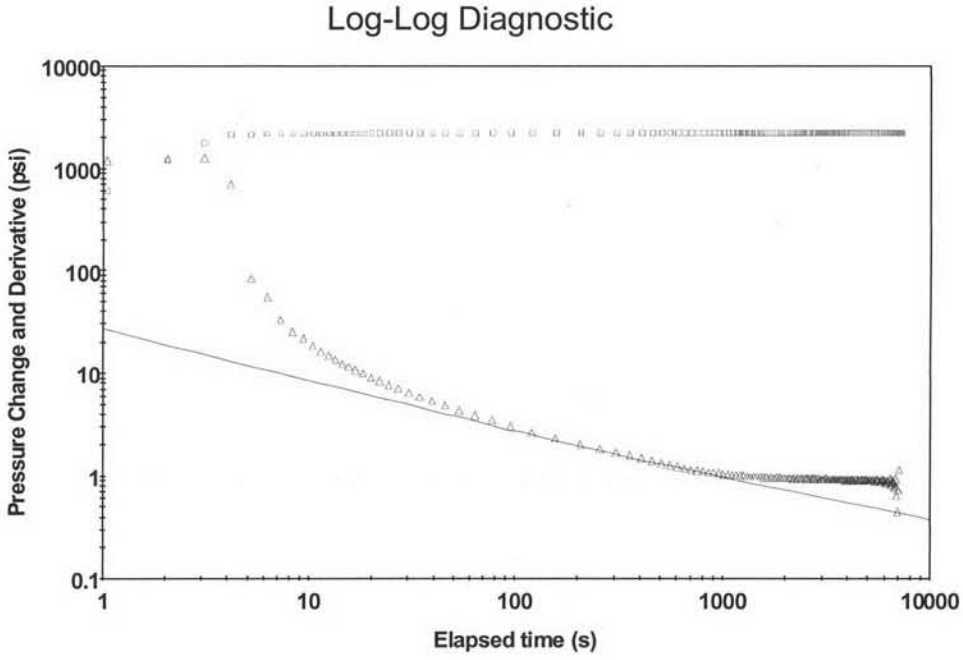


(c) Drawdown for 60 minutes and buildup for 60 minutes (case t14).

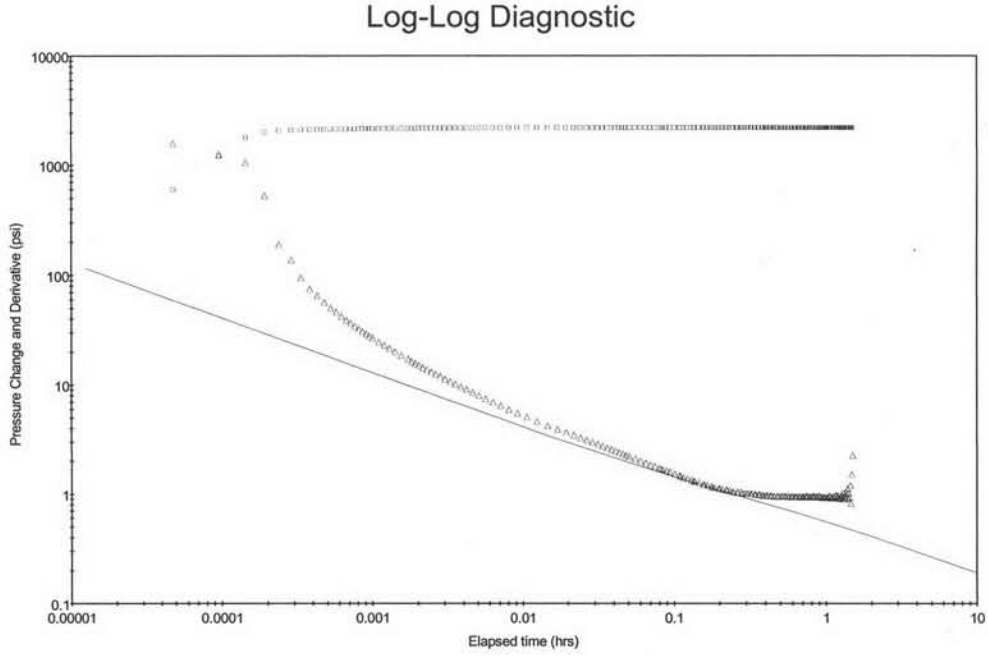


(d) Drawdown for 30 minutes and buildup for 90 minutes (case t15).

Figure 4.11: Diagnostic plots for different test durations (continued).

### 4.1.3 Effects of Probe Positions

To determine the effect of the probe position to the pressure response, a set of simulations was carried out. The probe position was set at the middle of the formation, 0.5, 1, 2, 5, and 8 feet away from the middle of the formation as shown in Figure 4.12. As a result, eleven different positions were studied. In these cases, grid sizes in the theta and radial directions are the same as those in the base case. The z-direction grids were resized corresponding to the probe position. The grid cell at the probe was set to be 0.0833 foot, and the rest of the grids were increased logarithmically. The horizontal permeability ($k_{xy}$) was set equal to 10 mD, and the vertical permeability ($k_z$) was set equal to 1 mD. Thus, from Equation 3.6, the calculated spherical permeability is 4.642 mD. The flow rate of the test was set at 2.54 bbl/day (4.67 cc/sec). The flow period consists of a 30-minute drawdown and a 90-minute buildup.

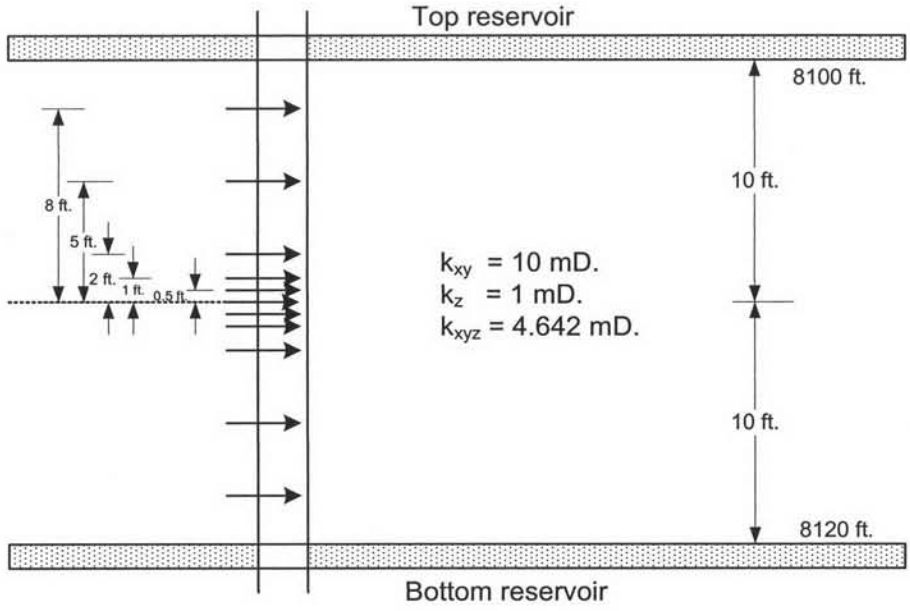


Figure 4.12: Schematic of different probe positions.

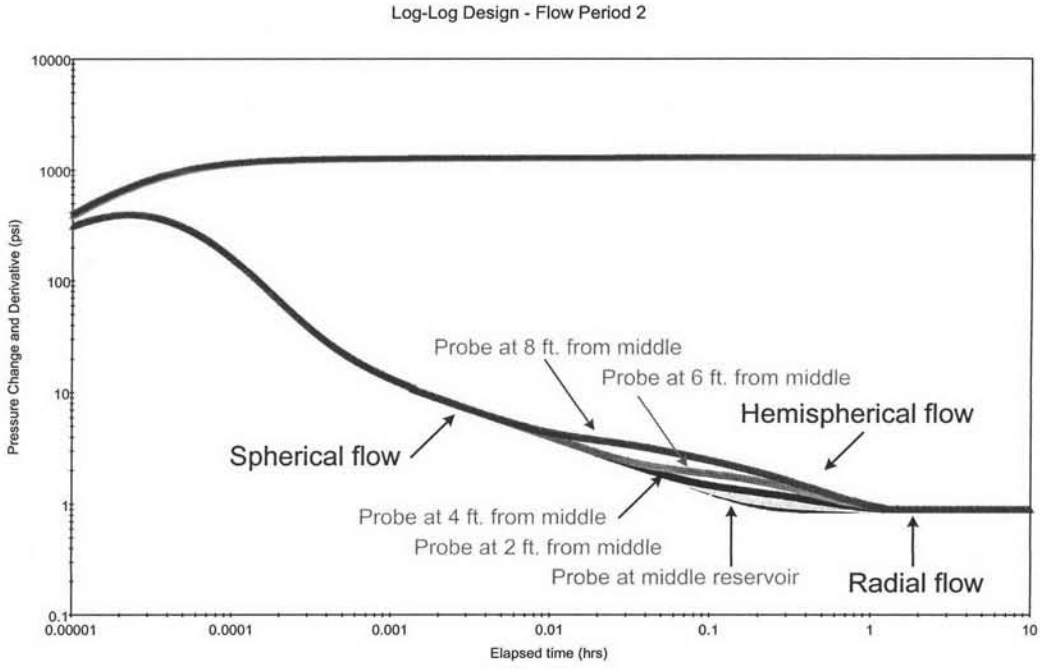


Figure 4.13: Diagnostic plot of the pressure response obtained from a well test interpretation software.

Theoretically, when the probe position is not at the middle of the formation, hemispherical flow, apart from spherical and radial flow, is also present. Figure 4.13 is the diagnostic plot of the pressure response when the probe position was varied from 2 feet beneath the reservoir top to 2 feet above the reservoir bottom at an interval of 2 feet. It can be seen that when the probe is placed closer to the top or the bottom of the reservoir, spherical flow occurs for a shorter period of time, and the derivative plot enters the hemispherical flow before reaching radial flow. The closer to the boundary the probe is, the more noticeable the hemispherical flow. Due to symmetry, the probe at the same distance from top or bottom boundary gives the same pressure response. After the pressure signal reaches both the top and bottom boundaries, the radial flow develops as shown in Figure 4.14.

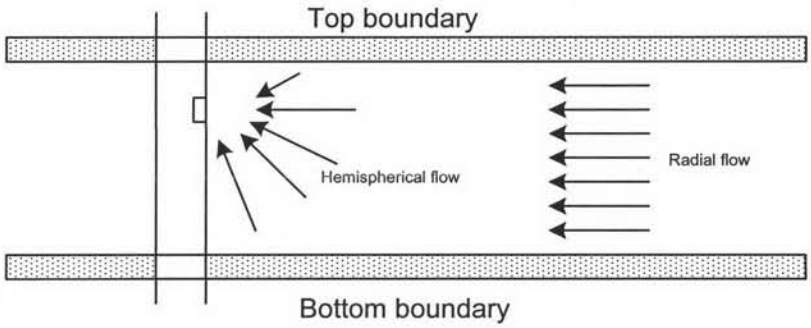


Figure 4.14: Schematic of pressure response.

From Figure 4.15, it can be seen that when the probe is placed at 8 feet above the middle of the formation, which is 2 beneath the top of the reservoir, the spherical flow occurs for a short period of time. The spherical permeability estimated from this spherical flow is 3.673 mD. Then, the derivative plot enters the hemispherical flow. The permeability estimated from this hemispherical flow is 3.085 mD. At late times, the radial flow can be seen. This radial flow gives the estimated horizontal permeability of 8.190 mD. The spherical and horizontal permeabilities obtained from interpreting the pressure response for this probe position is lower than that used in the simulation (4.642 mD) with an error of -20.87 and -18.10 %, respectively. This is due to the fact that the flow regime in simulation is hemispherical flow while a well test interpretation software is applied the spherical source solution. Thus, there is a little inconsistency between these two flow models.

From Figure 4.16, when the probe is at 5 feet above the middle of the formation, which is at 5 feet beneath the top boundary, the spherical flow occurs for a longer period of time compared to the previous case. The spherical permeability estimated from this spherical flow is 4.087 mD. Then, the derivative plot enters the hemispherical flow. The permeability estimated from this flow regime is 3.162 mD. At late times, the radial flow appears in the derivative plot, this flow regime gives the estimated horizontal permeability of 8.846 mD. Similar to the previous case, the spherical and horizontal permeabilities obtained from interpreting the pressure response for this probe position is lower than that used in the simulation with an error of -11.95 and -11.54 %, respectively.

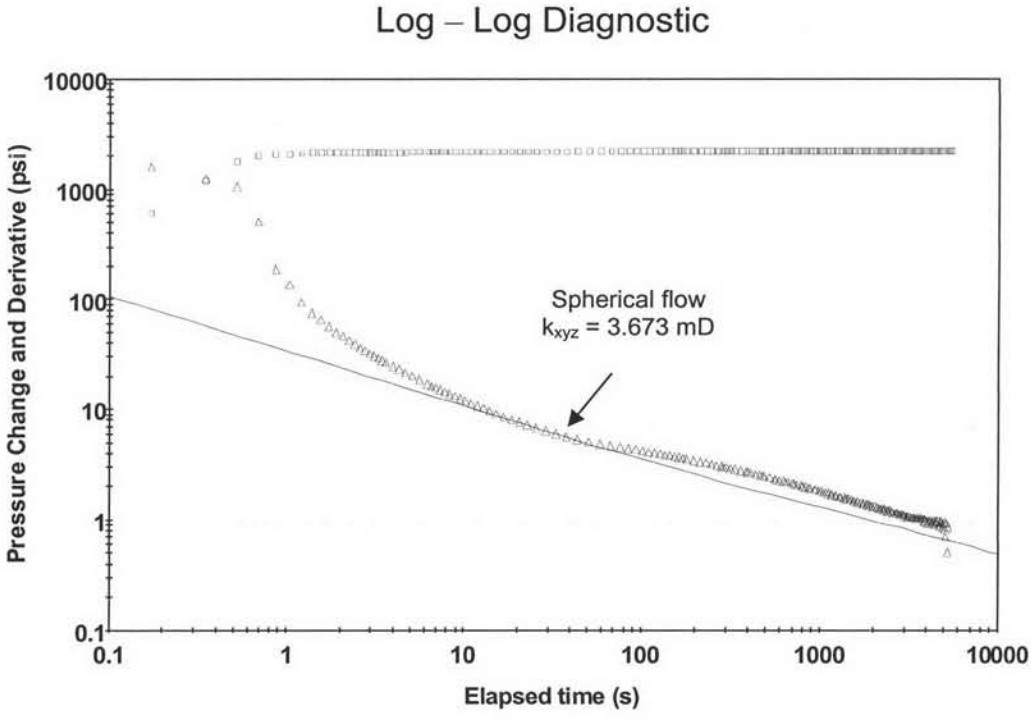


(a) Spherical flow.

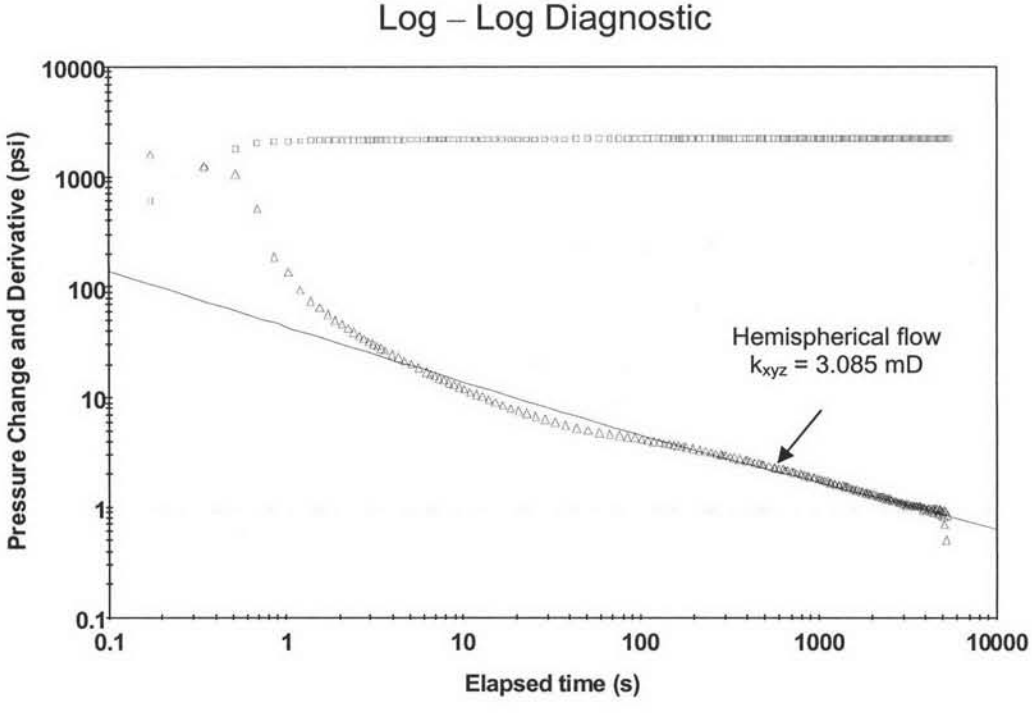


(b) Hemispherical flow.

Figure 4.15: Diagnostic plot when the probe is 8 feet above the middle of the formation.

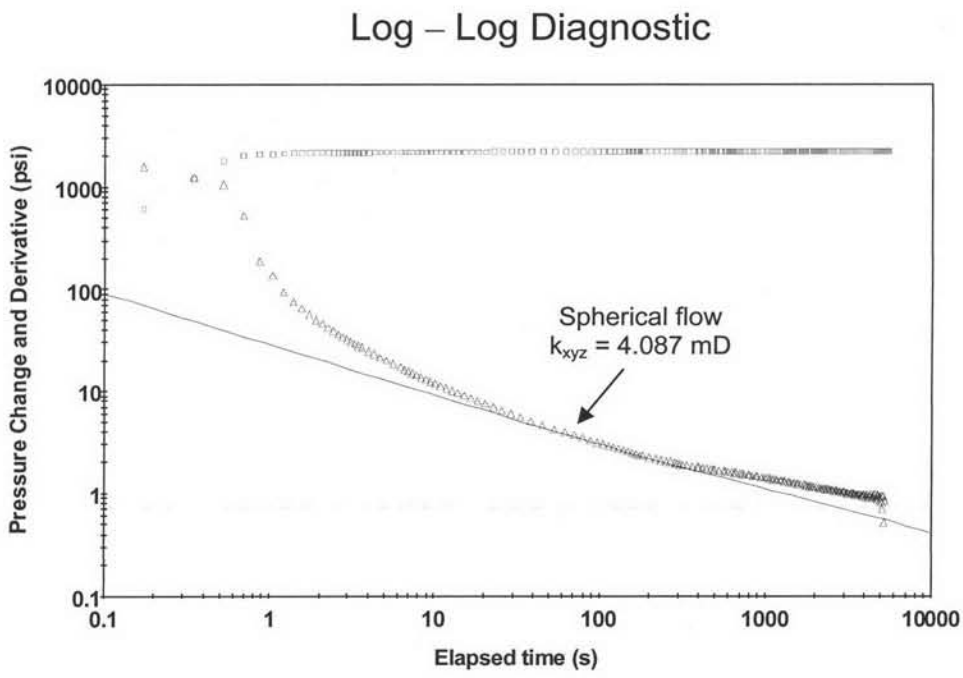


(a) Spherical flow.

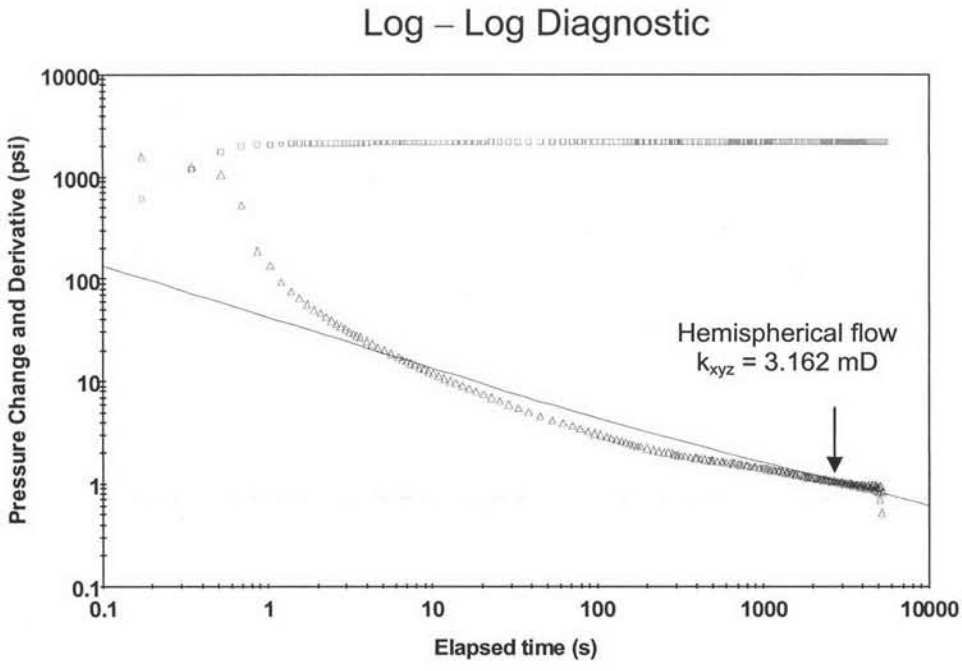


(b) Hemispherical flow.

Figure 4.16: Diagnostic plot when the probe is 5 feet above the middle of the formation.

From Figure 4.17, it can be seen that when the probe is at 0.5 foot above the middle of the formation, only one negative half slope which indicates spherical flow is present. Since the probe is very close to the middle of the formation, the pressure response is very similar to that of the case when the probe is set at the middle of the formation. The spherical and horizontal permeabilities obtained from this case, 4.502 and 9.920 mD, respectively. These values are very close to the permeabilities obtained from the case that the probe is at the middle of the formation, 4.515 and 9.864 mD, respectively.

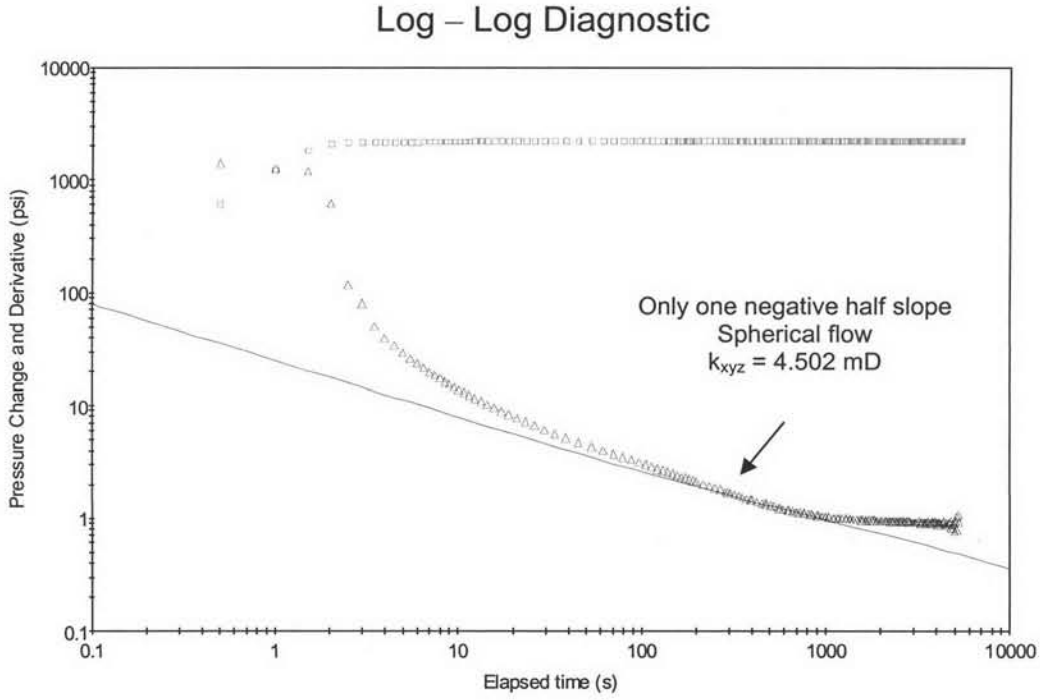


Figure 4.17: Diagnostic plot when probe position at 0.5 foot above the middle of the formation.

The interpreted results from different probe positions described before were summarized in Table 4.5. It can be concluded that when the probe position is at the middle of the formation, the estimated spherical and horizontal permeability (4.515 and 9.864 mD) give the most consistent results with the values used in the simulation (4.642 and 10 mD) with an error of -2.74 and -1.36 %, respectively. Table 4.5 also compares the radius of investigation when the probe is placed at different positions. Thus, when considering the radius of investigation ($r_{inv}$), the probe at the middle of the formation has the highest value of radius of investigation showing that the pressure response traveled for the longest distance.

In Figure 4.13, it can be seen that the further from the middle of the formation the probe is, the longer it takes for the pressure response to fully develop into radial flow. Therefore, it is recommended that the probe should be positioned in the middle of the formation.

Table 4.5: Interpreted results from different probe positions.

| **Probe position from the middle of the formation** | **Input $k_{xyz}$** | **Interpreted $k_{xyz}$** | **Error** | **Input $k_{xy}$** | **Interpreted $k_{xy}$** | **Error** | **$r_{inv}$** |
|---|---|---|---|---|---|---|---|
| ft | mD | mD | % | mD | mD | % | ft |
| 8 (above) | 4.642 | 3.673 | -20.87 | 10 | 8.190 | -18.10 | 113 |
| 5 (above) | 4.642 | 4.087 | -11.95 | 10 | 8.846 | -11.54 | 117 |
| 2 (above) | 4.642 | 4.398 | -5.25 | 10 | 9.621 | -3.79 | 122 |
| 1 (above) | 4.642 | 4.486 | -3.35 | 10 | 9.795 | -2.05 | 124 |
| 0.5 (above) | 4.642 | 4.502 | -3.01 | 10 | 9.920 | -0.80 | 124 |
| 0 | 4.642 | 4.515 | -2.74 | 10 | 9.864 | -1.36 | 124 |
| 0.5 (below) | 4.642 | 4.524 | -2.54 | 10 | 9.836 | -1.64 | 124 |
| 1 (below) | 4.642 | 4.452 | -4.08 | 10 | 9.700 | -3.00 | 123 |
| 2 (below) | 4.642 | 4.435 | -4.45 | 10 | 9.638 | -3.62 | 123 |
| 5 (below) | 4.642 | 4.099 | -11.69 | 10 | 8.870 | -11.30 | 118 |
| 8 (below) | 4.642 | 3.698 | -20.33 | 10 | 8.122 | -18.78 | 112 |

### 4.1.4 Effects of Formation Permeability

To determine the effect of formation permeability on the pressure response, several simulation runs were performed by varying the permeability. The permeability ratio $(k_z/k_{xy})$ was kept constant and equal to 0.1. The horizontal permeability ($k_{xy}$) was set to 1, 10, 100, and 1000 mD, and vertical permeability ($k_z$) was respectively set to 0.1, 1, 10 and 100 mD. The spherical permeability is calculated using Equation 3.6 and equal to 0.4642, 4.642, 46.42, 464.2 mD, respectively. The grid sizes are the same as those in the base case. The probe position was set at the middle of the formation. Figure 4.18 shows a schematic of the model. The flow rate of the test was set at 2.54 bbl/day (4.67 cc/sec).

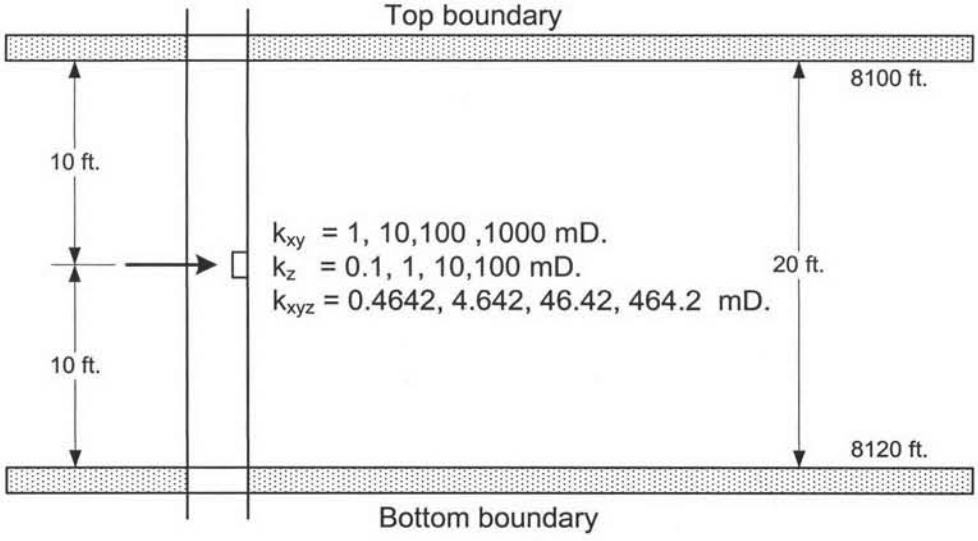


Figure 4.18: Schematic of a single layer reservoir with varying permeability.

Figure 4.19 shows the diagnostic plot of a test conducted in a reservoir with a horizontal permeability of 1 mD. The test was conducted with 30 minutes of drawdown and 90 minutes of buildup. In this case, the negative half slope which is the indicator of spherical flow appears for a short period of time, yielding the estimated permeability of 0.5222 mD with an error of 12.50 % as tabulated in Table 4.6. The permeability is so low that the pressure response did not go far enough to get information that can fully represent the entire reservoir. It can be seen that the radius

of investigation is only 29 feet. The test duration was then extended to see if the pressure response could go any further. When the test was conducted at 180 minutes of drawdown and 540 minutes of buildup, the estimated spherical permeability is 0.4610 mD with an error of -0.65 % and the radius of investigation increases to 68 feet. Thus, for a tight reservoir, wireline formation test would have to be conducted for a longer period of time.

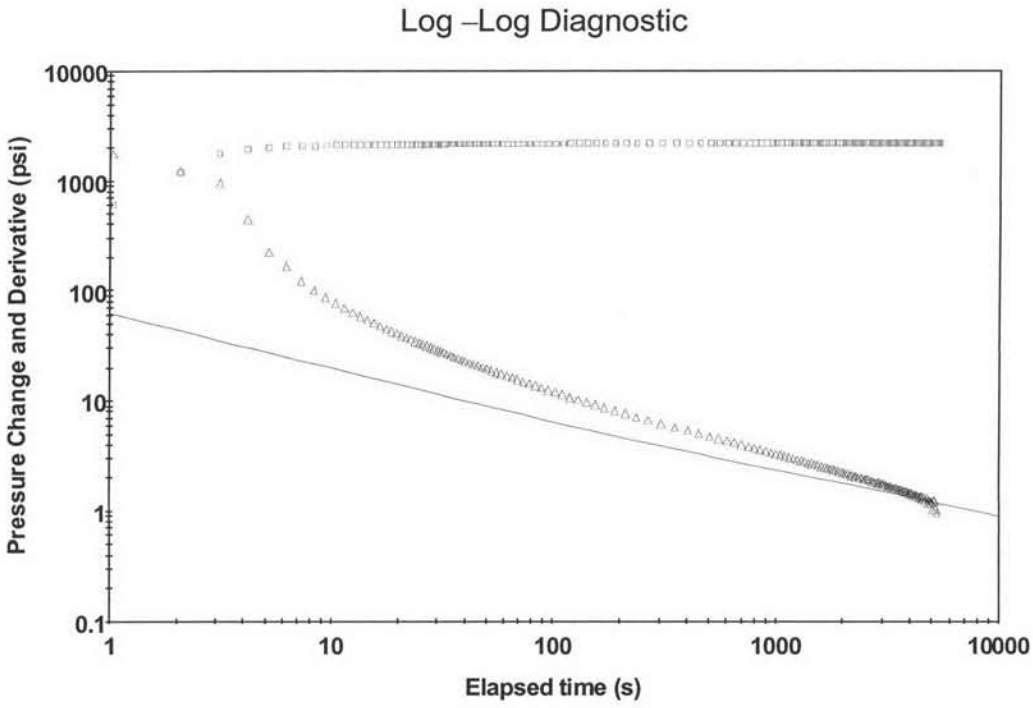


Figure 4.19: Diagnostic plot of a test conducted in a reservoir with horizontal permeability of 1 mD.

Table 4.6: Interpreted results of extended test duration of tests conducted in a reservoir with horizontal permeability of 1 mD.

| **Drawdown time** | **Buildup time** | **Cumu. time** | **Input $k_{xyz}$** | **Interpreted $k_{xyz}$** | **Error** | **Input $k_{xy}$** | **Interpreted $k_{xy}$** | **Error** | **$r_{inv}$** |
|---|---|---|---|---|---|---|---|---|---|
| mins | mins | mins | mD | mD | % | mD | mD | % | ft |
| 30 | 90 | 120 | 0.464 | 0.5222 | 12.50 | 1 | - | - | 29 |
| 60 | 180 | 240 | 0.464 | 0.5009 | 7.95 | 1 | - | - | 40 |
| 120 | 360 | 480 | 0.464 | 0.4679 | 0.84 | 1 | 0.9969 | -0.31 | 56 |
| 180 | 540 | 720 | 0.464 | 0.4610 | -0.65 | 1 | 0.9993 | -0.07 | 68 |

Figure 4.20 shows diagnostic plot of a test conducted in a reservoir with a horizontal permeability of 10mD. The tests were conducted with 30 minutes of drawdown and 90 minutes of buildup. In this case, the permeability is quite good. As seen in the figures, the spherical response can be observed as well as the radial response. The interpreted results are summarized in Table 4.7 with the permeabilities obtained from Interpret2005 are close to those used in the simulation. In addition, case t15 gives the radius of investigation of 124 feet so the pressure response went approximately half way to the boundary. The permeability obtained from this test is close to that used in the simulation. In order to get the permeability that can represent the entire reservoir, the test needs to be extended until the pressure response reaches the boundary.

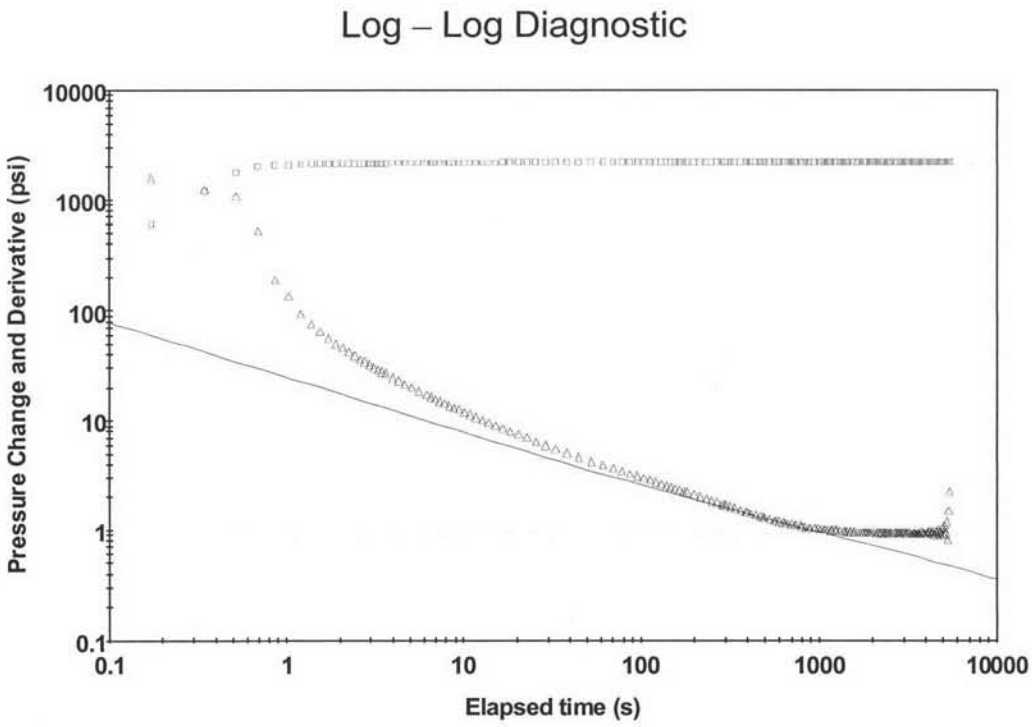


Figure 4.20: Diagnostic plot of test conducted in a reservoir with horizontal permeability of 10 mD.

Figure 4.21 show diagnostic plot of a test conducted in a reservoir with a horizontal permeability of 100 mD. The tests were conducted with 30 minutes of drawdown and 90 minutes of buildup. In this case, the permeability is better than the previous case. As seen in the figures, the spherical and response can be observed as well as the boundary effect. The interpreted results are summarized in Table 4.7 with the permeabilities obtained from a well test interpretation software are close to those used in the simulation. Furthermore, case t152 gives the radius of investigations of 364 feet which is larger than the actual distance to the boundary indicating that the pressure response has reached the boundary. This permeability can be used to represent the permeability of the whole reservoir. In this case, the reservoir permeability can be obtained by using wireline formation test that takes only a total of 120 minutes of test duration.

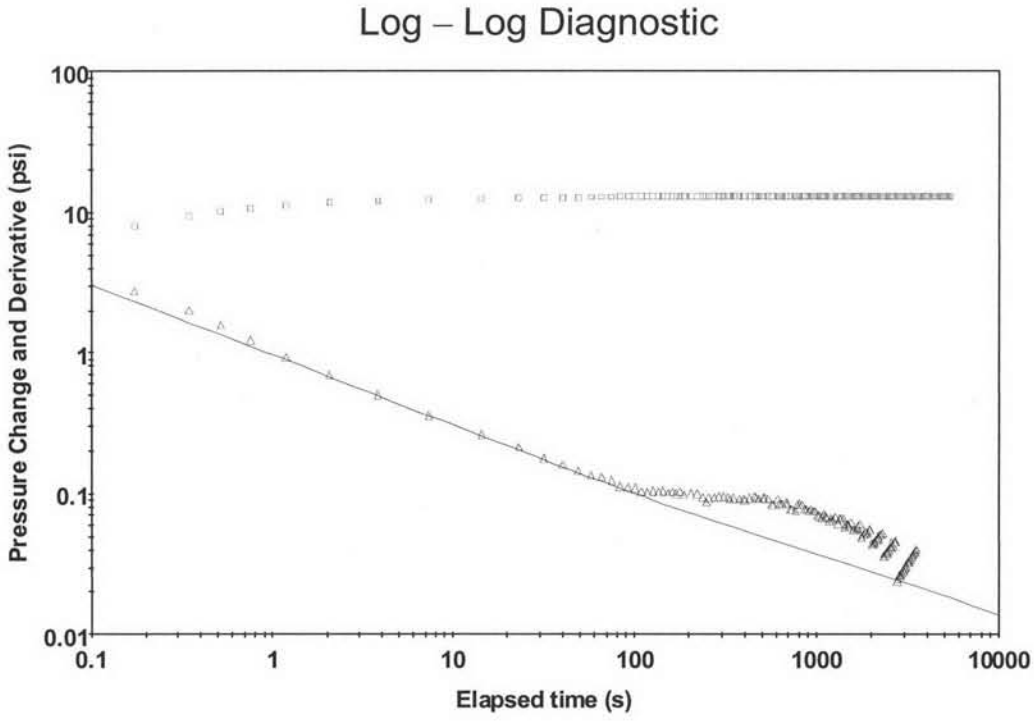


Figure 4.21: Diagnostic plot of test conducted in a reservoir with horizontal permeability of 100 mD.

Figure 4.22 shows the diagnostic plot of a test conducted in a reservoir with a horizontal permeability of 1000 mD. The test was conducted with 30 minutes of drawdown and 90 minutes of buildup. In this case, the reservoir permeability is so high that the pressure change is very small (less than 0.5 psi). It is hard to see any trend in the pressure behavior and identify any flow regime. As a result, the derivative is scattering. Thus, in a loose reservoir, the flowrate needs to be as high as the tool can handle in order to be able to detect the change in pressure.

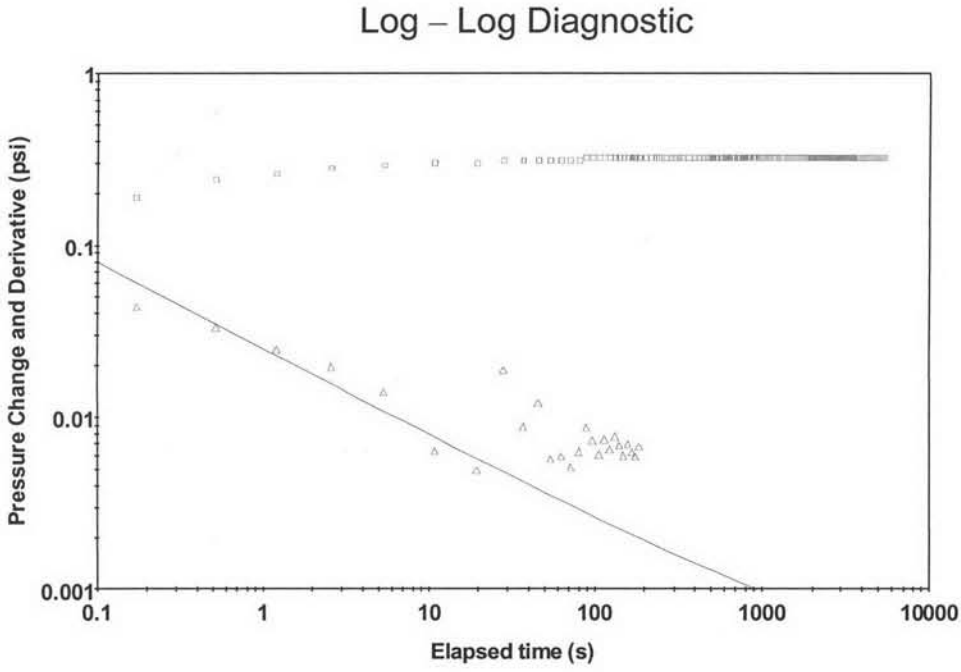


Figure 4.22: Diagnostic plot of test conducted in a reservoir with horizontal permeability of 1000 mD.

Table 4.7: Interpreted results of tests conducted in a reservoir with different permeabilities.

| Case | Input $k_{xy}$ | Input $k_z$ | Input $k_{xyz}$ | Interpreted $k_{xyz}$ | Error | Interpreted $k_{xy}$ | Error | $r_{inv}$ |
|---|---|---|---|---|---|---|---|---|
| | mD | mD | mD | mD | % | mD | % | ft |
| t151 | 1 | 0.1 | 0.464 | 0.5222 | 12.54 | - | - | 29 |
| t15 | 10 | 1 | 4.642 | 4.515 | -2.74 | 9.86 | -1.36 | 124 |
| t152 | 100 | 10 | 46.42 | 41.20 | -11.25 | 84.92 | -15.08 | 364 |
| t153 | 1000 | 100 | 464.2 | 441.9 | -4.80 | 966.40 | -3.36 | 1227 |

## 4.2 Simulation of Two-layer Reservoir

This section is to examine the applicability of WFT in mutilayer reservoirs. To keep the model as simple as possible, a two-layer reservoir was selected for the study. Simulations and interpretations were performed under different scenarios to see whether wireline formation testing with a single probe would be able to appraise reservoir parameters beyond the adjacent layer.

The grid sizes of reservoir model are the same as those in the base case and so are the reservoirs conditions and fluid properties. The flow rate of the test was set at 2.54 bbl/day (4.67 cc/sec) over a total flow period of 120 minutes consisting of a 30-minute drawdown and a 90-minute buildup.

The reservoir model was divided into two layers with equal thickness of 10 feet. Two different sets of horizontal permeabilities were used in the study. In the first set of study, one of the layers has a permeability of 10 mD while the other has the value of 100 mD. In the second set, the horizontal permeabilities of the layers are 10 and 1000 mD. The first one represents a low contrast permeability system while the second one represents a high contrast permeability system. The vertical to horizontal permeability ratio $(k_z/k_{xy})$ for each layer was kept constant at 0.1. The reservoir porosity was set to be 0.18. The probe position was set at 0.5, 1, 2, 5, and 8 feet away from the interface between the two-layer formation as schematically shown in Figure 4.23.

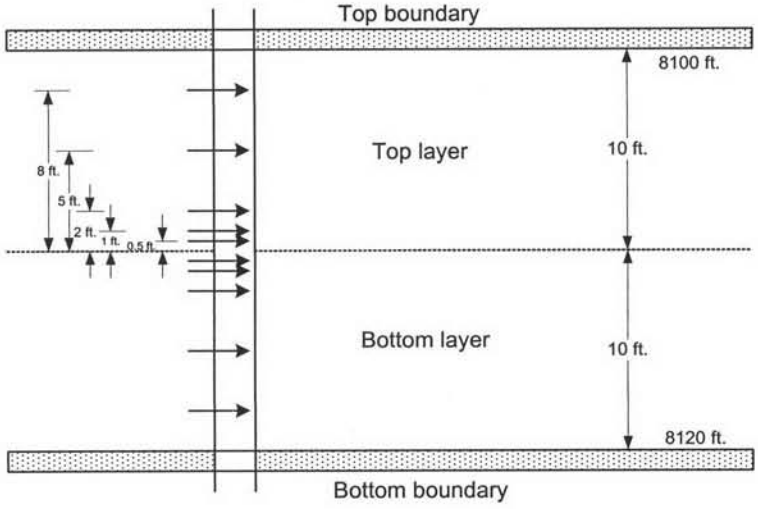


Figure 4.23: Schematic of a two-layer formation with different probe positions.

### 4.2.1 Case I: Horizontal permeability of 10 and 100 mD

In this case, the horizontal permeability of the top layer was set to be 10 mD, and the vertical permeability was set to be 1 mD. While, the horizontal permeability of the bottom layer was set equal to 100 mD and the vertical permeability was set equal to 10 mD. Thus, from Equation 3.6, the calculated spherical permeabilities of the top and bottom layer are 4.642 and 46.42 mD, respectively, as schematically shown in Figure 4.24. The probe was placed at 0.5, 1, 2, 5, and 8 feet away from the interface between the two-layer formation.

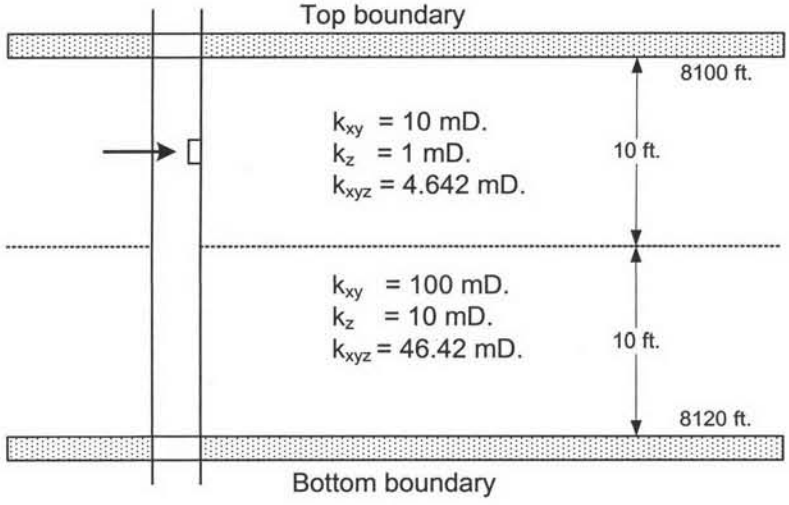


Figure 4.24: Schematic of a two-layer formation with horizontal permeabilities of 10 and 100 mD.

Figure 4.25 shows the diagnostic plot of a test conducted in a reservoir with the probe positioned at 8 feet above the middle of the formation which is 2 feet beneath the top of the reservoir. At middle times, a negative half slope which is an indicator of the hemispherical flow can be seen and results in interpreted permeability of 3.746 mD. At late times, the pressure derivative drops as if there were a constant pressure boundary. In fact, the higher permeability zone is contributing fluid into the lower permeability zone. Due to a layer permeability contrast between the two zones, the bottom zone acts as a large source of fluid. As a result, the pressure derivative follows the characteristic of a constant pressure boundary.

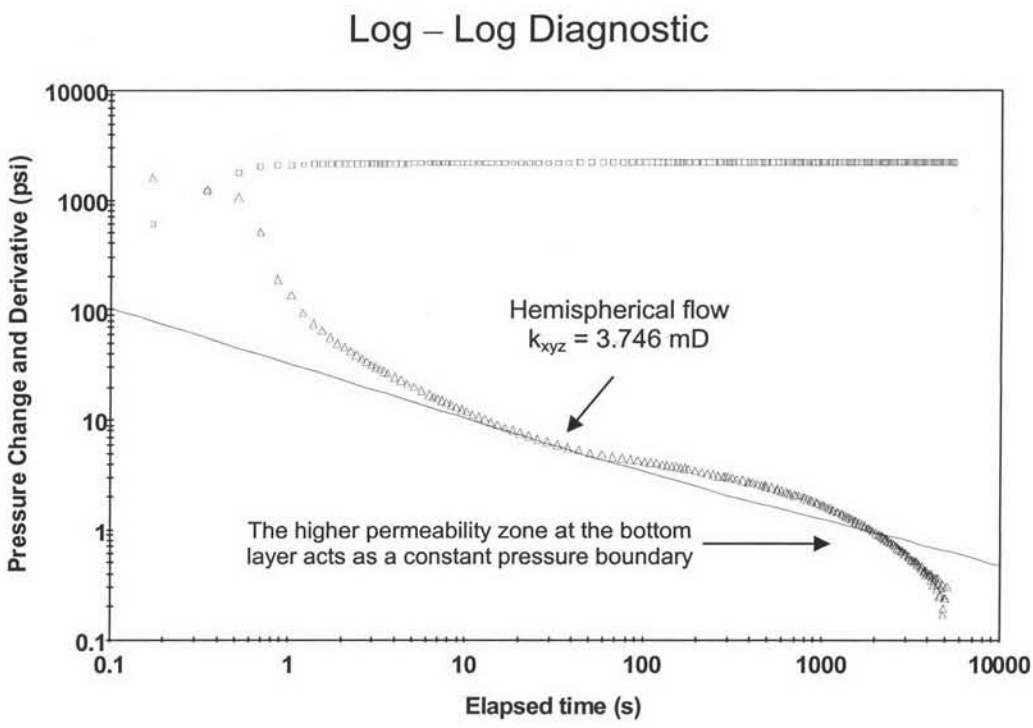


Figure 4.25: Diagnostic plot when the probe is 8 feet above the middle of the formation.

Figure 4.26 shows the diagnostic plot of a test conducted in a reservoir with the probe positioned at 5 feet above the middle of the formation which is at the middle of the top layer. The behavior of the pressure derivative is similar to that in the previous case. However, the spherical flow is longer since the probe is not as close to the top boundary. The permeability was estimated to be 4.204 mD. At late times, the pressure derivative descends due to a strong contribution of fluid from the higher permeability zone at the bottom layer.

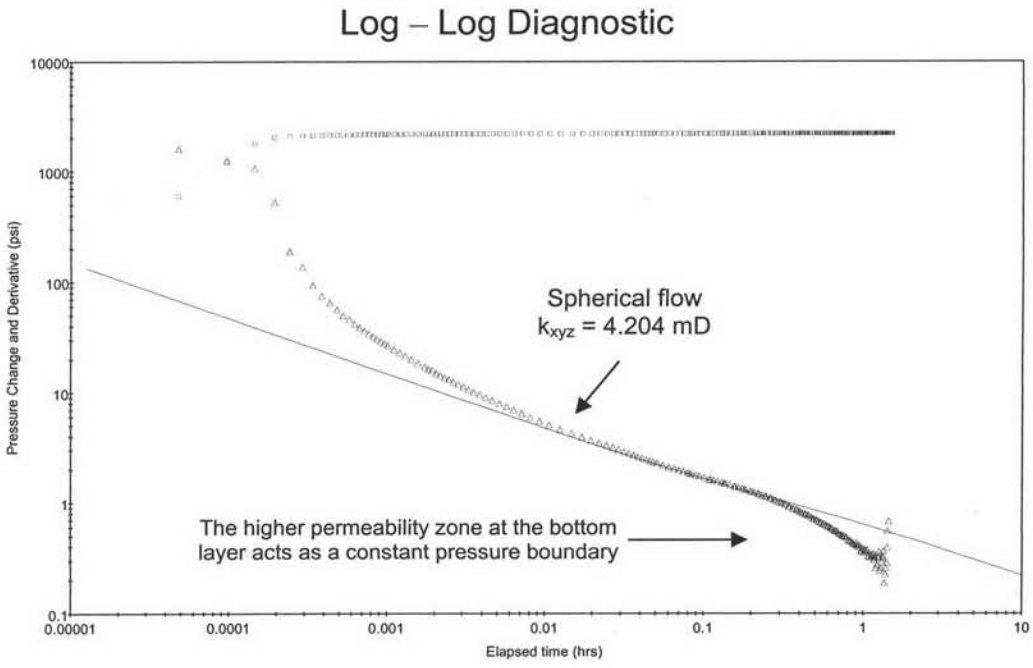


Figure 4.26: Diagnostic plot when the probe is 5 feet above the middle of the formation.

To examine the pressure response at late times, whether there was any possibility of the changing mobility or another flow regime contributing from the bottom layer, the test was extended longer to cover 60, 120, and 180 minutes of drawdown and 180, 360, 540 minutes of buildup. In these cases, the probe was still set at 5 feet from the top boundary. The derivative plots of these tests are shown in Figure 4.27. It can be seen that, at middle times, the spherical flow regime is present. The interpreted permeability is then the spherical permeability. At late times, even if the tests were conducted longer, pressure derivative still descends due to a strong contribution of fluid from the higher permeability zone at the bottom layer. Table 4.8 shows the interpreted results of spherical permeabilities obtained from the tests. The permeabilities obtained from longer tests are close to those obtained from a test conducted with 30 minutes of drawdown and 90 minutes of buildup. Thus, the original 30-minute drawdown and 90-minute buildup duration is enough.

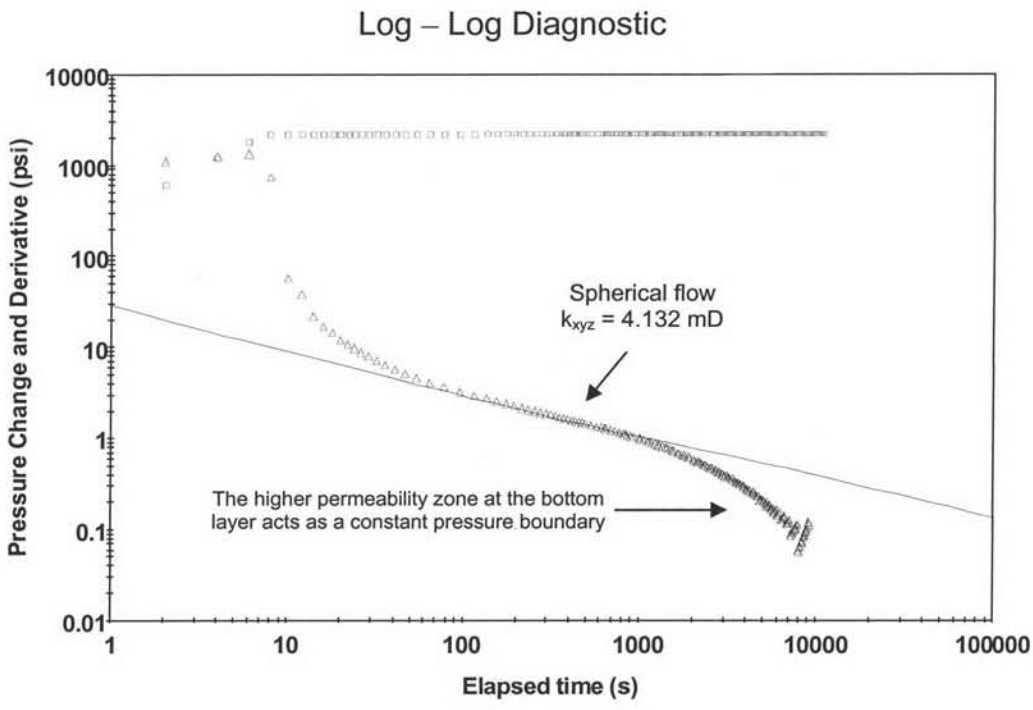


(a) Drawdown for 60 minutes and buildup for 180 minutes.

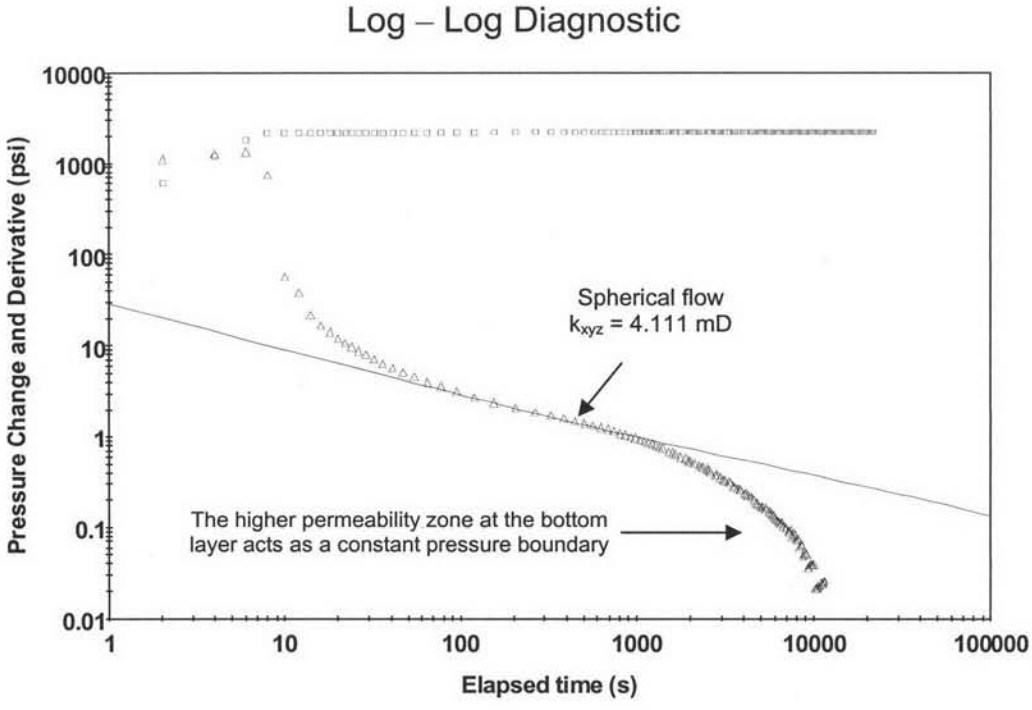


(b) Drawdown for 120 minutes and buildup for 360 minutes.

Figure 4.27: Diagnostic plot when the probe is 5 feet above the middle of the formation for extended test duration.

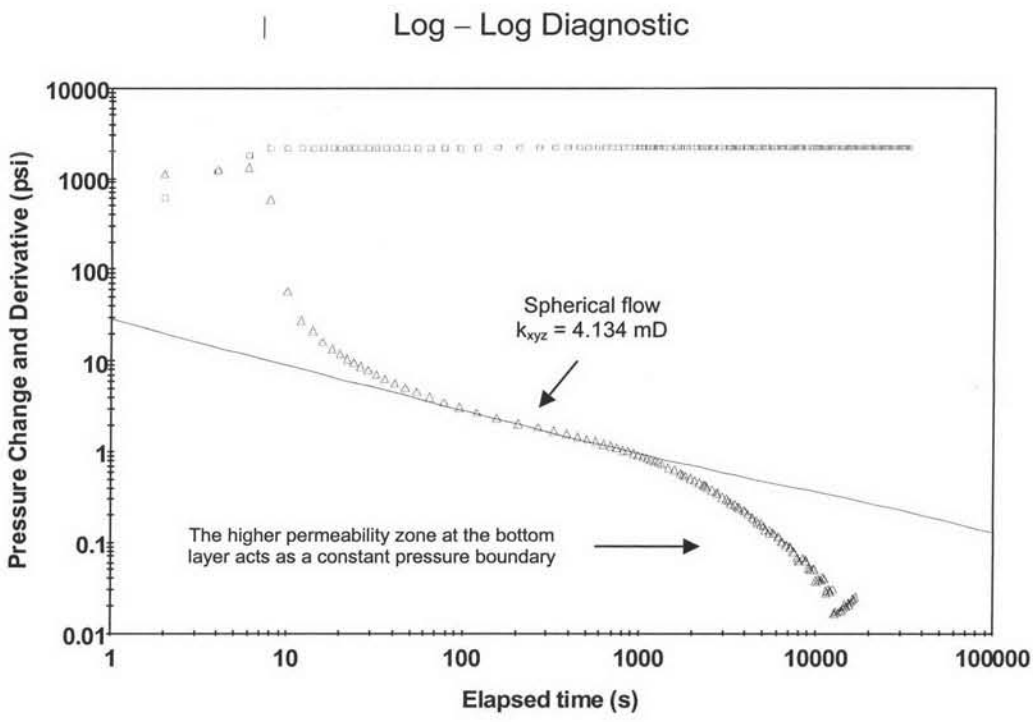


(c) Drawdown for 180 minutes and buildup for 540 minutes.

Figure 4.27: Diagnostic plots when the probe is 5 feet above the middle of the formation for extended test duration (continued).

Table 4.8: Interpreted results of extended time when the probe is at 5 feet above the middle of the formation

| **Drawdown time** | **Buildup time** | **Cumu. Time** | **Interpreted $k_{xyz}$** |
|---|---|---|---|
| mins | mins | mins | mD |
| 30 | 90 | 120 | 4.204 |
| 60 | 180 | 240 | 4.132 |
| 120 | 360 | 480 | 4.111 |
| 180 | 540 | 720 | 4.134 |

To continue study on the effect of probe position, the probe was moved further towards the interface between the two layers. Figure 4.28 shows the diagnostic plot of a test conducted in a reservoir with the probe positioned at 2 feet above the middle of the formation. A negative half slope straight line is fitted to the data in the spherical flow region, yielding a permeability estimate of 3.715 mD. This spherical flow occurs around the vicinity of the probe. Thus, the estimate of the permeability represents the permeability of the top layer. As the test was continued, a negative unit slope is present, indicating the change in mobility. After that, a negative half slope can be seen again, depicting the continuation of the spherical flow. The permeability estimated from this second spherical flow regime is 8.507 mD, which is influenced by the higher permeability zone at the bottom layer.

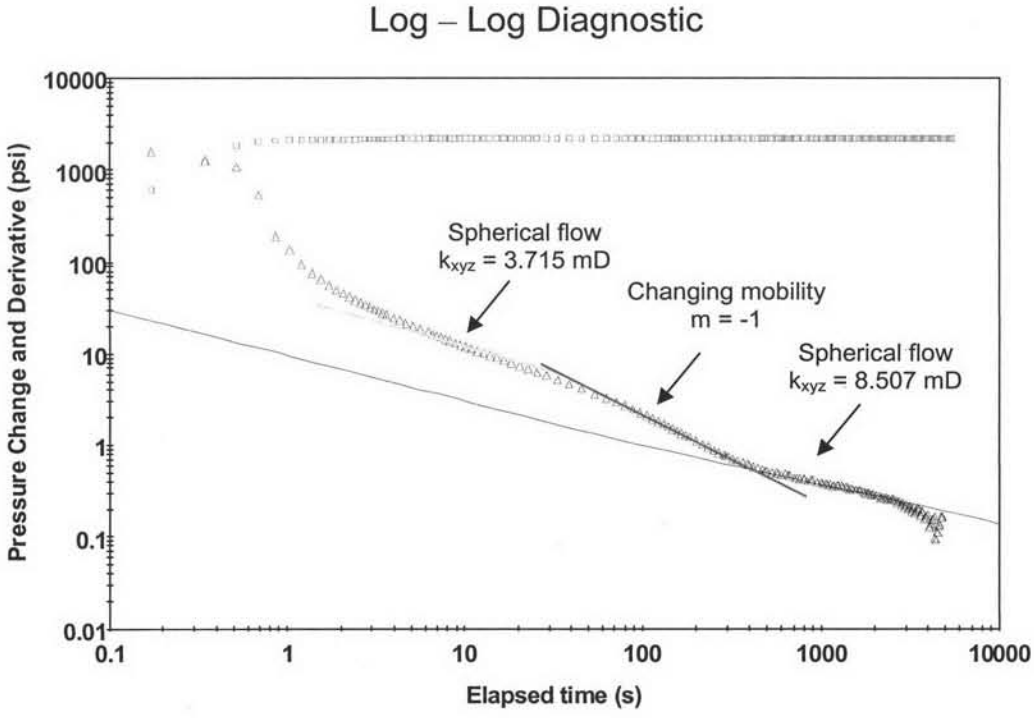


Figure 4.28: Diagnostic plots when the probe is 2 feet above the middle of the formation.

Figure 4.29 shows the diagnostic plot of a test conducted in a reservoir with the probe positioned at 1 foot above the middle of the formation. Similar to the previous case, two negative half slope straight lines were fitted to the derivative, the first one indicating spherical flow from the area very adjacent to the probe and the second one depicting spherical flow from a larger area which includes the bottom layer. Since the probe is very close to the interface between the two layers, the first spherical flow is very short. The permeability estimated from the first and second straight lines are 3.18 and 12.40 mD, respectively. The permeability estimated from the second spherical flow is more accurate than that estimated from the first one (see Figure 4.29). Between the spherical flows, a straight line with a unit slope was fitted to the data, signifying a change in mobility ratio. Although this straight line starts earlier than that in the previous case (Figure 4.28 a), both lines end approximately at the same time. Notice that the tail of the derivative no longer drops. This is due to the fact that the probe is very close to the permeable bottom layer, and the resulting permeability is close to that of the second layer. The probe does not see the second layer as a source of fluid to support the pressure in the first layer anymore. Thus, the constant pressure boundary behavior disappears.

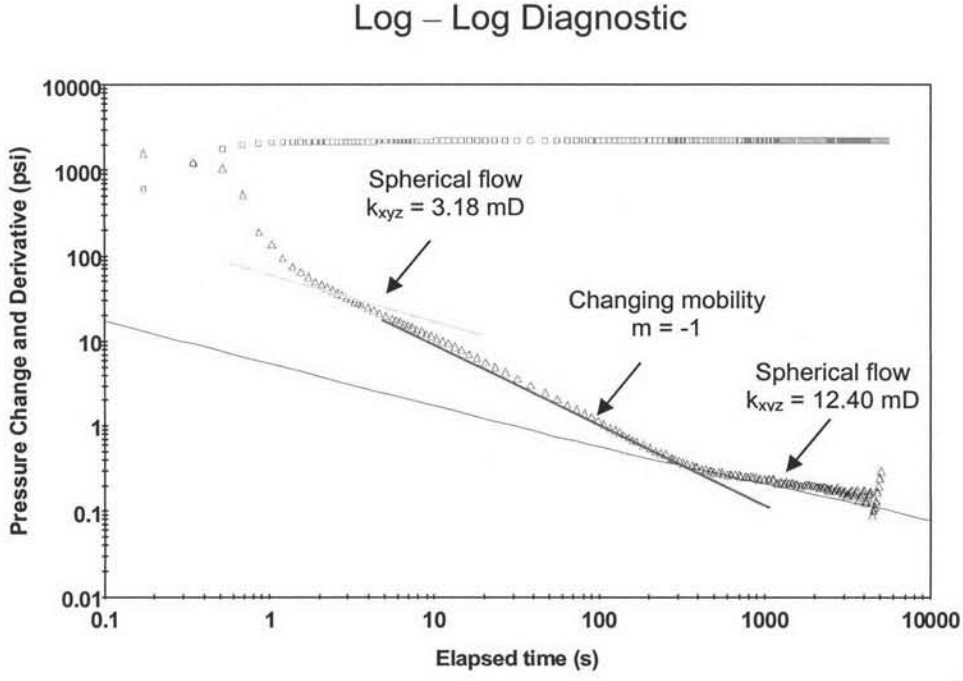


Figure 4.29: Diagnostic plot when the probe is 1 foot above the middle of the formation.

Figure 4.30 shows the diagnostic plot of a test conducted in a reservoir with the probe positioned at 0.5 feet above the middle of the formation. Since the probe is extremely close to the interface between the two layers, the first spherical flow cannot be seen. The first trend we see is the negative unit slope, indicating changing mobility from the top layer to the lower zone. After that, the negative half slope of spherical flow can be seen. The permeability estimated from this straight is 15.83 mD. This value is highly influenced by the permeability in the lower layer. Similar to the previous case, the derivative does not drop at the end of the test since the probe takes in majority of the fluid from the lower layer and thus does not see the lower layer as a pressure support anymore.

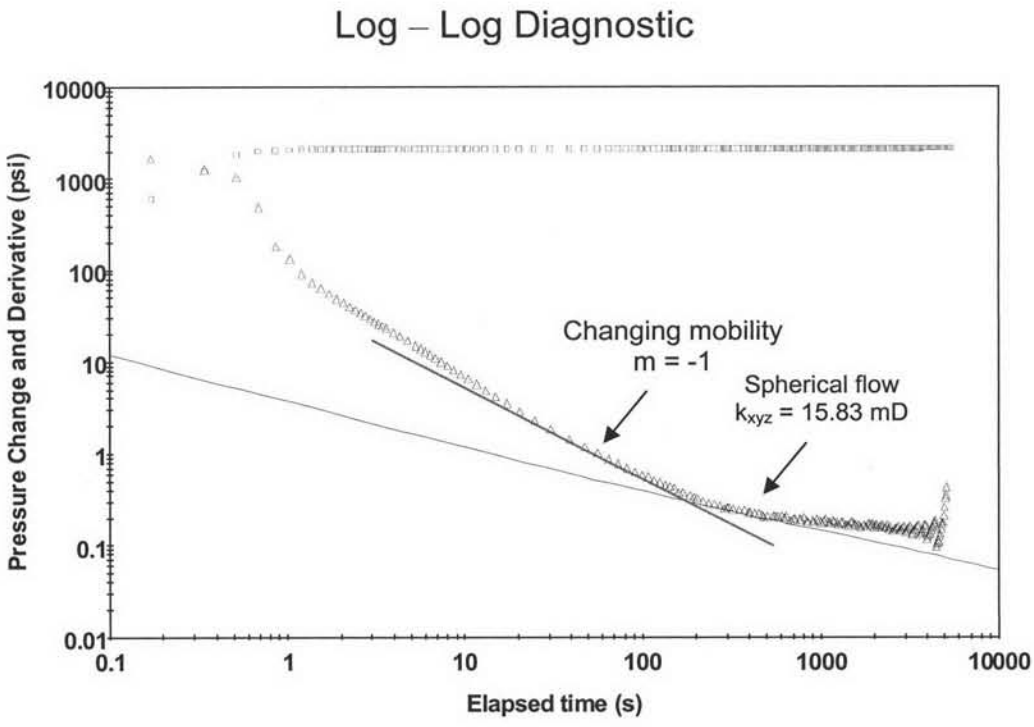


Figure 4.30: Diagnostic plot when the probe is 0.5 foot above the middle of the formation.

Figure 4.31 shows the diagnostic plot of a test conducted in a reservoir with the probe located at 0.5 foot below the middle of the formation. In this case, the probe is located in a more permeable layer. The derivative depicts a negative half slope behavior indicating spherical flow which corresponds mainly to the flow in the lower layer and partly to the flow in the top layer. The spherical permeability estimated from this straight line is 25.46 mD, which is highly influenced by the permeability in the bottom layer.

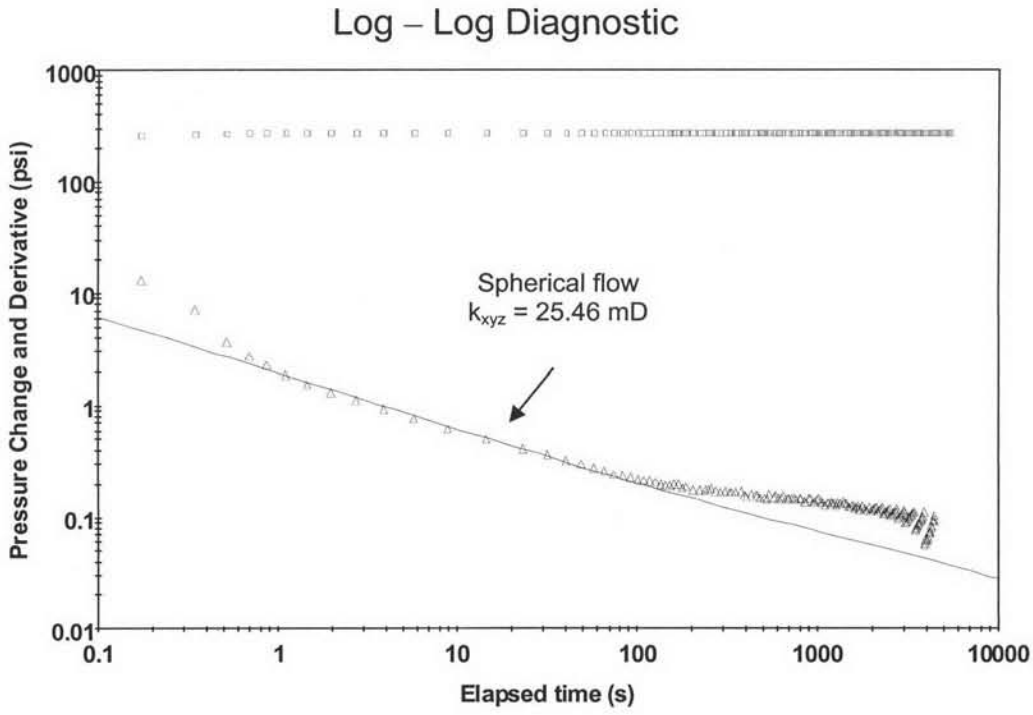


Figure 4.31: Diagnostic plot when the probe is 0.5 foot below the middle of the formation.

Figure 4.32 shows the diagnostic plot of a test conducted in a reservoir with the probe positioned at 1 foot below the middle of the formation. Similar to the previous case, the probe is located in a more permeable layer. At first, a negative half slope straight line is fitted to the data in the spherical flow region, yielding a permeability estimate of 32.96 mD, which is mostly influenced by the permeability in the bottom layer. As the test was continued, the second negative half slope can be seen again, depicting the continuation of the spherical flow. The permeability estimated from this second spherical flow regime is 25.56 mD, which has less value than the first one. At late times, the stabilization of the derivative which indicates the radial flow can be seen. This radial flow gives the estimated horizontal permeability of 54.72 mD.

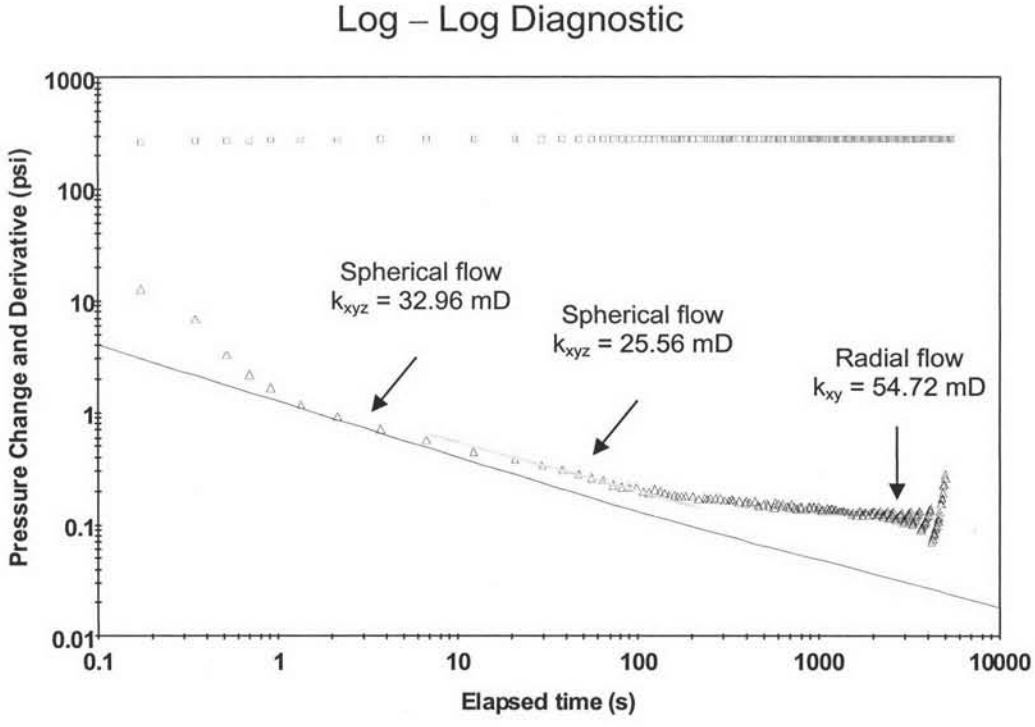


Figure 4.32: Diagnostic plot when the probe is 1 foot below the middle of the formation.

Figure 4.33 shows the diagnostic plot of a test conducted in a reservoir with the probe positioned at 2 feet below the middle of the formation. Again, the probe is located in a more permeable layer. The derivative depicts a negative half slope behavior indicating spherical flow which corresponds mostly to the flow in the bottom layer. The permeability estimated from this straight line is 38.70 mD, being mostly influenced by higher permeability at the bottom layer. At late times, radial flow can be seen. This radial flow gives the estimated horizontal permeability of 83.73 mD.

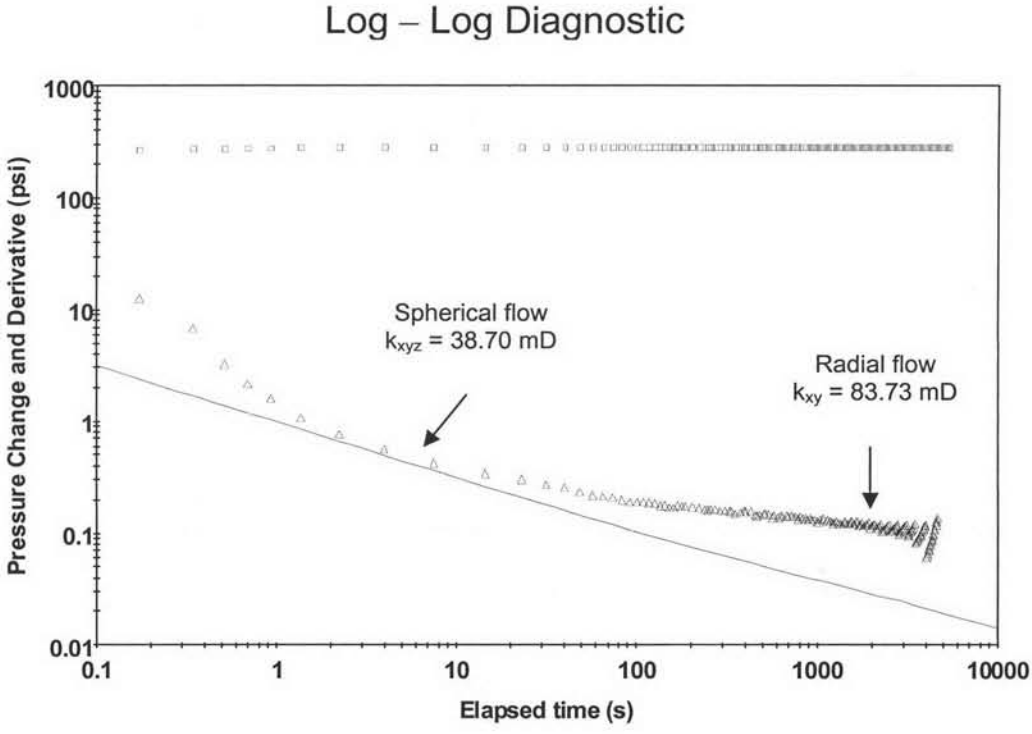


Figure 4.33: Diagnostic plot when the probe is 2 feet below the middle of the formation.

Figure 4.34 shows the diagnostic plot of a test conducted in a reservoir with the probe positioned at 5 feet below the middle of the formation, which is 5 feet from the bottom of the reservoir. Similar to the previous case, the probe is located in more permeable layer. The derivative depicts a negative half slope behavior indicating spherical flow which corresponds mostly to the flow in the bottom layer. The permeability estimated from this straight line is 39.63 mD, which is slightly higher than the value obtained when the probe is only 2 feet beneath the interface between the two layers. At late times, the radial flow can be seen. The horizontal permeability estimated from this radial flow is 85.81 mD.

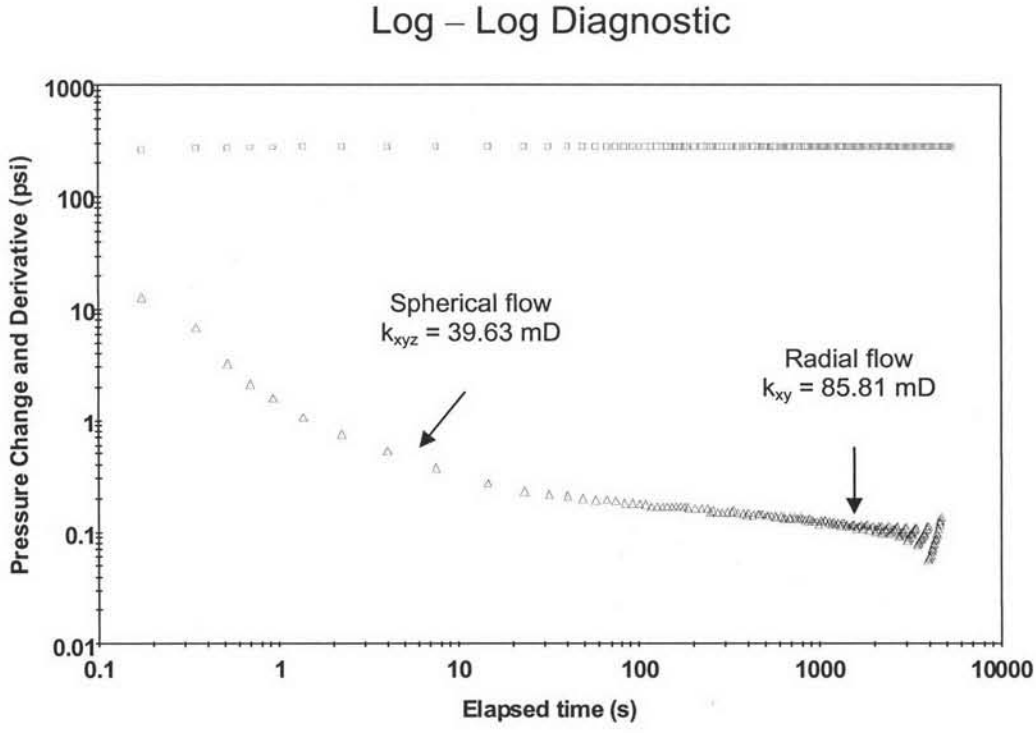


Figure 4.34: Diagnostic plot when the probe is 5 feet below the middle of the formation.

Figure 4.35 shows the diagnostic plot of a test conducted in a reservoir with the probe positioned at 8 feet beneath the middle of the formation which is 2 feet from the bottom of the reservoir. Again, the probe is located in a more permeable layer and close to the bottom boundary. Two negative half slope straight lines were fitted to the derivative, the first one indicating spherical flow from the area very adjacent to the probe and the second one depicting hemispherical flow when the pressure response hits the bottom boundary. Since the probe is very close to the bottom boundary, the first spherical flow is very short. The permeability estimated from the first and second straight lines are 38.52 and 26.24 mD, respectively. At late times, the radial flow can be seen. The estimate of horizontal permeability from this radial flow is 82.91 mD.

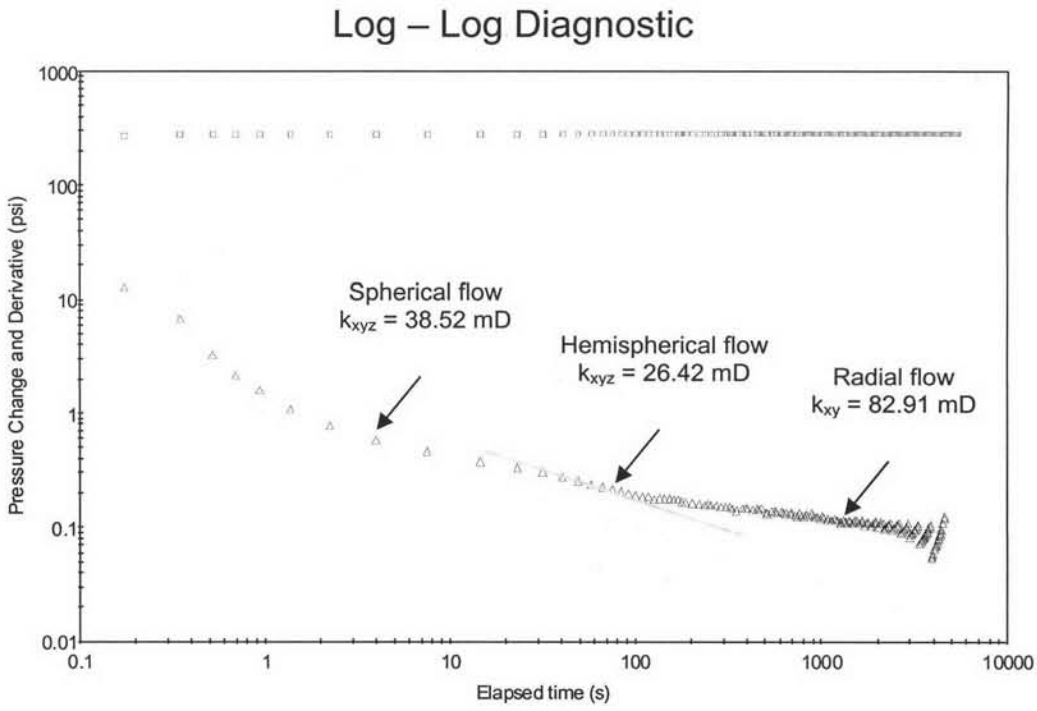


Figure 4.35: Diagnostic plot when the probe is 8 feet below the middle of the formation

In order to compare the permeabilities estimated from WFT with different permeability averaging techniques, the average spherical and horizontal permeability for each layer based on arithmetic, geometric and harmonic average was computed and is shown in Table 4.9. The estimated permeabilities and the differences between their values and average permeabilities base on the three averaging techniques are tabulated in Table 4.10. Figure 4.36 and 4.37 compare the value of spherical permeabilities estimated at different probe positions with the actual values and the three average values. Table 4.10 and Figure 4.36 show that the estimated spherical permeability when the probe is in low permeable zone at top layer and further away above the interface between the two layers, the estimated spherical permeability is represent the low permeability of that layer. Comparing to the value from a test conducted in a single layer and at the same depth ( 8 and 5 feet above the middle of the formation), the values from this case ( 3.746 and 4.204 mD ) is close to those values from a single layer reservoir ( 3.673 and 4.415 mD). If the prove is moved downward to the interface between the two layers, at 2 feet above the middle of the formation, the estimated permeability is close to the harmonic mean of two-layer system with an error of 0.79 %. When the probe is closer to the interface between the two layers, at 1 and 0.5 foot above the middle of the formation, the estimated spherical permeabilities are close to the geometric mean of the two-layer system. As the study was continued, the probe is located in high permeable zone at the bottom layer and close to the interface between the two layers, the spherical permeability obtained from the test is close to the arithmetic mean of the two-layer system with an error of -0.27 %. If the probe was set further away below the interface between the two layers, the spherical permeability obtained from the test is close to the high permeability value of that bottom layer. In addition, these estimated permeabilities from these tests are close to the value obtained from a test conducted in a single layer reservoir (41.42 mD)

Although the spherical permeability can be estimated in all the cases, the horizontal permeability can be estimated only in cases when the probe was set in the high permeable zone at the bottom layer. This is due to the fact that the pressure response can travel for a longer distance in a more permeable zone. When radial flow is present, the horizontal permeability can be estimated. The estimated permeabilities are different depending on the position of the probe. The results in Table 4.10 indicate

that the estimated horizontal permeability of the probe at 1 foot below the middle of the formation is close to the arithmetic mean of two-layer system with an error of -0.51 %. In addition, the chart from Figure 4.37 illustrates that if the probe is set close to the interface between the two layers and in the high permeability zone, the horizontal permeability obtained from the test is the arithmetic mean of the two-layer system. If the probe is set further away from the interface between the two layers and in the high permeability layer, the horizontal permeability obtained from the test is close to the high permeability of that bottom layer. Note that, when the probe is quite far from the interface between the two layers, the estimated horizontal permeability is influenced mostly by the high permeability of the bottom layer, its value is as accurate as the value estimated from a test in a single layer reservoir (84.92 mD).

Table 4.9: Spherical and horizontal permeabilities using different averaging techniques for case I.

| | **Top layer Permeability** | **Bottom layer Permeability** | **Averaging Technique** | | |
|---|---|---|---|---|---|
| | | | **Arithmetic mean** | **Geometric mean** | **Harmonic mean** |
| | mD | mD | mD | mD | mD |
| Spherical | 4.642 | 46.42 | 25.53 | 14.68 | 8.44 |
| Horizontal | 10 | 100 | 55 | 31.62 | 18.18 |

Table 4.10: Interpreted results of tests conducted in a reservoir with different probe positions for case I.

| Probe position from the middle of the formatiom | | Difference when compared to | | | | Differnce when compared to | | |
|---|---|---|---|---|---|---|---|---|
| | Interpreted $k_{xyz}$ | Arithmetic mean | Geometric mean | Harmonic mean | Interpreted $k_{xy}$ | Arithmetic mean | Geometric mean | Harmonic mean |
| ft | mD | % | % | % | mD | % | % | % |
| 8 (above) | 3.746 | -85.33 | -74.48 | -55.62 | - | - | - | - |
| 5 (above) | 4.204 | -83.53 | -71.36 | -50.19 | - | - | - | - |
| 2 (above) | 8.507 | -66.68 | -42.05 | 0.79 | - | - | - | - |
| 1 (above) | 12.40 | -51.43 | -15.53 | 46.92 | - | - | - | - |
| 0.5 (above) | 15.83 | -37.99 | 7.83 | 87.56 | - | - | - | - |
| 0.5 (below) | 25.46 | -0.27 | 73.43 | 201.66 | - | - | - | - |
| 1 (below) | 32.96 | 29.10 | 124.52 | 290.52 | 54.72 | -0.51 | 73.06 | 200.99 |
| 2 (below) | 38.70 | 51.59 | 163.62 | 358.53 | 83.73 | 52.24 | 164.80 | 360.56 |
| 5 (below) | 39.63 | 55.23 | 169.96 | 369.55 | 85.81 | 56.02 | 171.38 | 372.00 |
| 8 (below) | 38.52 | 50.88 | 162.40 | 356.40 | 82.91 | 50.75 | 162.21 | 356.05 |

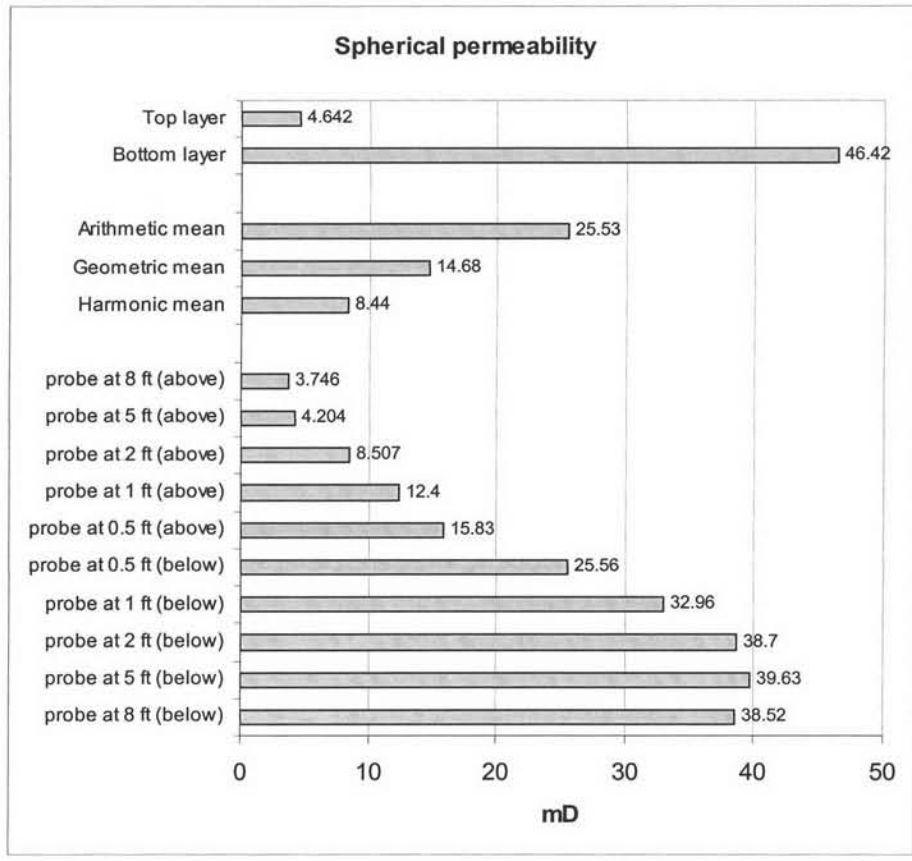


Figure 4.36: Chart comparing spherical permeability for case I.

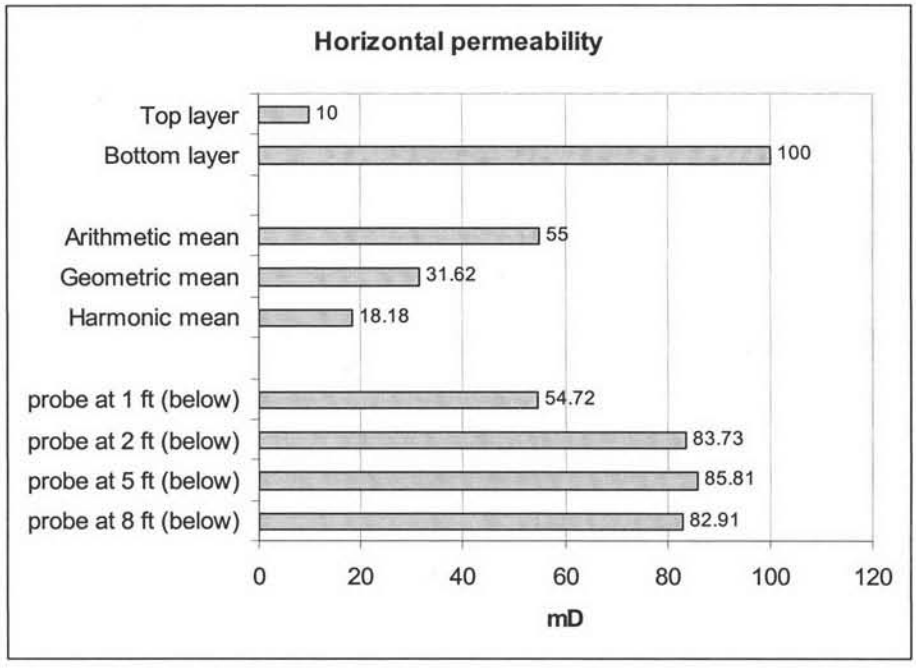


Figure 4.37: Chart comparing horizontal permeability for case I.

### 4.2.2 Case II: Horizontal permeability of 100 and 10 mD

Additionally, to examine the effect of order of layer permeability, the layer permeabilities from case I were adversely set. The horizontal permeability of the top layer was set to be 100 mD, and the vertical permeability was set to be 10 mD. While the horizontal permeability of the bottom layer was set equal to 10 mD and the vertical permeability was set equal to 1 mD. Thus, from Equation 3.6, the calculated spherical permeabilities of the top and bottom layer are 46.42 and 4.642 mD, respectively, as schematically shown in Figure 4.38. The probe was placed at 0.5, 1, 2, 5, and 8 feet away from the middle of the formation.

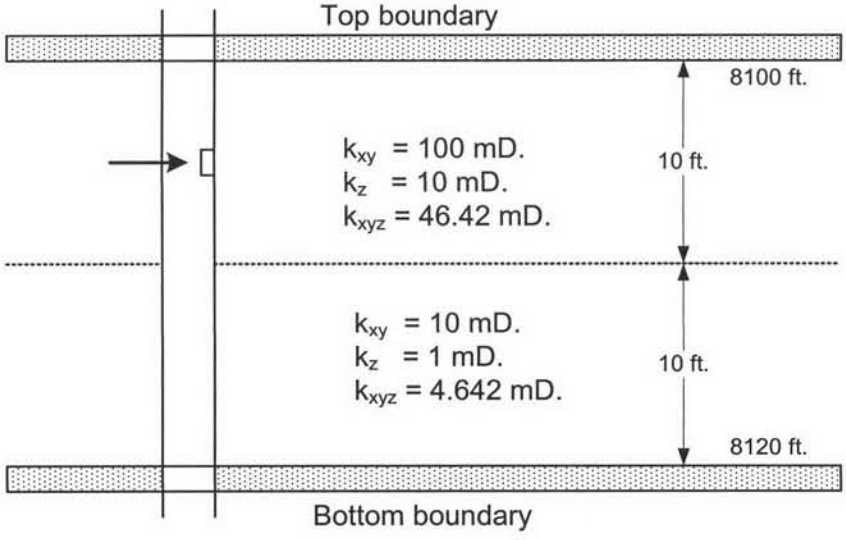


Figure 4.38: Schematic of two layer with horizontal permeabilities of 100 and 10 mD.

Figure 4.39 shows the diagnostic plot of a test conducted in a reservoir with probe position at 8 feet above the middle of the formation which is 2 feet beneath the top of the reservoir. In this case, the probe is set in a more permeable layer and close to the top boundary. Two negative half slope straight lines were fitted to the derivative, the first one indicating spherical flow from the area very adjacent to the probe and the second one depicting hemispherical flow when the pressure response hits the top boundary. Since the probe is very close to the top boundary, the first spherical flow is very short. The permeability estimated from the first and second straight lines are 38.32 and 26.91 mD, respectively. At late times, the horizontal straight line in the derivative which indicates radial flow can be seen. The estimated horizontal permeability from the radial flow is of 83.86 mD.

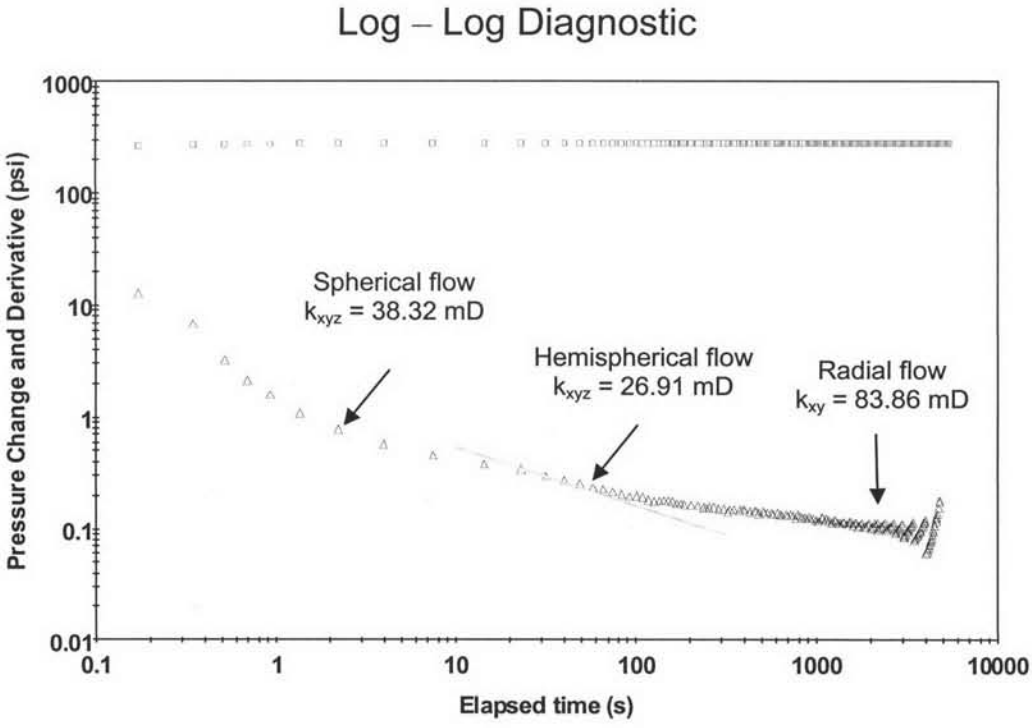


Figure 4.39: Diagnostic plot when the probe is at 8 feet above the middle of the formation.

Figure 4.40 shows diagnostic plot of a test conducted in a reservoir with probe position at 5 feet above the middle of the formation which is at the middle of the top layer. Similar to the previous case, the probe is located in a more permeable layer. The derivative depicts a negative half slope behavior indicating spherical flow which corresponds mostly to the flow in the top layer. The permeability estimates from this spherical flow is 40.33 mD, which is slightly higher than the value obtained when the probe is 2 feet from the top boundary. At late times, the radial flow can be seen. This radial flow gives the estimated horizontal permeability of 84.35 mD.

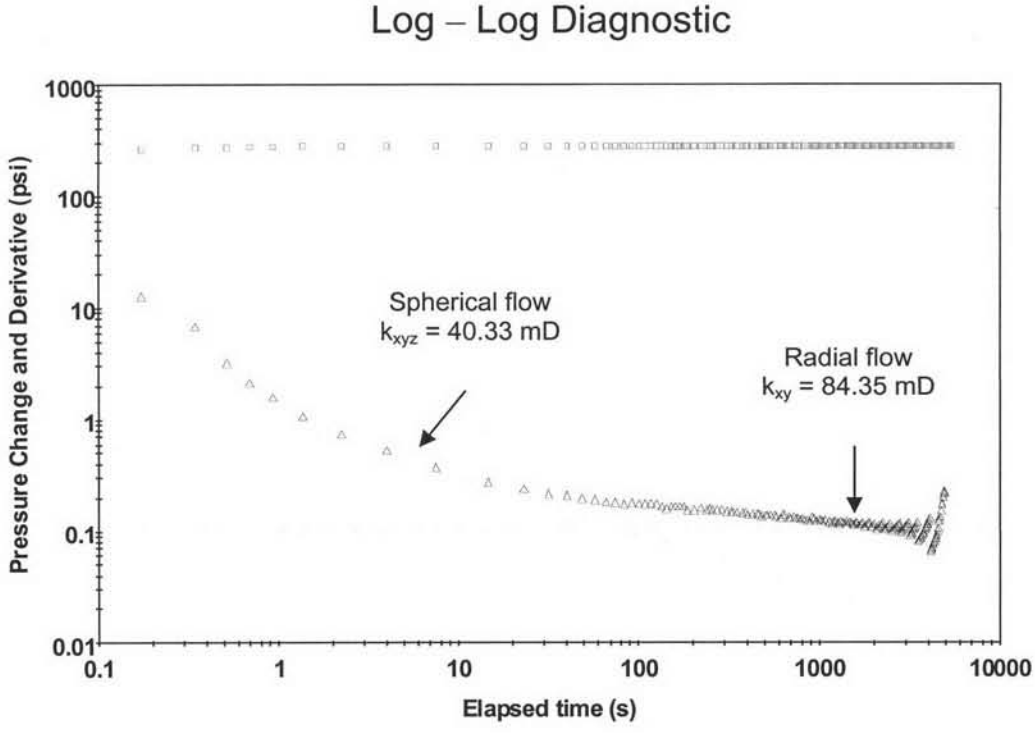


Figure 4.40: Diagnostic plot when the probe is at 5 feet above the middle of the formation.

Figure 4.41 shows the derivative plot of a test conducted in a reservoir with probe position at 2 feet above the middle of the formation. Again, the probe is located in a more permeable layer. The derivative depicts a negative half slope behavior indicating spherical flow which corresponds mostly to the flow in the top layer. The permeability estimates from this straight line is 38.78 mD, being mostly influenced by the higher permeability at the top layer. At late time, it can be seen the radial flow. This radial flow yields the estimate of horizontal permeability of 83.93 mD.

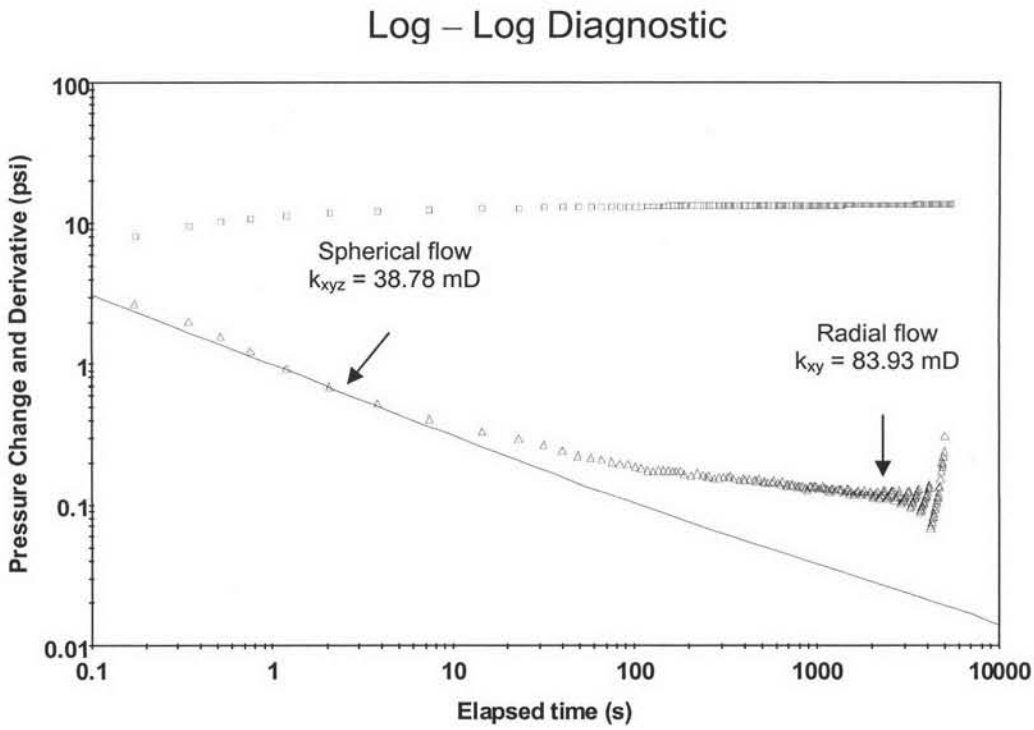


Figure 4.41: Diagnostic plot when the probe is at 2 feet above the middle of the formation.

Figure 4.40 shows the derivative plot of a test conducted in a reservoir with probe position at 1 foot above the middle of the formation. The probe is still located in a more permeable layer but closer to the lower permeable zone of the bottom layer. At first, a negative half slope straight line is fitted to the data in the spherical flow region, yielding a permeability estimate of 35.88 mD, which is highly influenced by the permeability in the top layer. As the test was continued, the second negative half slope can be seen again, depicting the continuation of the spherical flow. The permeability estimated from this second spherical flow regime is 25.89 mD, which has less value than the first one. At late times, it can be seen the radial flow. The horizontal permeability estimated from the radial flow is 78.93 mD.

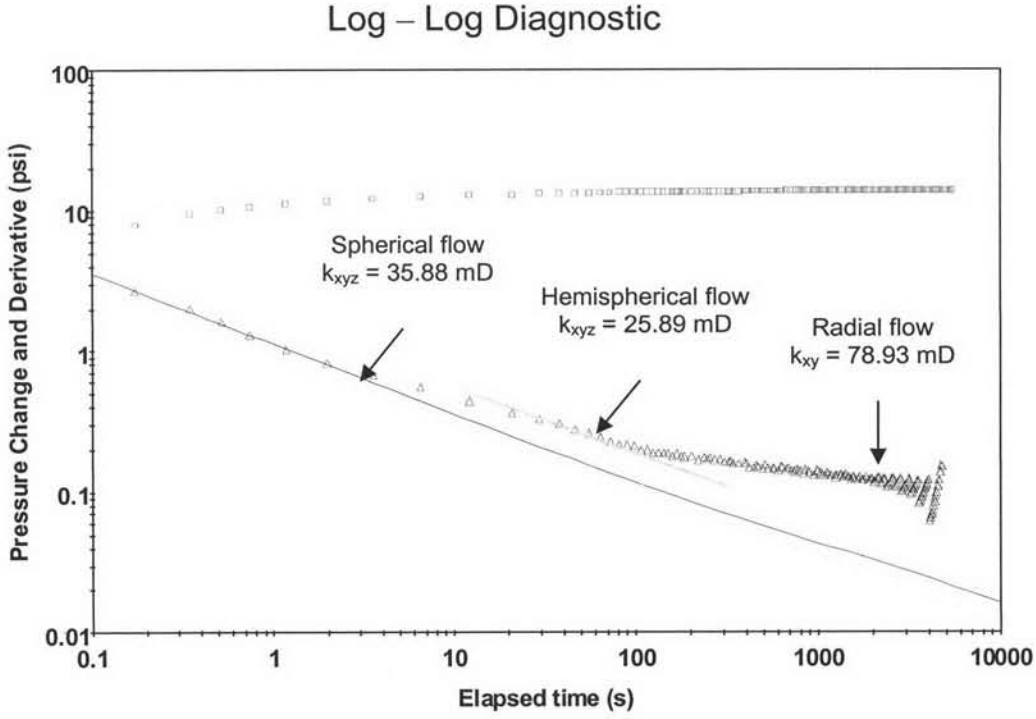


Figure 4.42: Diagnostic plot when the probe is at 1 foot above the middle of the formation.

Figure 4.43 shows the diagnostic plot of a test conducted in a reservoir with the probe positioned at 0.5 foot above the middle of the formation. According to the probe is in a more permeable layer and extremely close to the interface between the two layers, the derivative depicts a negative half slope indicating spherical flow which corresponds mainly to the flow in the top layer and partly to the flow in the lower layer. The spherical permeability estimated from this straight line is 24.24 mD, which is highly influenced by the permeability in the top layer. At late times, similar to the previous case, it still can be seen the radial flow. This flow regime gives the estimated horizontal permeability of 52.14 mD.

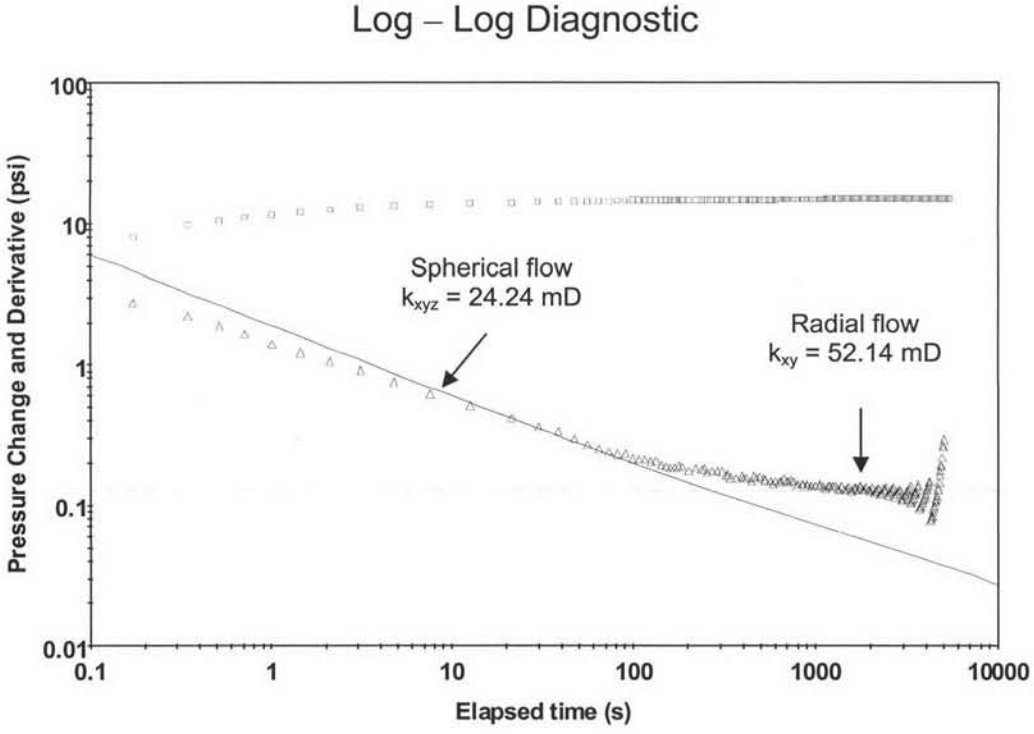


Figure 4.43: Diagnostic plot when the probe is at 0.5 foot above the middle of the formation.

Figure 4.44 shows the diagnostic plot of a test conducted in a reservoir with the probe positioned at 0.5 foot below the middle of the formation. The probe is now in low permeable layer. Since the probe is very close to the interface between the two layers, at first, a negative unit slope can be seen, indicating changing mobility from the top layer to the lower zone. After that, the negative half slope of spherical flow can be seen. The permeability estimated from this straight is 15.84 mD. This value is highly influenced by the permeability in the bottom layer since the probe takes in majority of the fluid from the bottom layer.

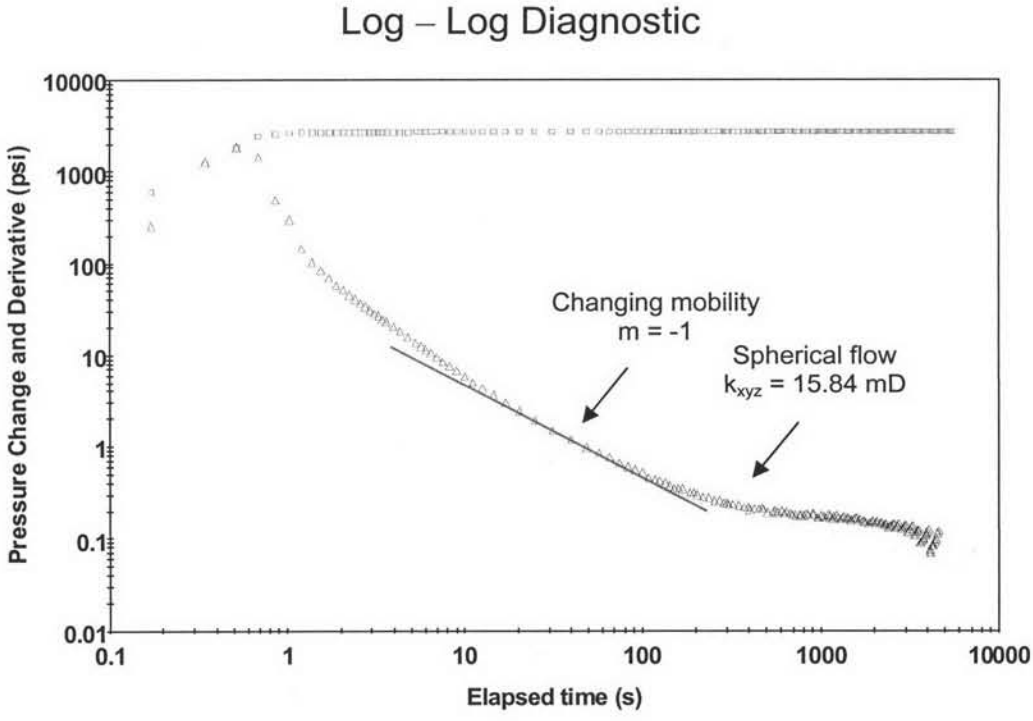


Figure 4.44: Diagnostic plot when the probe is at 0.5 foot below the middle of the formation.

Figure 4.45 shows the diagnostic plot of a test conducted in a reservoir with the probe positioned at 1 foot above the middle of the formation. A negative half slope straight line is fitted to the data in the spherical flow region. Since the probe is very close to the interface between the two layers, the first spherical flow is very short. The spherical permeability estimated from the straight line is 3.41 mD. This spherical flow occurs around the vicinity of the probe. Thus, the estimate of the permeability represents the permeability of the bottom layer. As the test was continued, a negative unit slope is present, indicating the change in mobility. After that, a negative half slope can be seen again, depicting the continuation of the spherical flow. The permeability estimated from this second spherical flow regime is 12.22 mD, which is influenced by the higher permeability zone at the top layer.

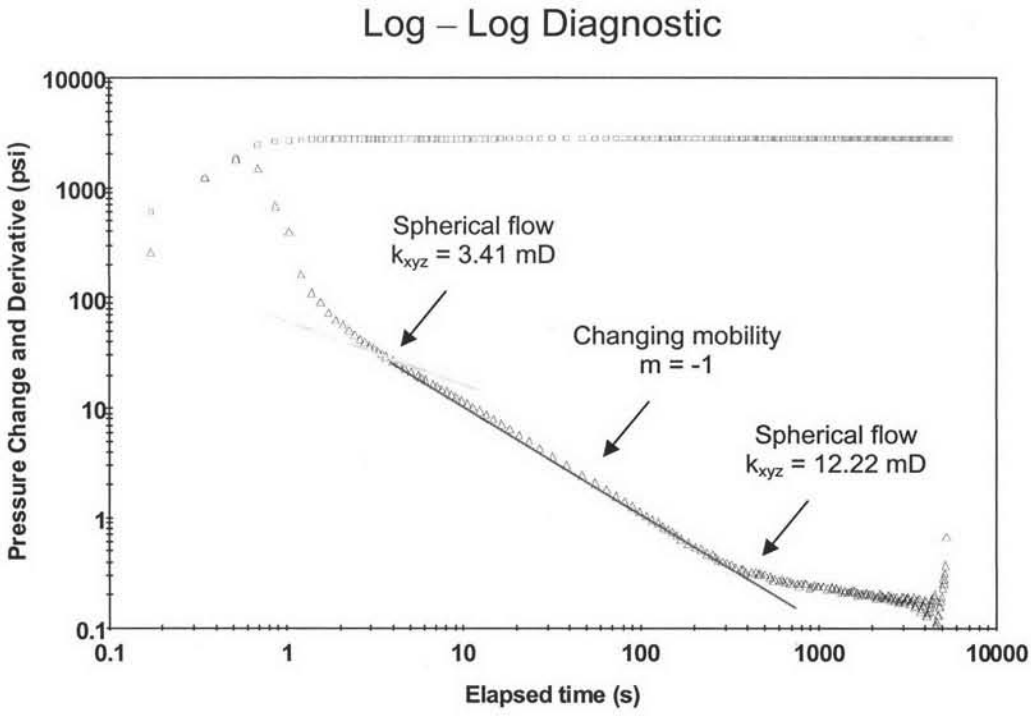


Figure 4.45: Diagnostic plot when the probe is 1 foot below the middle of the formation.

Figure 4.46 shows the diagnostic plot of a test conducted in a reservoir with the probe positioned at 2 feet below the middle of formation. Similar to the previous case, two negative half slope straight lines were fitted to the derivative, the first one indicating spherical flow from the area very adjacent to the probe and the second one depicting spherical flow from a larger area which includes the bottom layer. Since the probe is very close to the interface between the two layers, the first spherical flow is very short. The permeability estimated from the first and second straight lines are 3.415 and 8.634 mD, respectively. The permeability estimated from the second spherical flow is more accurate than that estimated from the first one. Between the spherical flows, a straight line with a unit slope was fitted to the data, signifying a change in mobility ratio. Although this straight line starts earlier than that in the previous case (Figure 4.45), both lines end approximately at the same time.

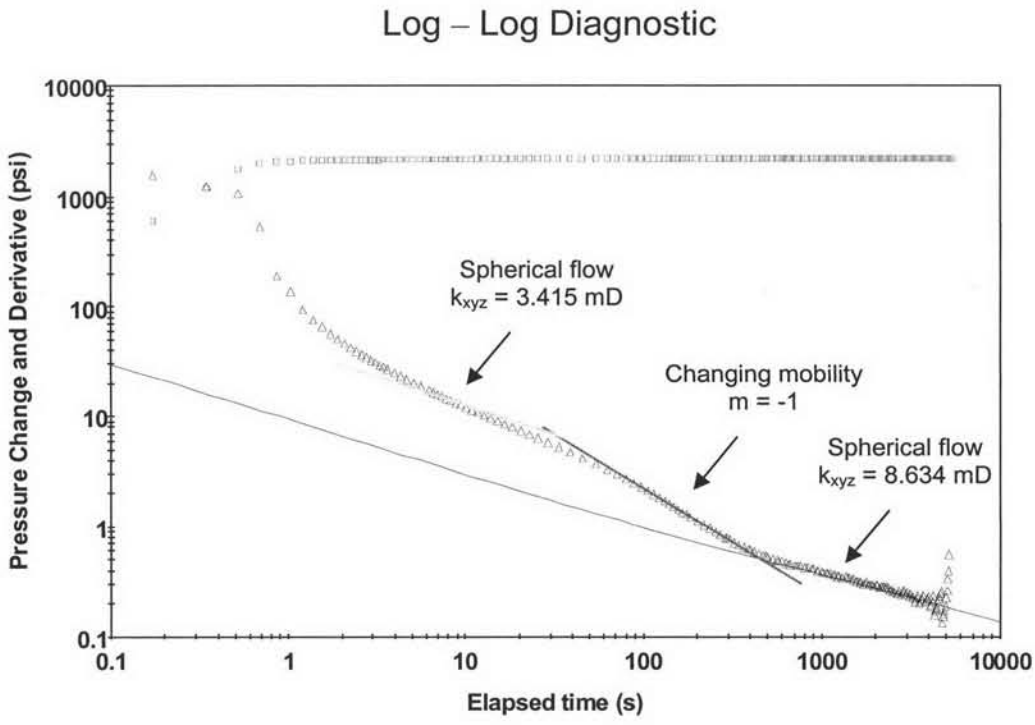


Figure 4.46: Diagnostic plot when the probe is 2 feet below the middle of the formation.

Figure 4.47 shows the diagnostic plot of a test conducted in a reservoir with the probe positioned at 5 feet below the middle of the formation which is at the middle of the bottom layer. At middle times, the negative half slope which is an indicator of the spherical flow can be seen and results in interpreted permeability of 4.222 mD. At late times, the pressure derivative drops as if there were a constant pressure boundary. In fact, the higher permeability zone is contributing fluid into the lower permeability zone. Due to a layer permeability contrast between the two zones, the top zone acts as a large source of fluid. As a result, the pressure derivative follows the characteristic of a constant pressure boundary.

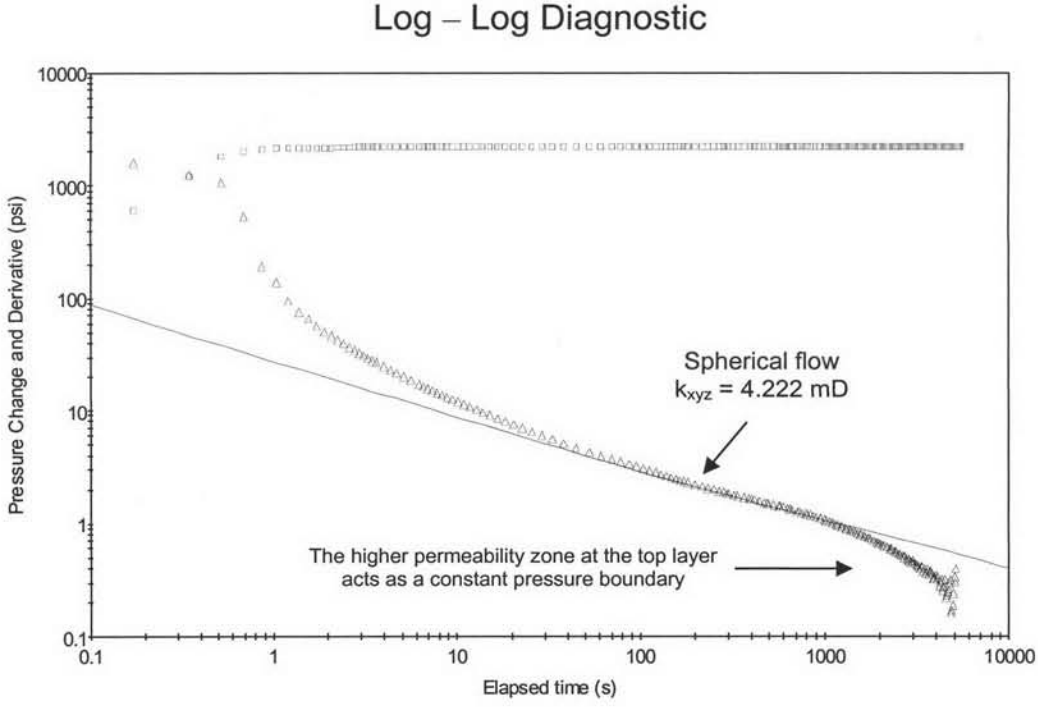


Figure 4.47: Diagnostic plot when the probe is at 5 feet below the middle of the formation.

Figure 4.26 shows the diagnostic plot of a test conducted in a reservoir with the probe positioned at 8 feet below the middle of the reservoir which is 2 feet from the bottom of the reservoir. The behavior of the pressure derivative is similar to that in the previous case. At middle times, the negative half slope indicating the hemispherical flow can be seen and results in interpreted permeability of 3.906 mD. At late times, the pressure derivative descends due to a strong contribution from the higher permeability zone at the top layer.

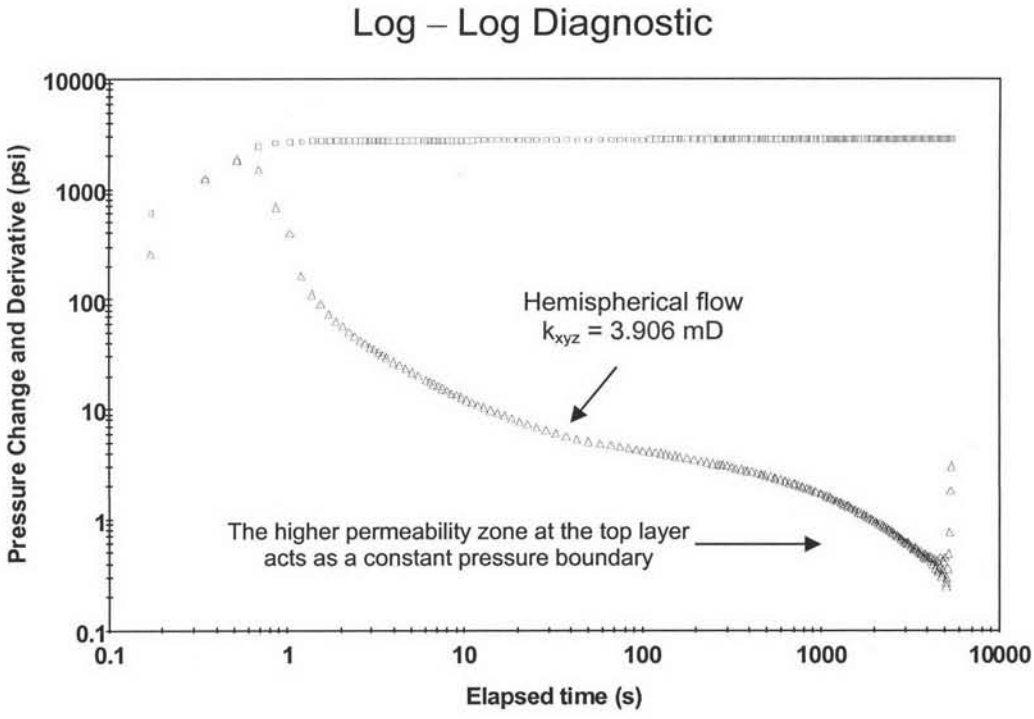


Figure 4.48: Diagnostic plot when the probe is at 8 feet below the middle of the formation.

Similar to case I, in order to compare the permeabilities estimated from WFT with different permeability averaging techniques, the average spherical and horizontal permeability for each layer based on arithmetic, geometric and harmonic average was computed and is shown in Table 4.10. The estimated permeabilities and the differences between their values and average permeabilities base on the three averaging techniques are tabulated in Table 4.12. Figure 4.49 and 4.50 compare the value of spherical permeabilities estimated at different probe positions with the actual values and the three average values. Table 4.11 and Figure 4.49 show that, when the probe is located in high permeable zone at the top layer and the probe was set further away above the interface between the two layers, the spherical permeability obtained from the test is close to the high permeability value of the top layer. The estimated permeabilities obtained from these are close to the estimated value from a test conducted in a single layer reservoir (41.42 mD) As the probe was moved downward and very close to the interface between the two layers at 0.5 foot from the middle of the reservoir, the spherical permeability obtained from the test is close to the arithmetic mean of two-layer system with an error of -5.05 %. As the test was continued, the probe then located at the bottom layer. The estimated spherical permeability when the probe is in low permeable zone and closer to the interface between the two layers, at 0.5 and 1 foot below the middle of the formation, the estimated spherical permeabilities are close to the geometric mean of the two-layer system. If the probe is at 2 feet below the middle of the formation, the estimated spherical permeability is close to the harmonic mean of two-layer system with an error of 2.30 %.

Although the spherical permeability can be estimated in all the cases, similar to case I, the horizontal permeability can be estimated only in cases when the probe was set in the high permeablezone at the bottom layer. This is due to the fact that the pressure response can travel for a longer distance in a more permeable zone. When radial flow is present, the horizontal permeability can be estimated. The estimated permeabilities are different depending on the position of the probe. If the probe is set further away above the interface between the two layers and in high permeable zone at top layer, the horizontal permeability obtained from the test is close to the high permeability of that layer. The estimated horizontal permeability is influenced mostly by the high permeable zone of that top layer. Its value is as accurate as the value

estimated from a test in a single layer reservoir (84.92 mD). When the probe is at 1 foot above to the interface between the two layers, the chart from Figure 4.50 illustrates that if the probe is set close to the interface between the two layers and in the high permeability zone, the horizontal permeability obtained from the test is the arithmetic mean of two-layer system with an error of -5.20 %.

According to case II is adverse to case I, even the pressure responses in the derivative plots are not exactly the same, there is no significant effect of the order of the layer permeability on the estimated permeability.

Table 4.11: Spherical and horizontal permeabilities using different averaging techniques for case II.

| | **Top layer Permeability** | **Bottom layer Permeability** | **Averaging Technique** | | |
|---|---|---|---|---|---|
| | | | **Arithmetic mean** | **Geometric mean** | **Harmonic mean** |
| | mD | mD | mD | mD | mD |
| Spherical | 46.42 | 4.642 | 25.53 | 14.68 | 8.44 |
| Horizontal | 100 | 10 | 55 | 31.62 | 18.18 |

Table 4.12: Interpreted results of tests conducted in a reservoir with different probe positions for case II.

| Probe position from the middle of the formatiom | | Difference when compared to | | | | Differnce when compared to | | |
|---|---|---|---|---|---|---|---|---|
| | Interpreted $k_{xyz}$ | Arithmetic mean | Geometric mean | Harmonic mean | Interpreted $k_{xy}$ | Arithmetic mean | Geometric mean | Harmonic mean |
| ft | mD | % | % | % | mD | % | % | % |
| 8 (above) | 38.32 | 50.10 | 161.04 | 354.03 | 83.86 | 52.47 | 165.21 | 361.28 |
| 5 (above) | 40.33 | 57.97 | 174.73 | 377.84 | 84.35 | 53.36 | 166.76 | 363.97 |
| 2 (above) | 38.78 | 51.90 | 164.17 | 359.48 | 83.93 | 52.60 | 165.43 | 361.66 |
| 1 (above) | 35.88 | 40.54 | 144.41 | 325.12 | 78.93 | 43.51 | 149.62 | 334.16 |
| 0.5 (above) | 24.24 | -5.05 | 65.12 | 187.20 | 52.14 | -5.20 | 64.90 | 186.80 |
| 0.5 (below) | 15.84 | -37.96 | 7.90 | 87.68 | - | - | - | - |
| 1 (below) | 12.22 | -52.13 | -16.76 | 44.79 | - | - | - | - |
| 2 (below) | 8.634 | -66.18 | -41.19 | 2.30 | - | - | - | - |
| 5 (below) | 4.222 | -83.46 | -71.24 | -49.98 | - | - | - | - |
| 8 (below) | 3.906 | -84.70 | -73.39 | -53.72 | - | - | - | - |

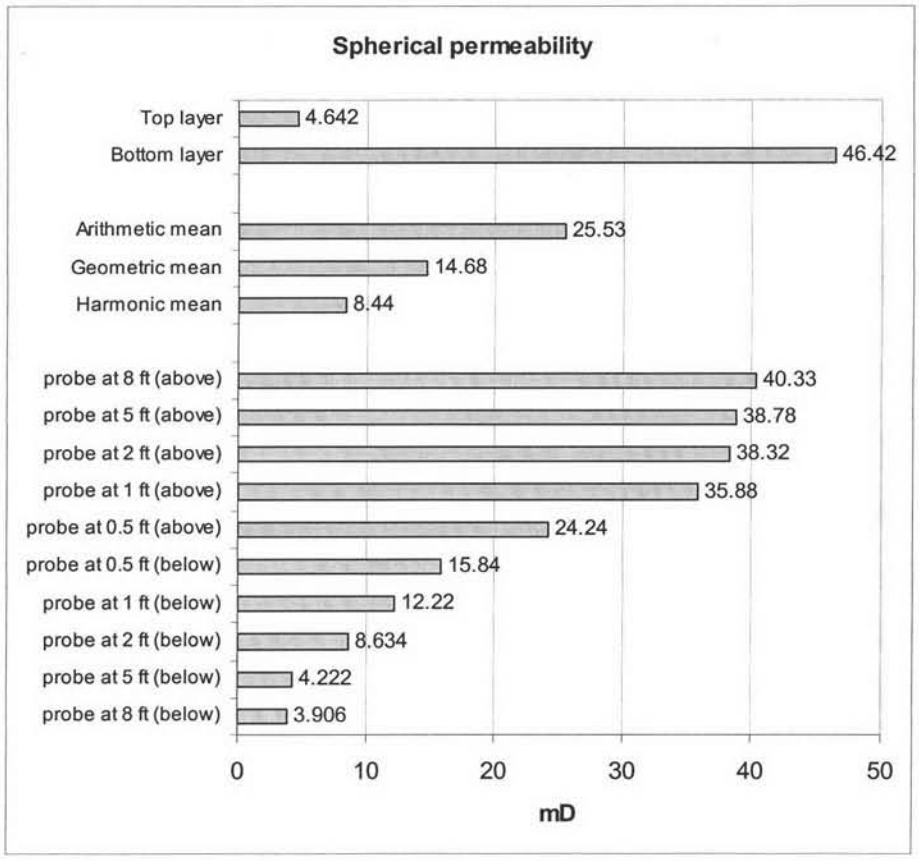


Figure 4.49: Chart comparing spherical permeability for case II.

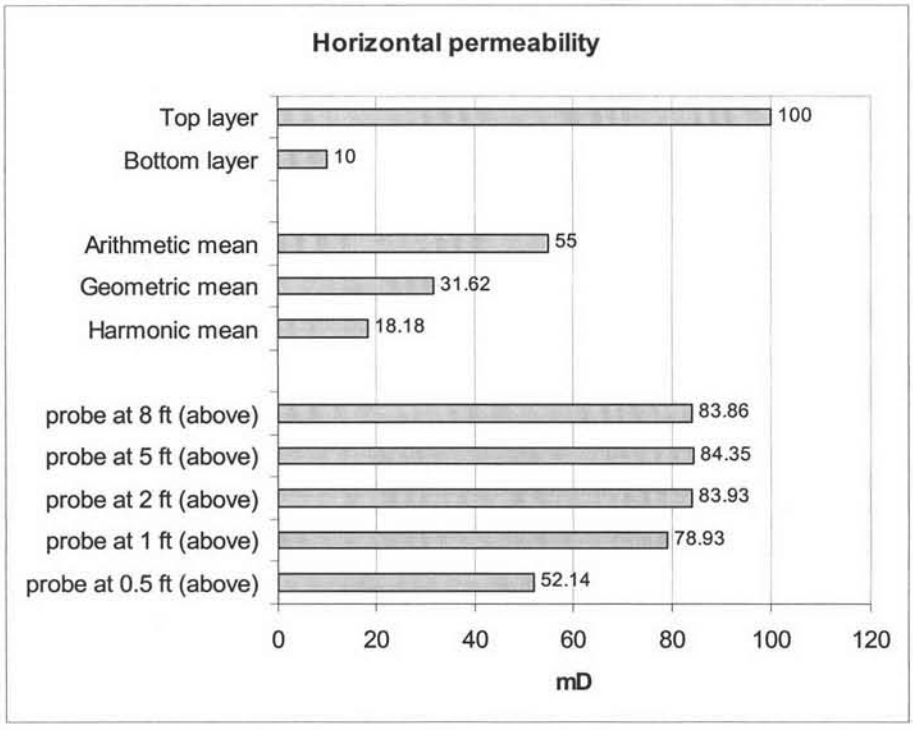


Figure 4.50: Chart comparing horizontal permeability for case II.

### 4.2.3 Case III: Horizontal permeability of 10 and 1000 mD

To examine the pressure response in a high contrast permeability system, the horizontal permeability of the top layer was set to be 10 mD, and the vertical permeability was set to be 1 mD. While, the horizontal permeability of the bottom layer was set equal to 1000 mD and the vertical permeability was set equal to 100 mD. Thus, from Equation 3.6, the calculated spherical permeabilities of the top and bottom layer are 4.642 and 464.2 mD, respectively, as schematically shown in Figure 4.51. The probe was placed at 0.5, 1, 2, 5, and 8 feet away from the middle of the formation.

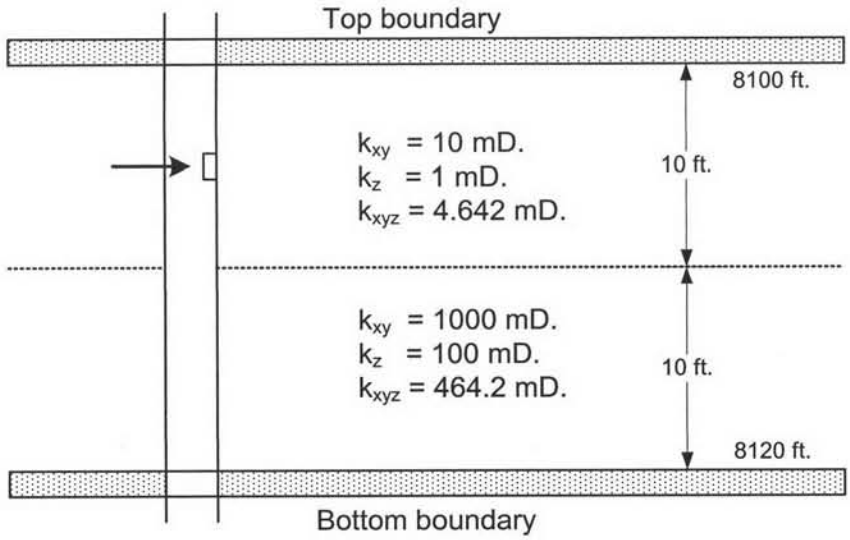


Figure 4.51: Schematic of two layer reservoir with horizontal permeability of 10 and 1000 mD.

Figure 4.52 shows the diagnostic plot of a test conducted in a reservoir with the probe positioned at 8 feet above the middle of the formation which is 2 feet from the top of the reservoir. At middle times, the negative half slope which is an indicator of the spherical flow can be seen, yielding the estimated permeability of 3.781 mD. At late times, the pressure derivative drops as if there were a constant pressure boundary. Similar to the test conducted in two layers reservoir consisting of horizontal permeability of 10 and 100 mD but this case the bottom layer has very high permeability with horizontal permeability of 1000 mD, the higher permeability zone is contributing fluid into the lower permeability zone. Due to a layer permeability contrast between the two zones, the bottom zone acts as a large source of fluid. As a result, the pressure derivative follows the characteristic of a constant pressure boundary. Note that the tail of the derivative drops lower than that of the system with a layer permeability contrast is not high.

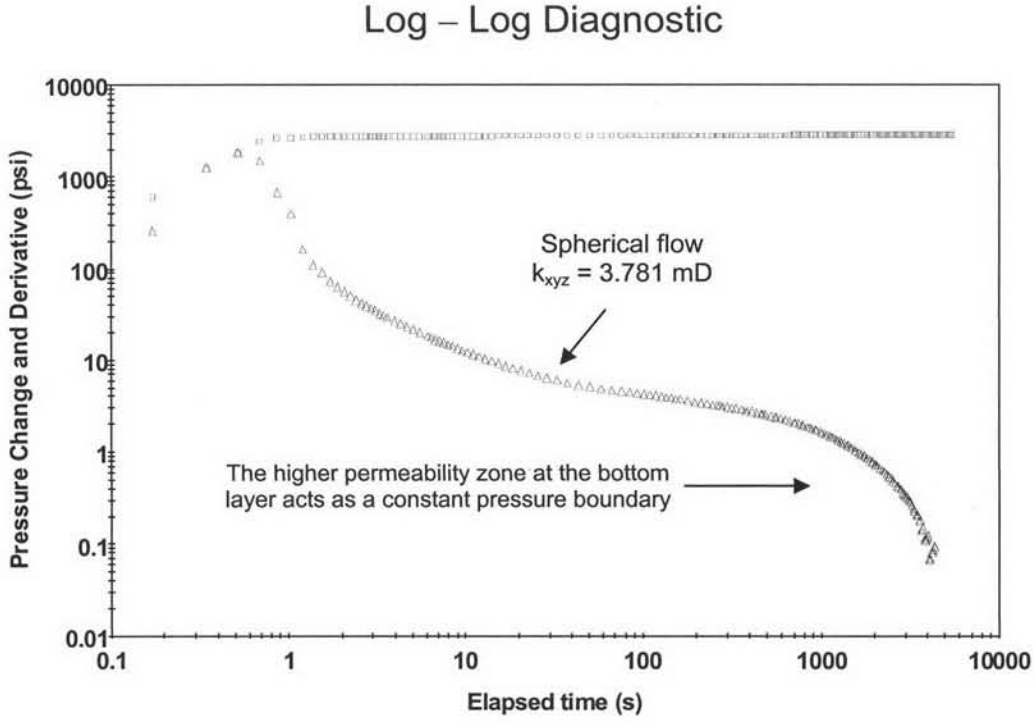


Figure 4.52: Diagnostic plot when the probe is at 8 feet above the middle of the formation.

Figure 4.53 shows the diagnostic plot of a test conducted in a reservoir with the probe positioned at 5 feet above the middle of the reservoir which is at the middle of the top layer. The behavior of the pressure derivative is similar to that in the previous case. The negative half slope indicating the spherical flow can be seen in the derivative. However, spherical flow is longer since the probe is not as close to the top boundary. The straight line results in spherical permeability of 4.142 mD. At late times, the pressure derivative descends due to a strong contribution of fluid from the higher permeability zone at the bottom layer.

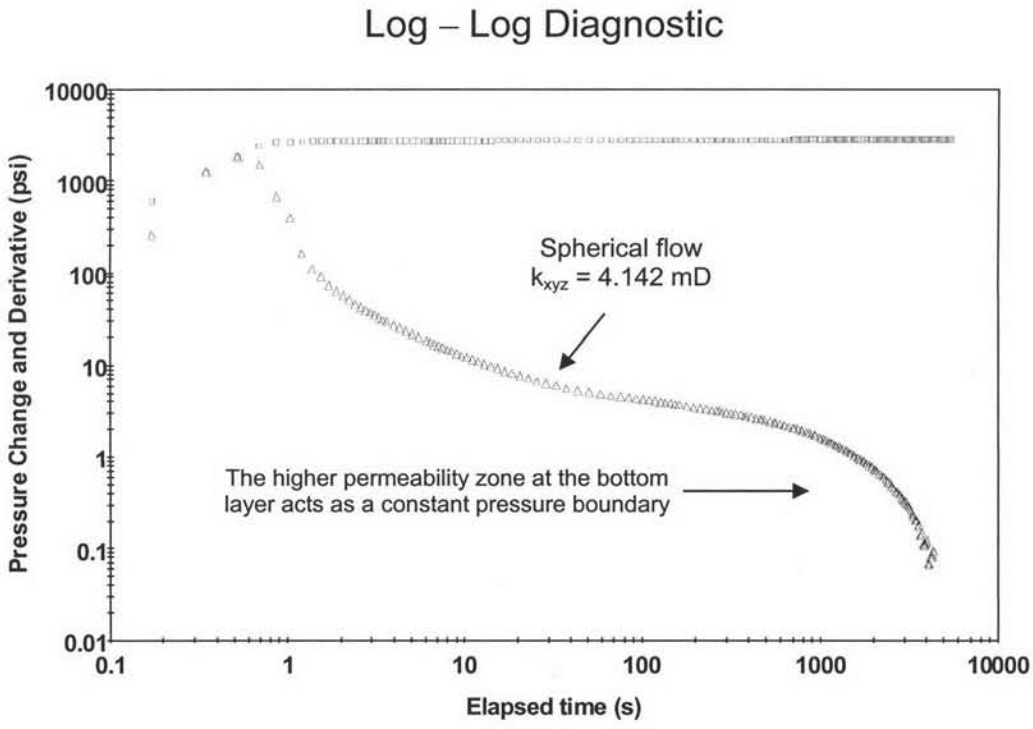


Figure 4.53: Diagnostic plot when the probe is at 5 feet above the middle of the formation.

Figure 4.54 shows the diagnostic plot of a test conducted in a reservoir with the probe positioned at 2 feet above the middle of the formation. A negative half slope straight line is fitted to the data in the spherical flow region, yielding a permeability estimate of 3.898 mD. This spherical flow occurs around the vicinity of the probe. Thus, the estimate of the permeability represents the permeability of the top layer. As the test was continued, a negative unit slope is present, indicating the change in mobility ratio. After that, a negative half slope can be seen again, depicting the continuation of the spherical flow. The permeability estimated from this second spherical flow regime is 11.69 mD, which is influenced by the higher permeability zone at the bottom layer. At late times, the tail of the derivative drops. This is due to the very high permeable zone at the top layer contributing the fluid to the upper layer.

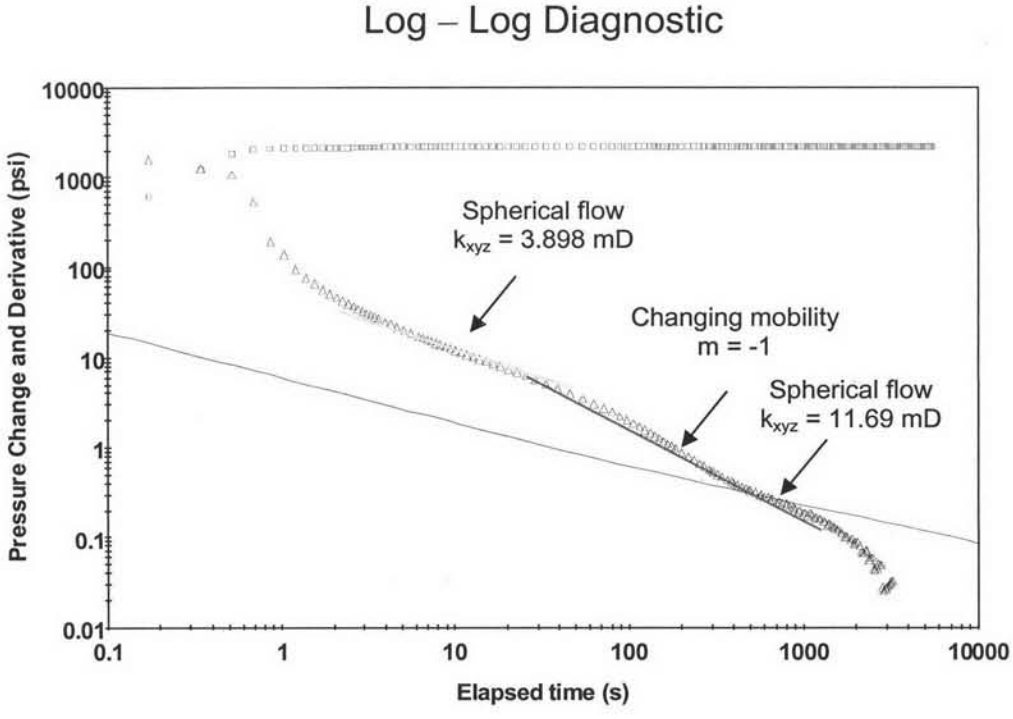


Figure 4.54: Diagnostic plots when the probe is 2 feet above the middle of the formation.

Figure 4.55 shows the diagnostic plot of a test conducted in a reservoir with the probe positioned at 1 foot above the middle of the formation. Similar to the previous case, two negative half slope straight lines were fitted to the derivative, the first one indicating spherical flow from the area very adjacent to the probe and the second one depicting spherical flow from a larger area which includes the bottom layer. Since the probe is very close to the interface between the two layers, the first spherical flow is very short. The permeability estimated from the first and second straight lines are 3.545 and 31.53 mD, respectively. Between the spherical flows, a straight line with a unit slope was fitted to the data, signifying a change in mobility ratio. Notice that the tail of the derivative starts to be noisy. This is due to the fact that the probe is very close to the very high permeable zone at the bottom layer.

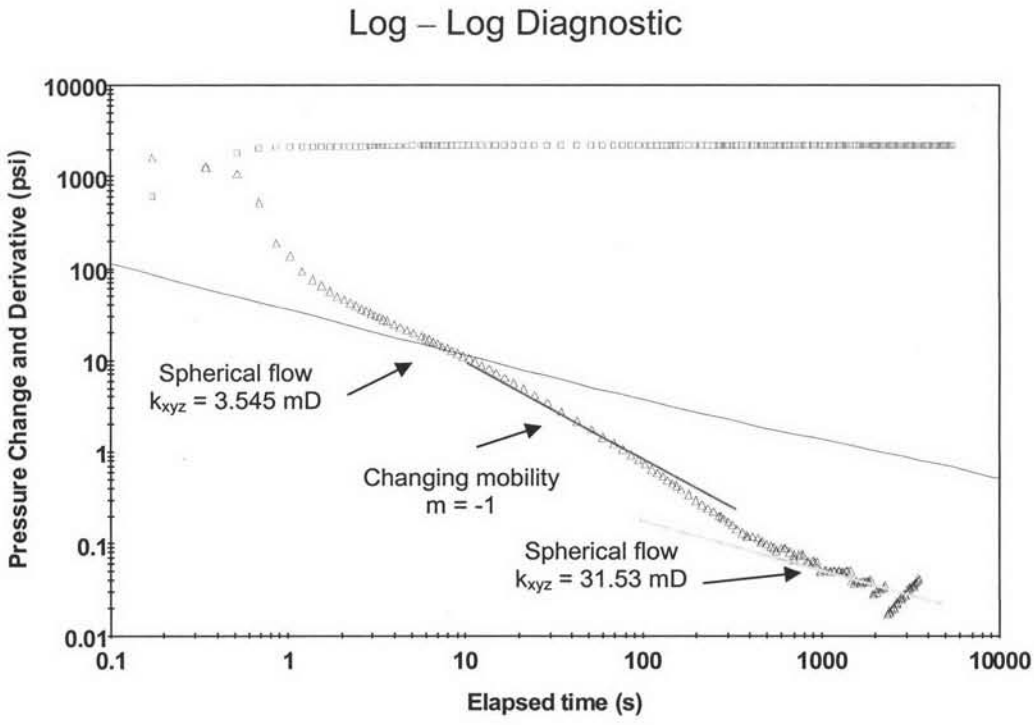


Figure 4.55: Diagnostic plot when the probe is 1 foot above the middle of the formation.

Figure 4.56 shows the diagnostic plot of a test conducted in a reservoir with the probe positioned at 0.5 foot above the middle of the formation. Since the probe is extremely close to the interface between the two layers and in the low permeability layer, the spherical flow cannot be seen. The only trend we see is the negative unit slope, indicating the change in mobility ratio from the top layer to the lower zone. This is highly influenced by the very high permeability in the lower layer.

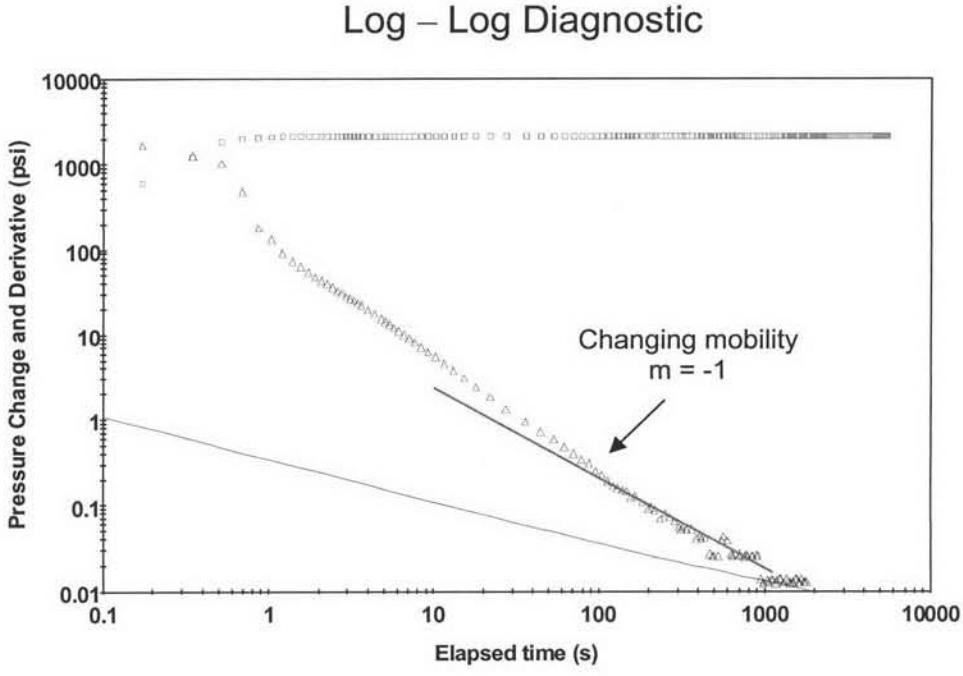


Figure 4.56: Diagnostic plot when the probe is 0.5 foot above the middle of the formation.

As the probe was placed at a very high permeability zone at the bottom layer, the pressure response in diagnostic plot depicting that the derivative have the same trend as the test conducted in a high permeability single layer even how close to the low permeability that probe was. Figure 4.57 illustrates diagnostic plots of the test conducted in a high permeability single layer reservoir and the tests with different probe positions in the bottom layer. It can be seen that pressure response behaves in similar way. At early times, the derivative depicts the negative half slopes which indicate spherical flow. At late times, it is hard to see any trend in the pressure behavior and identify any flow regime. The estimated permeabilities are tabulated in Table 4.14.

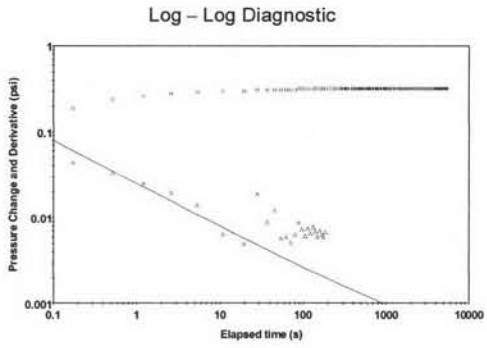


(a) The probe is at the middle of the high permeability single layer formation.

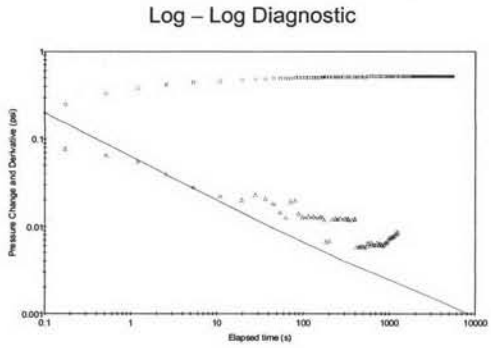


(b) The probe is 0.5 foot below the middle of the two-layer formation.

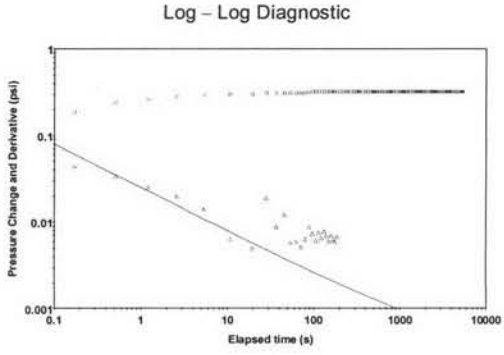


(c) The probe is 1 foot below the middle of the two-layer formation.

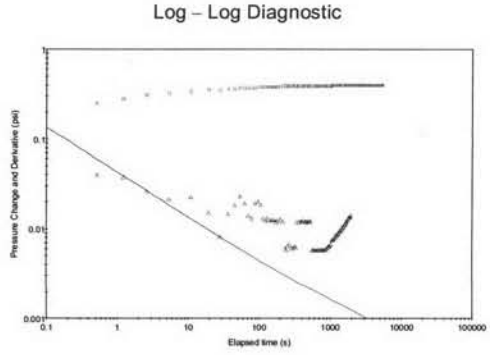


(d) The probe is 2 feet below the middle of the two-layer formation.

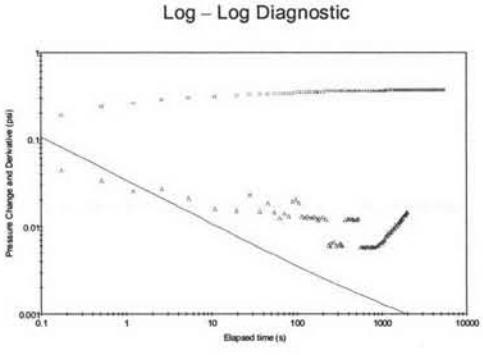


(e) The probe is 5 feet below the middle of the two-layer formation.

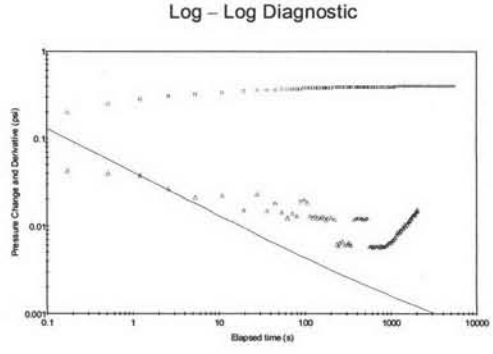


(f) The probe is 8 feet below the middle of the two-layer formation.

Figure 4.57: Diagnostic plots comparing a single layer and the two layers with different probe positions for case III.

In order to compare the permeabilities estimated from WFT with different permeability averaging techniques, the average spherical and horizontal permeability for each layer based on arithmetic, geometric and harmonic average was computed and is shown in Table 4.13. The estimated permeabilities and the differences between their values and average permeabilities base on the three averaging techniques are tabulated in Table 4.14. Figure 4.58 and 4.59 compare the value of spherical permeabilities estimated at different probe positions with the actual values and the three average values. Table 4.14 and Figure 4.58 show that when the probe is in low permeable zone at 2 feet above the middle of the formation, the estimated spherical permeability is closest the harmonic mean of two-layer system with an error of 27.20 %. When the probe is closer to the interface between the two layers at 1 foot above the middle of the formation, the estimated spherical permeabilities are close to the geometric mean of the two-layer system with an error of -32.08 %. As the probe was move downward at the location extremely close to the interface of the two layers, it can only see the change in mobility ratio. When the probe is located in high permeable zone at the bottom layer and very close to the interface between the two layers, the spherical permeability obtained from the test is close to the arithmetic mean of two-layer system with an error of 3.36 %. If the probe was set further away from the interface between the two layers, the spherical permeability obtained from the test is close to the high permeability value of the bottom layer. Note that, in this case, the estimated permeabilities have a larger error to the averaging values when compared to the two previous not-high contrast permeability systems.

Due to the derivative plots of these cases have the same trend as that of a very high permeability single layer which the plot is hard to be identified the radial flow regime, the estimated permeabiltiies cannot be compared with the averaging values.

Table 4.13: Spherical and horizontal permeabilities using different averaging techniques for case III.

| | **Top layer Permeability** | **Bottom layer Permeability** | **Averaging Technique** | | |
|---|---|---|---|---|---|
| | | | **Arithmetic mean** | **Geometric mean** | **Harmonic mean** |
| | mD | mD | mD | mD | mD |
| Spherical | 4.642 | 464.2 | 234.42 | 46.42 | 9.19 |
| Horizontal | 10 | 1000 | 505 | 100 | 19.80 |

Table 4.14: Interpreted results of tests conducted in a reservoir with different probe positions for case III.

| Probe position from the middle of the formatiom | | Difference when compared to | | | | Differnce when compared to | | |
|---|---|---|---|---|---|---|---|---|
| | Interpreted $k_{xyz}$ | Arithmetic mean | Geometric mean | Harmonic mean | Interpreted $k_{xy}$ | Arithmetic mean | Geometric mean | Harmonic mean |
| ft | mD | % | % | % | mD | % | % | % |
| 8 (above) | 3.781 | -98.39 | -91.85 | -58.86 | - | - | - | - |
| 5 (above) | 4.142 | -98.23 | -91.08 | -54.93 | - | - | - | - |
| 2 (above) | 11.69 | -95.01 | -74.82 | 27.20 | - | - | - | - |
| 1 (above) | 31.53 | -86.55 | -32.08 | 243.09 | - | - | - | - |
| 0.5 (above) | - | - | - | - | - | - | - | - |
| 0.5 (below) | 242.3 | 3.36 | 421.97 | 2536.56 | 522.1 | 3.39 | 422.10 | 2536.87 |
| 1 (below) | 293.0 | 24.99 | 531.19 | 3088.25 | 649.2 | 28.55 | 549.20 | 3178.79 |
| 2 (below) | 314.3 | 34.08 | 577.08 | 3320.02 | 700.5 | 38.71 | 600.50 | 3437.88 |
| 5 (below) | 366.4 | 56.30 | 689.31 | 3886.94 | 816.4 | 61.66 | 716.40 | 4023.23 |
| 8 (below) | 320.9 | 36.89 | 591.30 | 3391.84 | 690.4 | 36.71 | 590.40 | 3386.87 |

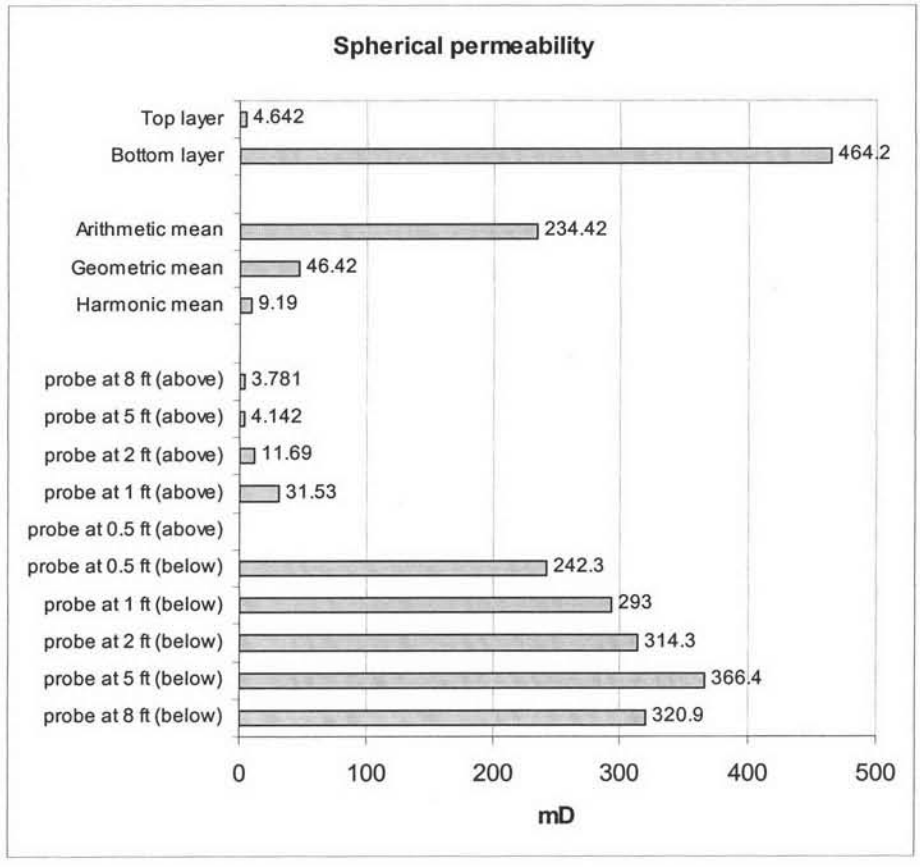


Figure 4.58: Chart comparing spherical permeability for case III.

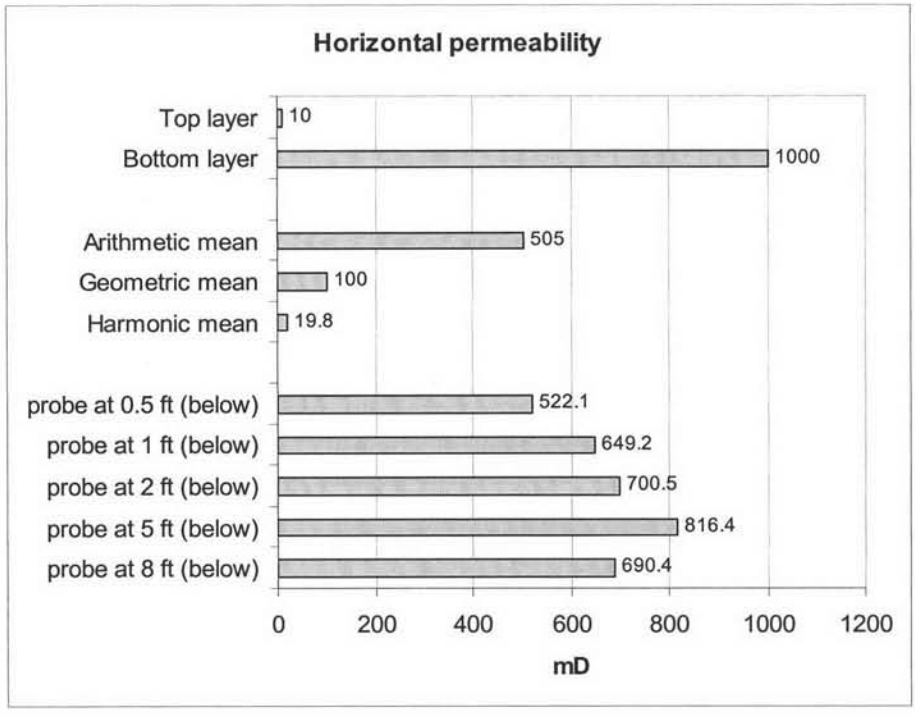


Figure 4.59: Chart comparing horizontal permeability for case III.

### 4.2.4 Case IV: Horizontal permeability of 1000 and 10 mD

Similar to the case III, the reservoir consisting of a high contrast permeability layer was applied. In contrary, to examine the effect of order of layer permeability, the layer permeabilities from the previous case were adversely set. The horizontal permeability of the top layer was set to be 1000 mD, and the vertical permeability was set to be 100 mD. While, the horizontal permeability of the bottom layer was set equal to 10 mD and the vertical permeability was set equal to 1 mD. Thus, from Equation 3.6, the calculated spherical permeabilities of the top and bottom layer are 464.2 and 4.642 mD, respectively, as schematically shown in Figure 4.51. The probe was placed at 0.5, 1, 2, 5, and 8 feet away from the middle of the formation.

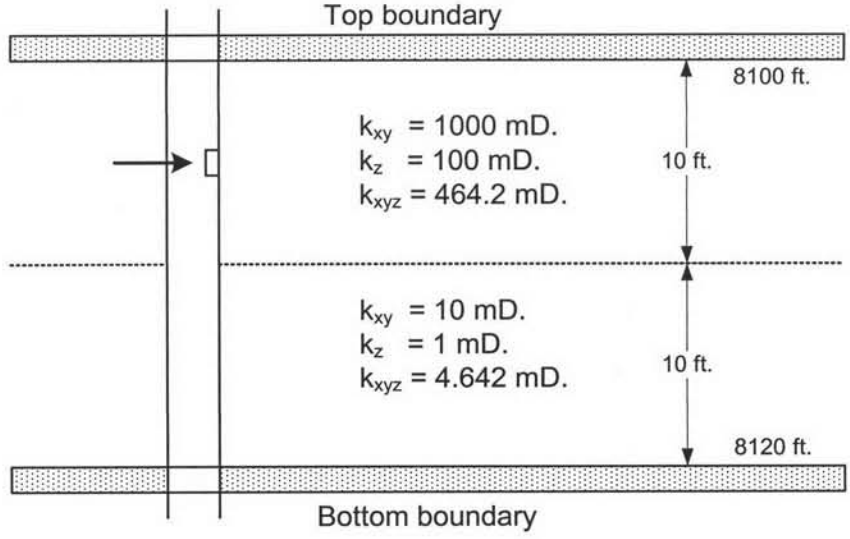


Figure 4.60: Schematic of two layer reservoir with horizontal permeabilities of 1000 and 10 mD.

Similar to case III, when the probe was placed at a very high permeability zone but adversely at the top layer, the pressure response in diagnostic plot depicting that the derivative plot have the same trend as the test conducted in a very high permeability single layer reservoir even how close to the low permeability that probe was. Figure 4.61 illustrates diagnostic plots of the test conducted in a high permeability single layer and the tests with different probe positions in the bottom layer. The figure shows that pressure response in the derivative plots of all these tests behave in similar way. At early times, the negative half slope straight lines are fitted to the data in the spherical flow region. These give spherical permeabilities as tabulated in Table 4.16. At late times, the derivative plot is scattering so that it is hard to identify any flow regime as seen in the figure.

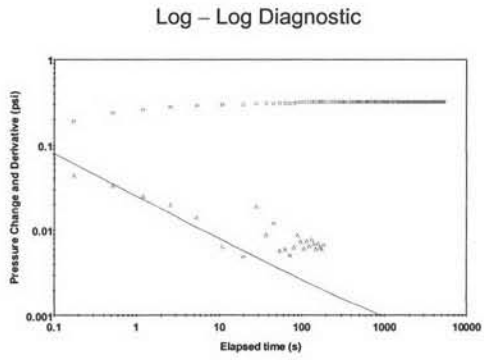


(a) The probe is at the middle of the high permeability single layer formation.

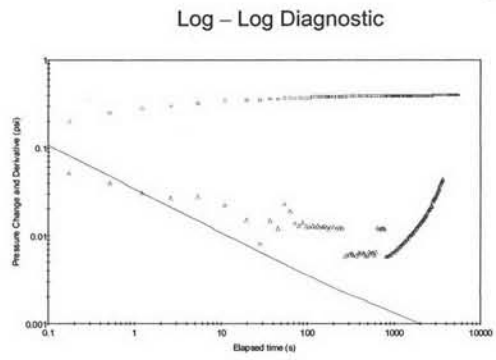


(b) The probe is 8 feet above the middle of the two-layer formation.

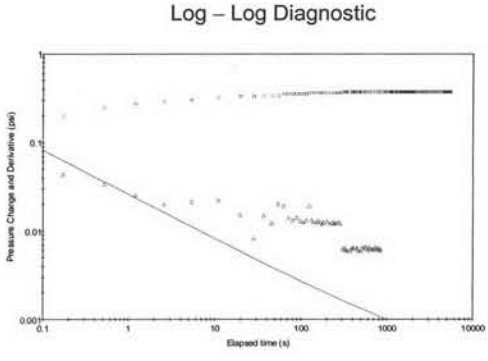


(c) The probe is 5 feet above the middle of the two-layer formation.

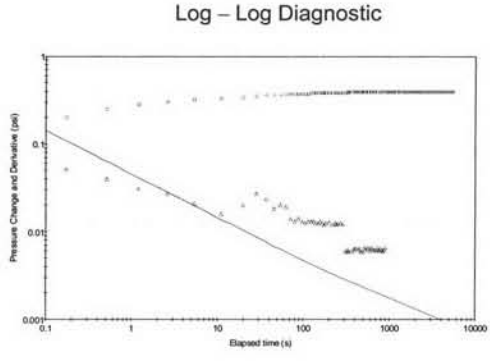


(d) The probe is 2 feet above the middle of the two-layer formation.

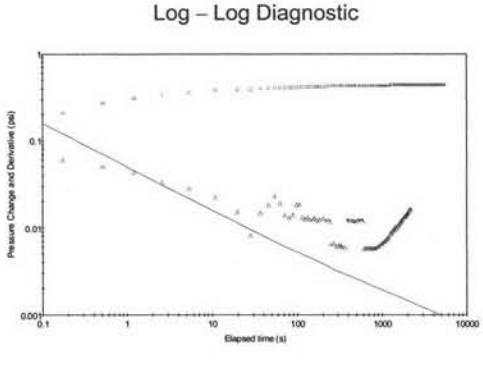


(e) The probe is 1 foot above the middle of the two-layer formation.

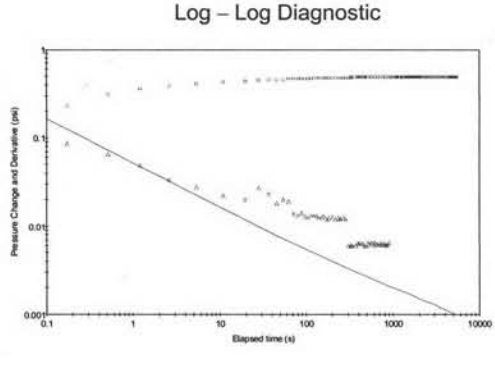


(f) The probe is 0.5 foot above the middle of the two-layer formation

Figure 4.61: Diagnostic plots comparing a single layer and the two layers with different probe positions for case IV.

To continue the study on the effect of the probe position, the probe was moved downward to the lower permeability at the bottom layer. Figure 4.62 shows the diagnostic plot of a test conducted in a reservoir with the probe positioned at 0.5 foot below the middle of the formation. Similar to the previous case, since the probe is extremely close to the interface between the two layers, the spherical flow cannot be seen. The only the negative unit slope indicating the change in mobility from the top layer to the lower zone is present. This is highly influenced by the very high permeability in the top layer.

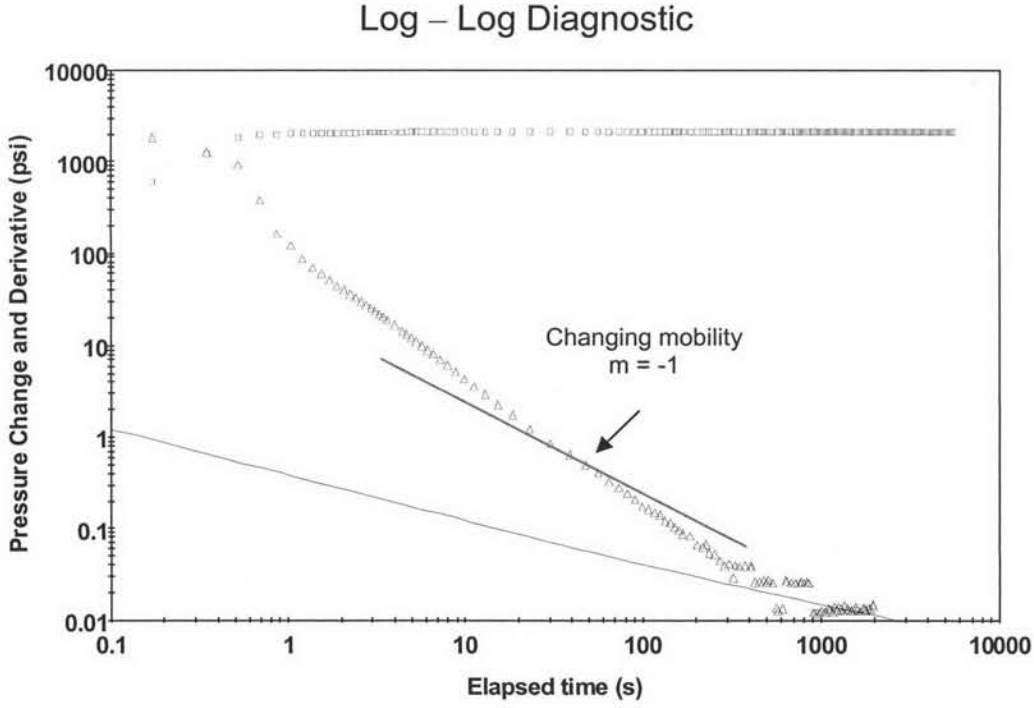


Figure 4.62: Diagnostic plot when the probe is 0.5 foot below the middle of the formation.

Figure 4.63 shows the diagnostic plot of a test conducted in a reservoir with the probe positioned at 1 foot below the middle of the formation. Two negative half slope straight lines were fitted to the derivative, the first one indicating spherical flow from the area very adjacent to the probe and the second one depicting spherical flow from a larger area which includes the top layer. Since the probe is very close to the interface between the two layers, the first spherical flow is very short. The permeability estimated from the first and second straight lines are 3.36 and 29.35 mD, respectively. Between the spherical flows, a straight line with a unit slope is present, signifying a change in mobility ratio. Notice that the tail of the derivative starts to be noisy. This is due to the fact that the probe is very close to the very high permeable bottom layer.

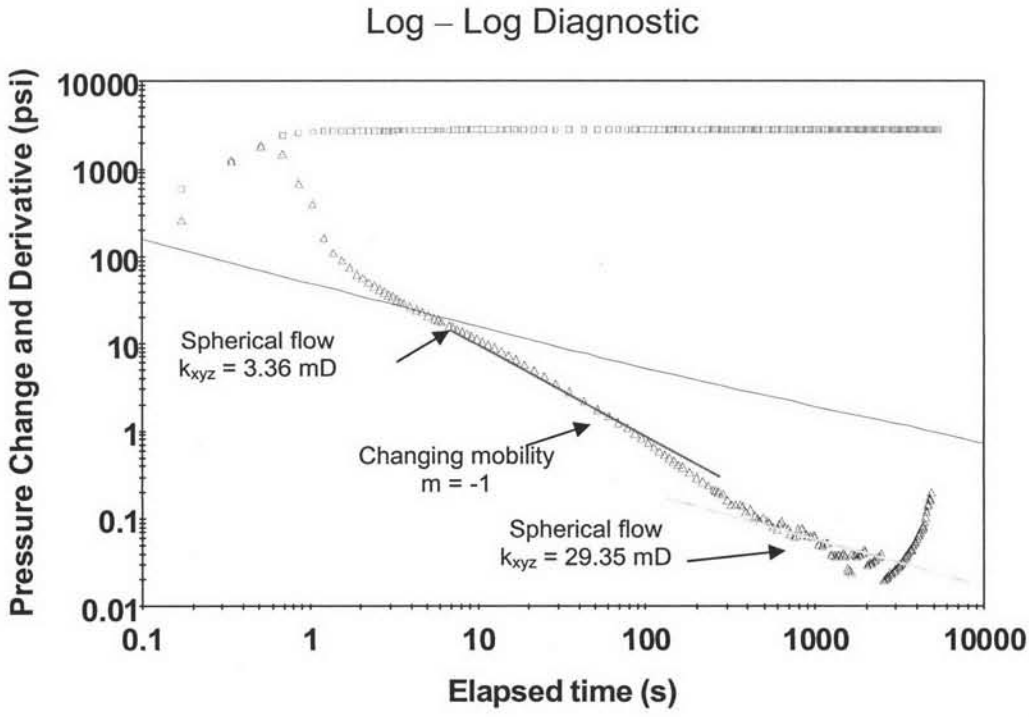


Figure 4.63: Diagnostic plot when the probe is 1 foot below the middle of the formation.

Figure 4.64 shows the diagnostic plot of a test conducted in a reservoir with the probe positioned at 2 feet below the middle of the formation. At early time, the negative half slope straight line can be seen, which is indicating the spherical flow region. This straight line gives the estimated horizontal permeability of 3.735 mD. This spherical flow occurs around the vicinity of the probe. Thus, the estimate of the permeability represents the permeability of the bottom layer. As the test was continued, a negative unit slope is present, indicating the change in mobility ratio. After that, a negative half slope can be seen again, depicting the continuation of the spherical flow. The permeability estimated from this second spherical flow regime is 13.08 mD, which is influenced by the higher permeability zone at the bottom layer. At late times, the tail of the derivative descends. This is due to the strong contribution of fluid from the very high permeable zone at the top layer.

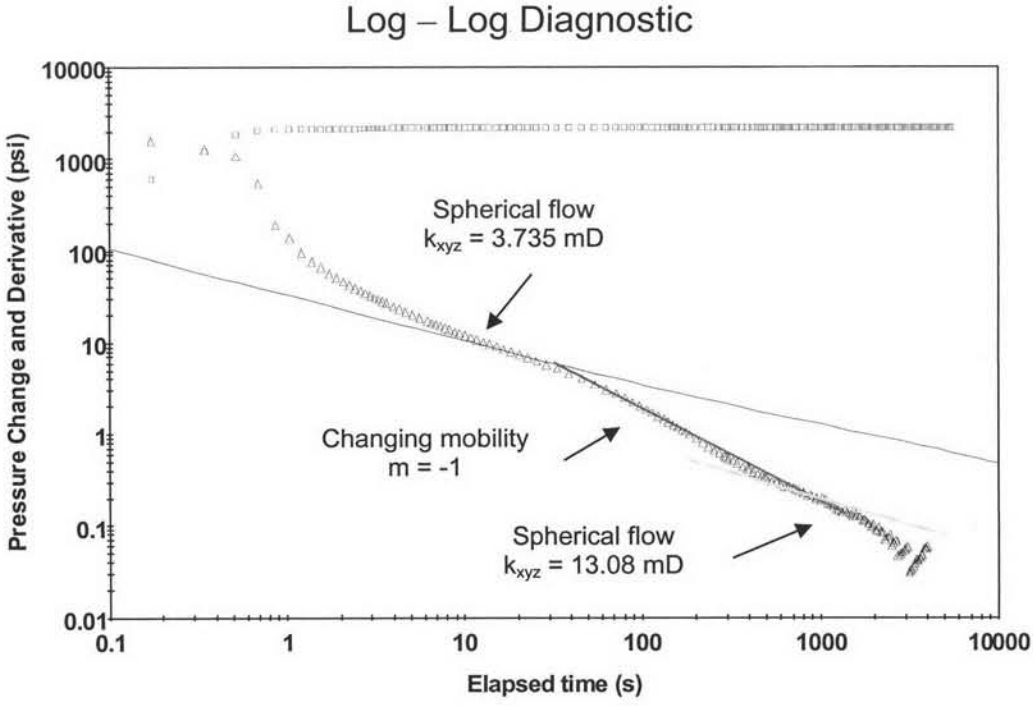


Figure 4.64: Diagnostic plot when the probe is 2 feet below the middle of the formation.

Figure 4.65 shows the diagnostic plot of a test conducted in a reservoir with the probe positioned at 5 feet below the middle of the reservoir which is at the middle of the bottom layer. At early times, the negative half slope indicating the spherical flow can be seen in the derivative. The straight line results in spherical permeability of 4.248 mD, which is close to the test conducted in a single layer reservoir (4.515 mD). At late times, the pressure derivative descends due to a strong contribution of fluid from the higher permeability zone at the bottom layer. It can be seen that, when the test was conducted at this position, the influence from the higher permeable zone from the top layer takes no effect on the pressure response, but acts as a constant pressure boundary.

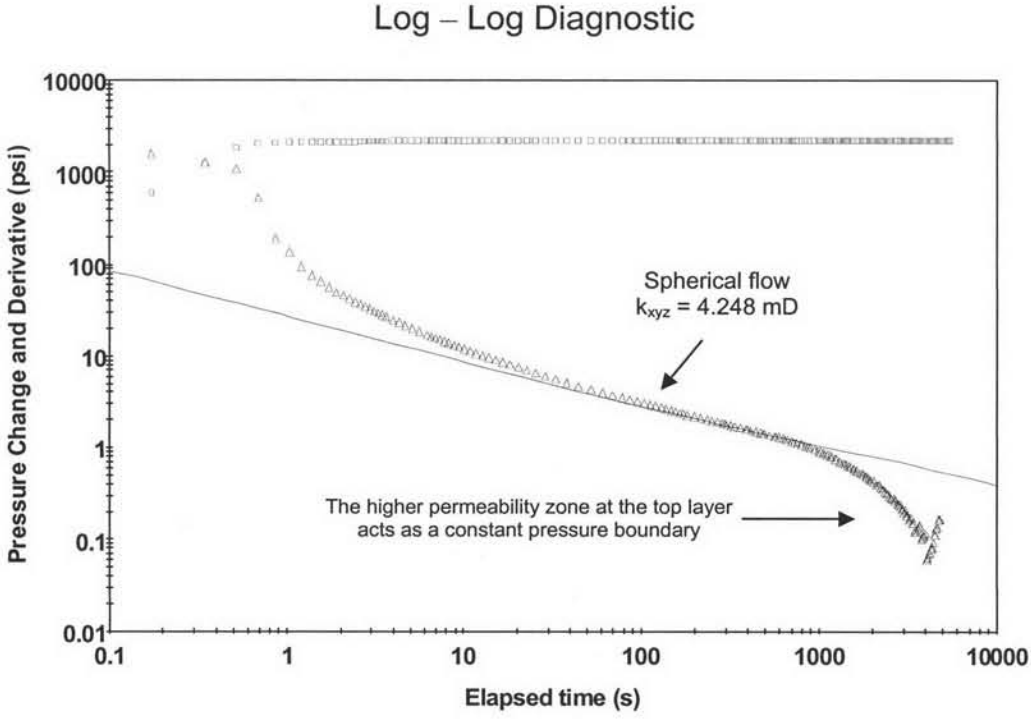


Figure 4.65: Diagnostic plot when the probe is 5 feet below the middle of the formation.

Figure 4.66 shows the diagnostic plot of a test conducted in a reservoir with the probe positioned at 8 feet below the middle of the formation which is 2 feet from the bottom of the reservoir. At middle times, the negative half slope which is an indicator of the spherical flow can be seen, yielding the estimated permeability of 3.779 mD. At late times, the pressure derivative drops as if there were a constant pressure boundary. The higher permeability zone at the top layer is contributing fluid into the lower permeability zone. Due to a strong contribution of fluid from the top zone, the very high permeable layer acts as a large source of fluid. As a result, the pressure derivative follows the characteristic of a constant pressure boundary.

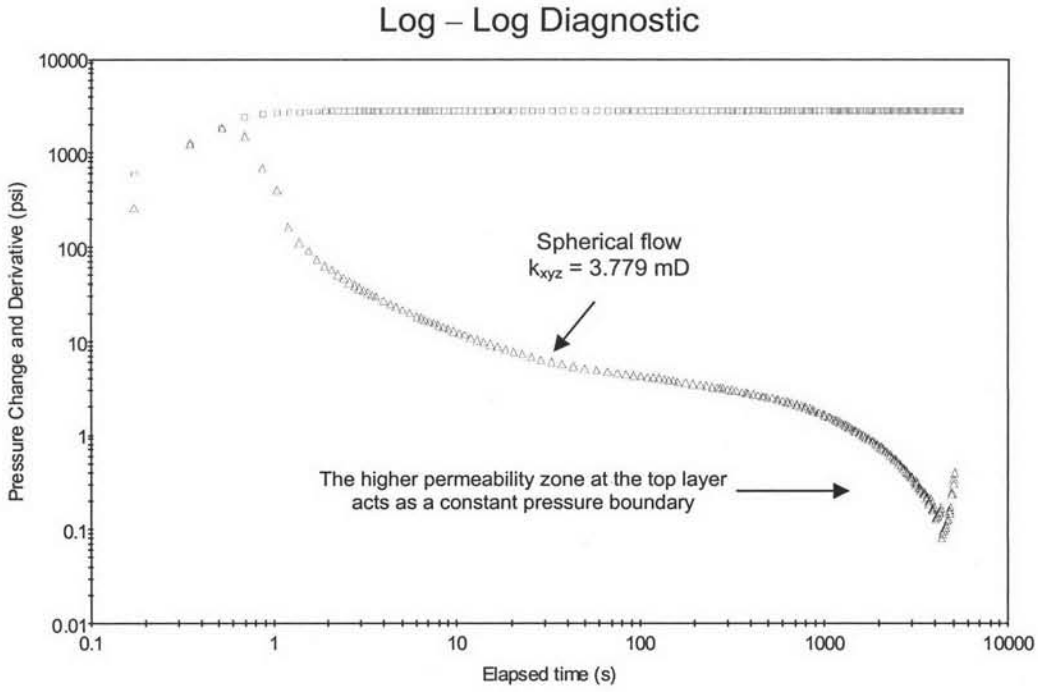


Figure 4.66: Diagnostic plot when the probe is 8 feet below the middle of the formation.

In order to compare the permeabilities estimated from WFT with different permeability averaging techniques, the average spherical and horizontal permeability for each layer based on arithmetic, geometric and harmonic average was computed and is shown in Table 4.15. The estimated permeabilities and the differences between their values and average permeabilities base on the three averaging techniques are tabulated in Table 4.16. Figure 4.67 and 4.68 compare the value of spherical permeabilities estimated at different probe positions with the actual values and the three average values. Table 4.16 and Figure 4.67 show that when the probe is in very high permeable zone above the middle of the formation and close to the interface of the two layers, the estimated spherical permeability is closest the arithmetic mean of two-layer system. As the probe was at the location extremely close to the interface of the two layers, it can only see the change in mobility ratio. When the probe is at the low permeable zone at the bottom layer, the estimated spherical permeabilities are influenced by the higher permeable zone at the top layer yielding high value of permeability. Table 4.16 and Figure 4.67 show that when the probe is in low permeable zone at 1 foot below the middle of the formation, the estimated spherical permeability is close to the geometric mean of two-layer system with an error of -36.77 %. When the probe is at 2 feet below the middle of the formation, the estimated spherical permeabilities are close to the harmonic mean of the two-layer system with an error of 42.33 %.

Similar to the previous case, the derivative plots of these cases have the same trend as that of a very high permeability single layer which the plot is hard to be identified the radial flow regime, the estimated permeablities cannot be compared with the averaging values.

Table 4.15: Spherical and horizontal permeabilities using different averaging techniques for case IV.

| | **Top layer Permeability** | **Bottom layer Permeability** | **Averaging Technique** | | |
|---|---|---|---|---|---|
| | | | **Arithmetic mean** | **Geometric mean** | **Harmonic mean** |
| | mD | mD | mD | mD | mD |
| Spherical | 464.2 | 4.642 | 234.42 | 46.42 | 9.19 |
| Horizontal | 1000 | 10 | 505 | 100 | 19.80 |

Table 4.16: Interpreted results of tests conducted in a reservoir with different probe positions for case IV.

| Probe position from the middle of the formatiom | | Difference when compared to | | | | Differnce when compared to | | |
|---|---|---|---|---|---|---|---|---|
| | Interpreted $k_{xyz}$ | Arithmetic mean | Geometric mean | Harmonic mean | Interpreted $k_{xy}$ | Arithmetic mean | Geometric mean | Harmonic mean |
| ft | mD | % | % | % | mD | % | % | % |
| 8 (above) | 365.8 | 56.04 | 688.02 | 3880.41 | 812.7 | 60.93 | 712.70 | 4004.55 |
| 5 (above) | 493.9 | 110.69 | 963.98 | 5274.32 | 994.3 | 96.89 | 894.30 | 4921.72 |
| 2 (above) | 302.1 | 28.87 | 550.80 | 3187.27 | 656.9 | 30.08 | 556.90 | 3217.68 |
| 1 (above) | 283.50 | 20.94 | 510.73 | 2984.87 | 610.4 | 20.87 | 510.40 | 2982.83 |
| 0.5 (above) | 275.80 | 17.65 | 494.14 | 2901.09 | 594.5 | 17.72 | 494.50 | 2902.53 |
| 0.5 (below) | - | - | - | - | - | - | - | - |
| 1 (below) | 29.35 | -87.48 | -36.77 | 219.37 | - | - | - | - |
| 2 (below) | 13.08 | -94.42 | -71.82 | 42.33 | - | - | - | - |
| 5 (below) | 4.248 | -98.19 | -90.85 | -53.78 | - | - | - | - |
| 8 (below) | 3.779 | -98.39 | -91.86 | -58.88 | - | - | - | - |

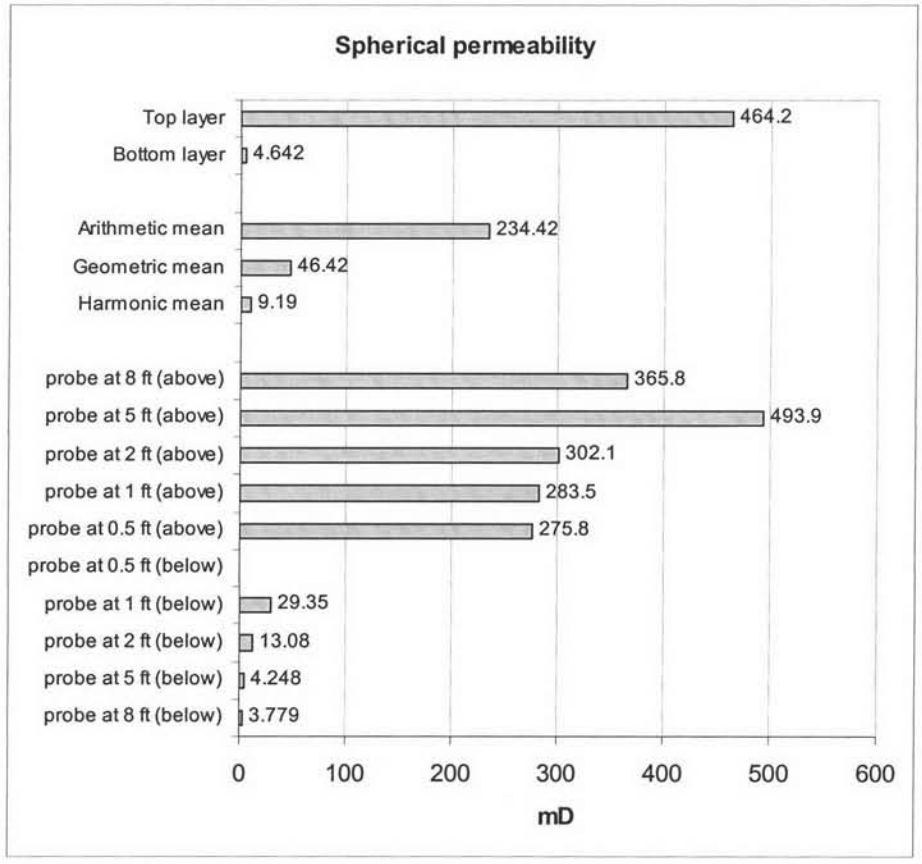


Figure 4.67: Chart comparing spherical permeability for case IV.

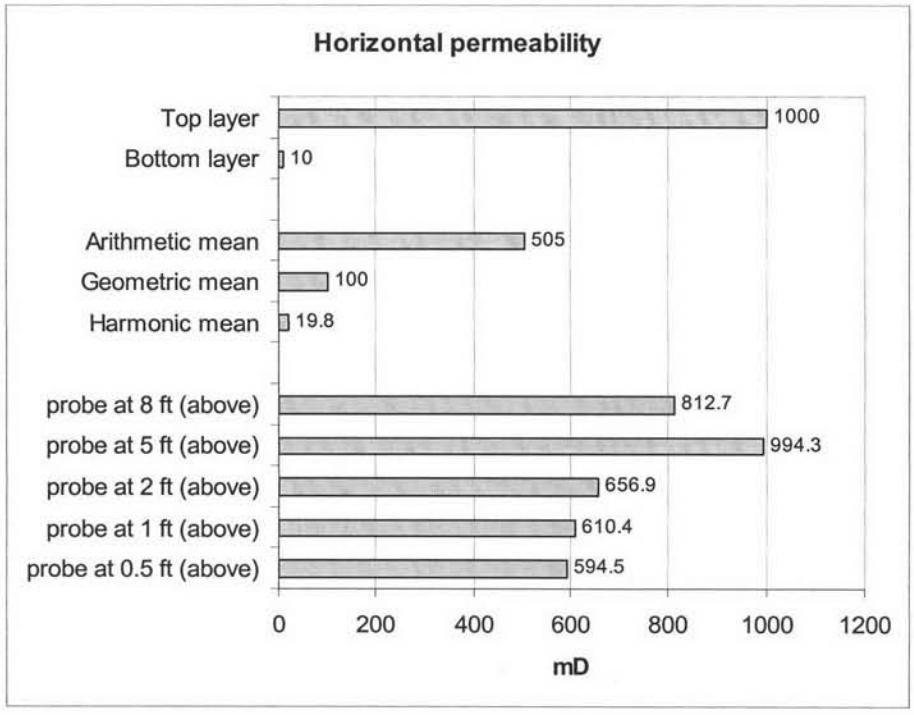


Figure 4.68: Chart comparing horizontal permeability for case IV.

## 4.3 Real Data

This section present the real data of WFT conducted in Asia Pacific region. Figure 4.69 shows an example of WFT data. The probe was in the less deplete zone (low permeability) at the top layer. The bottom zone is a high permeability layer. It can be seen that, at middle times, the derivative depicts the negative half slope indicating spherical flow. At late times, the tail of the derivative descends, which signifies a constant pressure boundary contributing from the high permeable zone at the bottom layer.

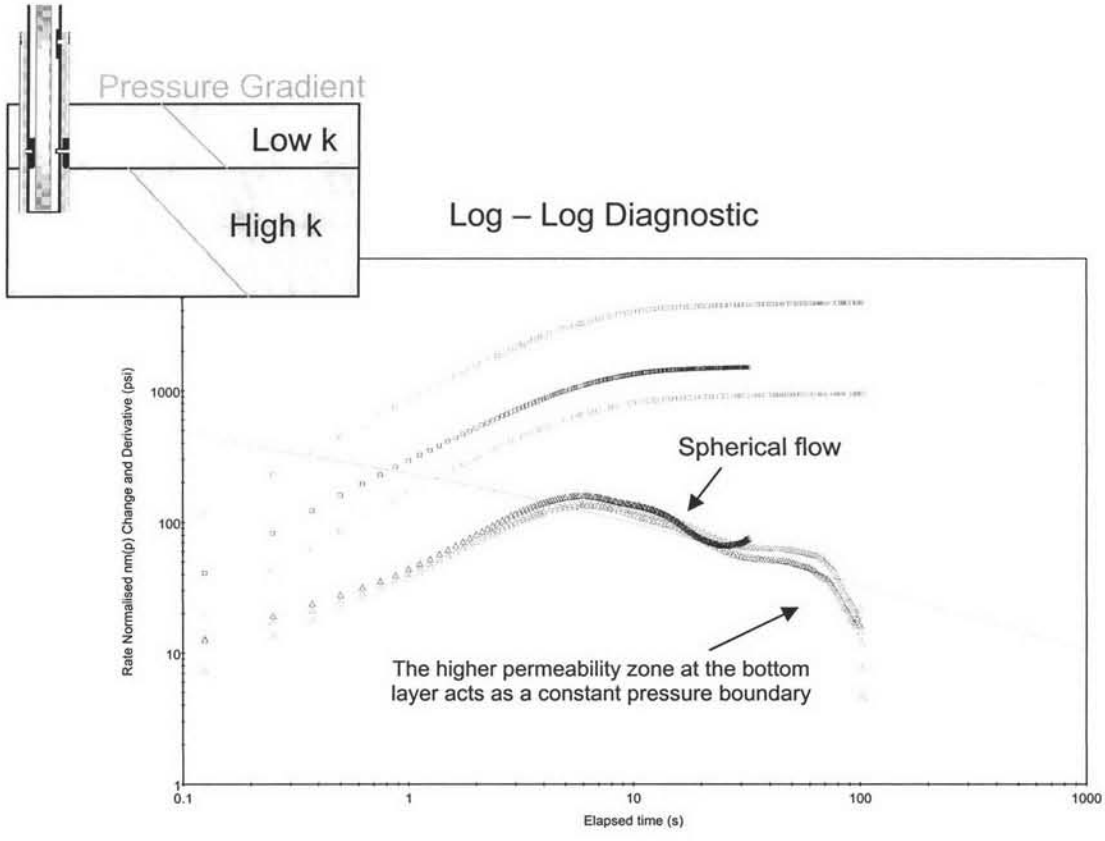


Figure 4.69: Real data of spherical flow regime and a high permeable zone acts as a constant pressure boundary.

Figure 4.70 shows the example of the tests when the changing mobility is present. At late times, the derivatives depict the negative unit slope indicating the change in mobility ratio.

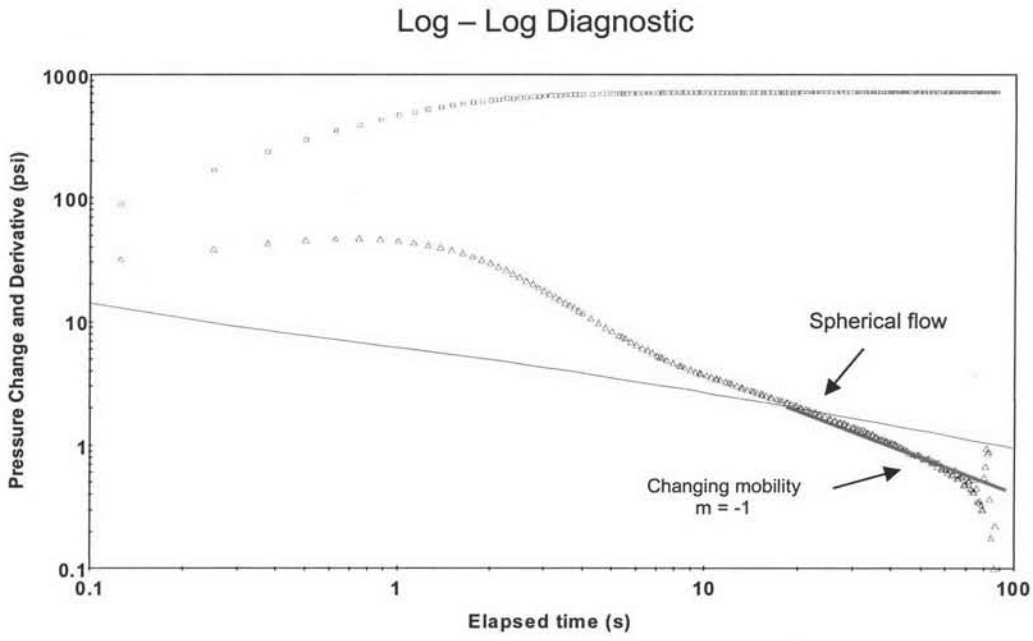


(a)

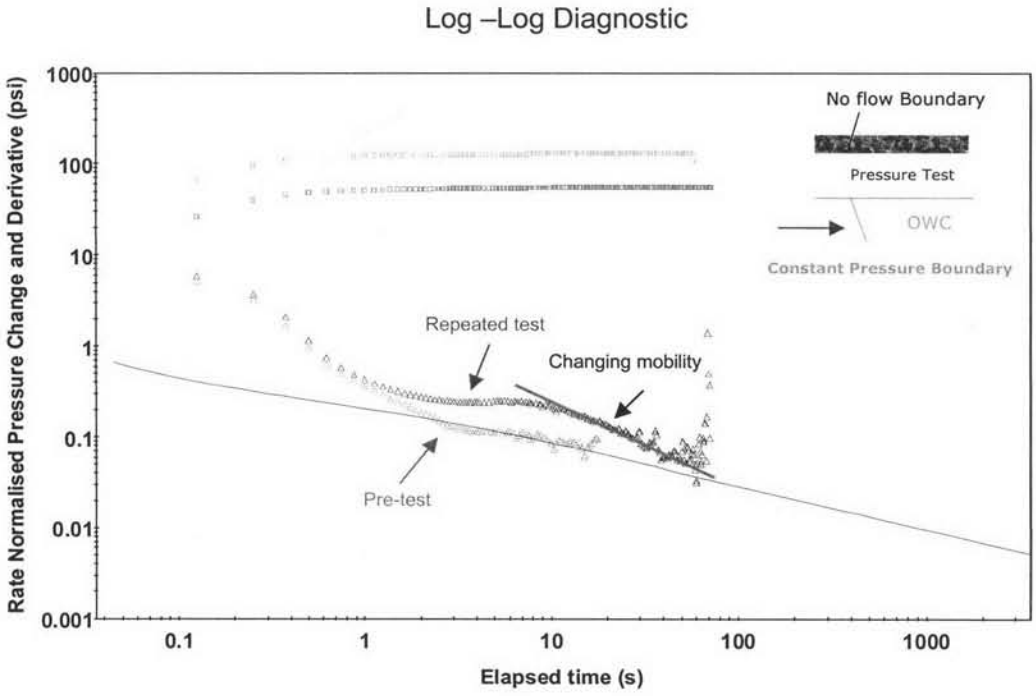


(b)

Figure 4.70: Real data of the changing mobility.